FUNCTIONAL STUDY FOR THE CHARACTERISATION AND VALIDATION OF *IFNA1* AS A TUMOUR SUPPRESSOR GENE IN MELANOMA PATHOGENESIS

A thesis submitted for the degree of
Doctor of Philosophy by

HIBA SERRAI

College of Health and Life Sciences

APRIL 2014

ABSTRACT

The complexity of melanoma is pronounced at many levels, whereby both environmental influences and genetic predisposition are involved and interact. Embedded within this complexity is heterogeneity, a defining characteristic of this malignancy. The rearrangement of genomic material on chromosomes 1p, 6q, 9p or 10q, 11q and 17q has been frequently reported during the development and progression of cutaneous malignant melanoma (CMM), suggesting several putative tumour suppressor genes and oncogenes in these regions.

The genomic complexity of chromosome 9p21 in melanoma development is well documented. This region encodes a potent cyclin-dependent kinase inhibitor *CDKN2*/*INK4A*/*p16* as a tumour suppressor gene (TSG) that is frequently inactivated in melanomas. Functional evidence suggested the presence of additional TSG loci in the 9p21-22 chromosome region (Parris et al., 1999). In pursuit of identifying novel TSG(s), our previous group's collaborative research provided experimental evidence that suggests *IFNA1* as a candidate TSG for melanoma development. Therefore, the aim of this work was to provide a further functional validation of such tumour-suppressive activity in CMM.

Firstly, I have successfully subcloned IFNA1 cDNA into pcDNA3 expression vector and established a panel of stably *IFNA1*-expressing clones. Subsequently, I have assessed their tumourigenicity in soft agar by measuring the colony-forming ability of each transfected clone. Expression analyses of IFNA1, at both post-transcriptional and translational levels, were also carried out. I have

also demonstrated a strong correlation between anchorage-independent growth in soft agar and *IFNA1* expression in qRT-PCR.

The antiproliferative and pro-apoptotic effects of IFNα have been widely documented, however, the precise mechanisms that trigger and potentiate this behaviour are not completely known. Based on previous findings, I have investigated whether *IFNA1* exerts its antitumoural activity through apoptosis. I was able to demonstrate a moderate relationship between anchorage-independent growth in soft agar and the apoptotic levels in the transfected clones. Although unpersuasive and inconclusive, the results seemed encouraging since this study was carried out using only the highly tumourigenic malignant melanoma UACC903 cell line.

ACKNOWLEDGEMENTS

The writing of this doctoral thesis required the concerted effort on the part of many brilliant, encouraging and loving people, and I would like to thank everyone involved, directly or indirectly, with this project for their professionalism, hard work, commitment, support and encouragement. It is virtually impossible to name every person associated with all the various facets of this project, but some have been particularly instrumental.

This thesis would have not been possible without the indefatigable help, support and motivation of my principal supervisor, Dr. Christopher Parris. His immense knowledge, resourceful ideas and guidance were the incontestable forces behind this thesis. A special thank you is also in order to the extraordinary members of my team, Dr. Emma Bourton, Gönül Ulus and Sheba Adam Zahir.

I would also like to thank Dr. Sahar Al-Mahdawi for her never ending support, guidance and encouragement. I would also like to thank Dr. Rana Hassan, Dr. Terry Roberts, and Dr. Evgeny Makarov for their valuable advice.

Many thanks to Maryam Ojani, Yaghoub Gozaly Chianea, Punamdip Bhullar, Ane Ogbe, Emma Ghaffari, Chiranjeevi Sandi and Vahid Ezzatizadeh, my most wonderful officemates. Thank you for your friendship and for always being upbeat and positive about the trials and tribulations of everyday life.

I gratefully acknowledge the funding received towards my PhD from the Ministry of Higher Education and Scientific Research of Algeria.

An immense thank you to my loving and most wonderful in-laws. Your love and support are truly appreciated and have made a world of difference in the pursuit of my studies. Your thoughtfulness, generosity and sound advice have been my guiding light.

I am indebted to my family, who have always inspired me to achieve great things and to pursue happiness. Thank you to my little sister, Oumnia. You are my sunshine and the source of excitement in my life. Thank you to my father and mother for being my parents and for ensuring that hard and honest work would wind up in my genes. Thank you for guiding me and encouraging me all the while loving me. Thank you for your generosity and your wise advice. Your examples of faith, hope, love, and respect will forever guide me in my life. Thank you for your unconditional love and support. Thank you for EVERYTHING!

Thank you to the man in my life, my husband Amine. You are my best friend and my partner. Your love of life continues to inspire me. You always encourage me to do what I love and never get tired of discussing my studies. Your enthusiasm is infectious and is a constant reminder of why I have embarked on this journey. Your mother's loving memory and footprint on my heart inspire me daily. Thank you for reassuring me and for motivating me.

To My Loving Family

TABLE OF CONTENTS

ABSTRACT ..... **I**
ACKNOWLEDGEMENTS ..... **III**
LIST OF FIGURES ..... **IIX**
LIST OF TABLES ..... **XII**
ABBREVIATIONS ..... **XIII**
INTRODUCTION **1**
1.1 Skin Cancer 1
1.1.1 Incidence 2
1.1.2 Skin Biology and Structure 3
1.1.3 Types of Skin Cancer 6
1.2. Cutaneous Malignant Melanoma 9
1.2.1. Epidemiology 9
1.2.2. History of Melanoma 10
1.2.3. Clinical Subsets of Malignant Melanoma 10
1.2.4 Etiologic and other Risk Factors: 14
1.2.5. Pathogenesis and Prognosis of Melanoma 20
1.3. Molecular Genetics of Cutaneous Malignant Melanoma 24
1.3.1. Chromosomal Aberrations in Melanoma 25
1.3.2. Alterations at Chromosome 9p21 in Melanoma 27
1.3.3. Melanoma Susceptibility Genes 27
1.3.4. A Melanoma Molecular Disease Model 32
1.4. Treatment of Cutaneous Malignant Melanoma 38
1.4.1. Surgical Treatment 38
1.4.2. Adjuvant Therapies 39
1.5. Interferon in Human Malignant Melanoma 42
1.5.1. Characterisation of the Type 1 Interferon Gene 43
1.5.2. Biological Effects of Interferons 44
1.5.3. Efficacy of IFNs in the Treatment of Melanoma 45

GENERAL MATERIALS AND METHODS 49
2.1. Cell Lines 49
2.2. General Cell Culture Equipment.....50
2.3. Cell Culture.....51
2.4. Cryopreservation of cells 51
2.5. Recovery of Cells from Cryopreservation 52
2.6. RNA Extraction Using Trizol® Reagent 52
2.6.1. Cell Homogenisation 53
2.6.2. Phase Separation 53
2.6.3. RNA Precipitation, Wash and Redissolving.....53
2.6.4. Quality Control 54
2.7. Standard Polymerase Chain Reaction (PCR).....54
2.8. Agarose Gel Electrophoresis 55
2.9 Statistical Analysis.....56
SUBCLONING AND CHARACTERISATION OF IFNA1 GENE.....57
3.1. INTRODUCTION 57
3.2. MATERIALS AND METHODS.....60
3.2.1. EcoRI Restriction Enzyme Digestion 61
3.2.2. Geneclean– Purifying DNA Fragments from TBE Agarose Gel 62
3.2.3. Preparation of LB Agar Plates 63
3.2.4. Ligation of cDNA into Expression Vector and Transformation.....63
3.3. RESULTS 69
3.4. DISCUSSION 72
EVALUATING THE TUMOURIGENICITY OF IFNA1-TRANSFECTED UACC-903 CLONES FOR ANCHORAGE-INDEPENDENT GROWTH IN SOFT AGAR ASSAY 75
4.1. INTRODUCTION 75
4.2. MATERIALS AND METHODS.....81
4.2.1. Selection with Geneticin® 81
4.2.2. Soft Agar Assay 85

4.3. RESULTS 87
4.4. DISCUSSION 91
DETERMINATION OF IFNA1 GENE EXPRESSION LEVELS USING REAL-TIME QUANTITATIVE REVERSE TRANSCRIPTION PCR 94
5.1. INTRODUCTION 94
5.2. MATERIALS AND METHODS 99
5.2.1. Nucleic Acid Purification and cDNA Synthesis 99
5.2.2. Primer Design 101
5.2.3. Reverse-Transcription PCR 102
5.2.4. Quantitative real-time PCR (qRT-PCR) 105
5.3. RESULTS 108
5.4. DISCUSSION 118
ASSESSMENT OF IFNA1 PROTEIN EXPRESSION 120
6.1. INTRODUCTION 120
6.2. MATERIALS AND METHODS 123
6.2.1. Sandwich ELISA 123
6.2.2. Quantitation of intracellular IFNA1 Protein Expression Using ImageStream^{x} 126
6.3. RESULTS 133
6.3.1. ELISA Analysis 133
6.3.2. Analysis of protein levels using Image stream 135
6.4. DISCUSSION 138
THE RELATIONSHIP BETWEEN IFNA1 EXPRESSION AND INDUCTION OF APOPTOSIS IN UACC-903 141
8.1. INTRODUCTION 141
7.2. MATERIALS AND METHODS 147
7.2.1. Cell Staining 147
7.2.2. Imaging Flow Cytometry 148
7.2.3. Image Compensation 148
7.2.4. ImageStream Analysis 149

7.3. RESULTS 151
7.4. DISCUSSION 153
CONCLUSION AND FURTHER RESEARCH 156
8.1. GENERAL DISCUSSION AND CONCLUSION 156
8.2. RESEARCH LIMITATIONS AND FUTURE WORK 162
REFERENCES 165

LIST OF FIGURES

Figure 1.1: Schematic representation of normal skin architecture 4
Figure 1.2: Hematoxylin and eosin (H&E) stained histological sections displaying melanocyte transformation progression.....5
Figure 1.3: Superficial Spreading Melanoma 11
Figure 1.4: Nodular Melanoma.....12
Figure 1.5: Lentigo Maligna Melanoma 13
Figure 1.6: Acral Lentiginous Melanoma.....14
Figure 1.7: Schematic illustration of transformed melanocytes progression.....22
Figure 1.8: Genomic organisation of the CDKN2A locus.....29
Figure 1.9: A simplified diagram of the fundamental signalling networks involved in melanoma tumourigenesis 34
Figure 1.10: Schematic illustration of HAS chromosome 9 with an enlarged exemplification, depicting type I IFN locus genes. 44
Figure 3.1: Schematic representation of the pcDNA3 expression vector.....58
Figure 3.2: Agarose gel image of plasmid cDNA treated with ECORI enzyme. ..60
Figure 3.3: 1 KB plus ladder.....61
Figure 3. 4: A picture of 1% agarose gel showing the treated plasmid DNA with EcoRI restriction enzyme. This plasmid was electrophoresed for 45 minutes at 35 volts. The upper band corresponds to the plasmid vector, whereas the lower one corresponds to IFNA1 cDNA with a size of 691 bp. The latter was carefully excised and eluted using GENECLEAN® 69
Figure 3.5: A picture of 1% agarose gel showing the 12 treated colonies with EcoRI. The gel was run for 35 minutes at 60 volts. U| uncut or control samples where no enzyme was added; C| cut or digested DNA plasmids with EcoRI. The upper band corresponds to the plasmid vector and the lower one to IFNA1 cDNA with a size of 691bp. 70
Figure 3.6: SnapGene analysis of IFNA1 cDNA sequencing 71
Figure 4.1: Schematic representation of the pcDNA3 vector.....81

Figure 4.2: UACC-903 cells transiently transfected with GFP. 87
Figure 4.3: Representative images of soft agar colony formation at day 21 89
Figure 4.4: Average colony-forming ability of the transfected clones against parental tumourigenic UACC-903 90
Figure 4.5: Chromosomal region 9p21-22 showing deletions in the two variants of chromosome 9 transferred to UACC-903 cell line 92
Figure 5.1: RT-PCR control gel demonstrating the quality of cDNA samples using "Set 1" GAPDH primers 109
Figure 5.2: GAPDH primer optimisation 109
Figure 5.3: IFNA1 primer optimisation using Set 2. 110
Figure 5.4: IFNA1 primer optimisation using Set 3 110
Figure 5.5: IFNA1 primer optimisation using Set 4 111
Figure 5.6: IFNA1 primer "set 4" optimisation using qRT-PCR amplification curve.....112
Figure 5.7: Post-amplification dissociation curves 112
Figure 5.8: Quantification of relative IFNA1 mRNA expression levels 114
Figure 5.9: Relative quantification analysis showing the fold-change of IFNA1 transcript abundance in test samples relative to UACC-903. 117
Figure 6.1: Extended range serial dilution (156-5000 pg/mL) of human IFN-α. 124
Figure 6.2: Snapshots of different objects that were captured in brightfield.....129
Figure 6.3: A building block tool showing a scatter plot of a defined single cell population 130
Figure 6.4: A predefined building block tool showing single cells distributed in histogram bins.....131
Figure 6.5: A scatter of single cells in focus that have been stained with both AF488 and Draq5.....132
Figure 6.6: ELISA standard curve using extended range serial dilution of the IFN-α standard. 133
Figure 6.7: Quantitative measurement of IFNA1 production in culture media using sandwich ELISA 134

Figure 6.8: Representative images derived from imagining flow cytometry displaying brightfield images along with AF488 and Draq5 staining 135
Figure 6.9: Representative ImageStream flow cytometry images showing IFNA1 protein expression in clone 8 136
Figure 6.10: Relative fluorescence levels of IFNA1 expression in UACC-903 cell variants. 137
Figure 7.1: A model for p53-mediated apoptosis in the intrinsic and extrinsic pathways 143
Figure 7.2: Gating for single cell population 149
Figure 7.3: Gating for single cells in focus 150
Figure 7.4: Gating for single cells in focus stained for both FITC and PI 150
Figure 7.5: Illustrative Images derived from imagestream analysis showing BF images along with annexin V-FITC and PI staining 151
Figure 7.6: Apoptosis levels in the transfected clones 152
Figure 7.7: A scatter diagram showing a weak negative correlation between anchorage-independence growth in soft agar and apoptosis levels 154
Figure 8.1: Chromosomal region 9p21 showing all the genes mapped between the markers D9S1846 and D9S171 159
Figure 8.2: A scatter graph showing a strong correlation between anchorage-independence growth in soft agar and IFNA1 expression in qRT-PCR 160

LIST OF TABLES

Table 1.1: Stage-specific survival estimates for melanoma patients, according to the AJCC staging system 23

Table 1.2: Chromosomal aberrations in cutaneous malignant melanoma 26

Table 5.1: Primer sequences for RT-PCR and qRT-PCR.....102

Table 5.2: Thermal Cycling Parameters 106

Table 5.3: Sample readings from total RNA extraction 108

ABBREVIATIONS

AF: Alexa Fluor

AK: Actinic Keratosis

ALM: Acral Lentiginous Melanoma

AMS: Atypical Mole Syndrome

ARF: Alternate Reading Frame

BCC: Basal Cell Carcinoma

BF: Brightfield

bp: base pair

BSA: Bovine Serum Albumin

CDK: Cyclin-Dependent Kinase

CFE: Colony Forming Efficiency

CMM: Cutaneous Malignant Melanoma

CMV: Cytomegalovirus

CPDs: Cyclobutane Pyrimidine Dimers

Ct: Threshold Cycle

DAPI: 4',6-Diamidino-2-Phenylindole

DEPC: Diethyl PyroCarbonate

DMEM: Dulbecco's Modified Eagle's Medium

DMSO: Dimethyl Sulfoxide

DNase I: Deoxyribonuclease I

DNS: Dysplastic Nevus syndrome

dNTP: DeoxyNucleoside TriPhosphate

ECM: Extracellular Matrix

EDTA: Ethylenediaminetetraacetic Acid

ELISA: Enzyme-Linked Immunosorbent Assay

ER: Endoplasmic Reticulum

EtBr: Ethidium Bromide

FDA: Food and Drug Administration

FITC: Fluorescein Isothiocyanate

H&E: Hematoxylin and Eosin

hTERT: Human Telomerase Transcriptase

HDI: High-Dose Interferon-α2b

IFN: Interferon

JAK-STAT: Janus Kinases-Signal Transducers and Activators of Transcription

Kb: Kilobase

kDa: Kilodalton

LB: Luria-Bertani

LOH: Loss of Heterozygosity

MDN: Melanocytic Dysplastic Naevi

MMCT: Microcell-Mediated Chromosome Transfer

MSI: Microsatellite Instability

OCA: Oculocutaneous Albinism

OD: Optical Density

PBS: Phosphate-Buffered Saline

PCR: Polymerase Chain reaction

PI: Propidium Iodide

PI3K: Phosphoinositide 3-Kinase

PTEN: Phosphatase and Tensin homolog

Rb: Retinoblastoma gene

RCF: Relative Centrifugal Force

RGP: Radial Growth Phase

Rpm: revolutions per minute

RPMI: Roswell Park Memorial Institute

RQ: Relative Quantification

RT-PCR: Reverse Transcription Polymerase Chain Reaction

SCC: Squamous Cell Carcinoma

SCID: Severe Combined Immunodeficiency Disease

SFM: Serum Free Medium

SLN: Sentinel Lymph Node

SOC: Super Optimal broth with Catabolic repressor

TBE: Tris/Borate/EDTA

TSG: Tumour Suppressor Gene

UPR: Unfolded Protein Response

UV: Ultraviolet

UVR: Ultraviolet Radiation

VGP: Vertical Growth Phase

XP: Xeroderma Pigmentosum

DECLARATION

I hereby declare that the research presented in this thesis is my own work except where explicitly stated otherwise, and has not been submitted in substance for any other degree.

HIBA SERRAI

CHAPTER 1

INTRODUCTION

1.1 Skin Cancer

The skin is the largest organ in the human body and a dynamic interface that protects us from various extrinsic factors, including ultraviolet radiation, climate, toxins, pollutants, and pathogens. Human skin falls into a cluster of different colours and gradations, ranging from pale white (type I) to black (type VI). Geographic distribution and environmental variables greatly influence the skin pigmentation, which is produced by a chemically inert and stable pigment known as melanin. Besides being the main determinant of skin colour, melanin plays a major photoprotective role by absorbing, scattering, photo-oxidising, scavenging free radicals, and therefore preventing DNA damage. However, failure to repair this damage leads to mutations, until eventually the accumulation of mutations in critical genes leads to skin cancer [Reviewed in (Costin and Hearing, 2007)].

The incidence, pathology, genetics and treatment of the major types of human skin cancer with emphasis on cutaneous malignant melanoma will be detailed further.

1.1.1 Incidence

The global incidence of skin cancer has been dramatically increasing among the Caucasian population over the past decades, making it a major global health problem. In fact, one in every three cancers is diagnosed as skin cancer with around 2 to 3 million non-melanoma skin cancers and 132,000 melanoma skin cancers occur each year worldwide (World Health Organization, 2012).

Non-melanoma skin cancers are the most prevalent yet the less lethal type of skin cancer. It is predominately common in ageing populations with a significantly varied epidemiological prevalence. Incidence rates are highest by far in Australia, with between 1% and 2% of the population developing NMSC annually. Moreover, the annual incidences in the United States are estimated at over one million cases (Ridky, 2007). In the United Kingdom, the number of newly diagnosed cases of NMSC has reached 99.549 cases per 100,000 population in 2010 (Cancer Research UK, 2012).

Over the past decades, melanoma diagnosis increased by 55% in the UK. From 1999 to 2010, melanoma incidence has risen from around 11 cases to 17 cases per 100,000 population. Estimates of the UK incidence and mortality of skin cancer in the year 2010 classified melanoma as the sixth most common cancer, and described 12 thousand new cases with a male to female ratio of around 10:11. The statistics described 2,203 deaths from melanoma, with a male to female ratio of 14:10 (Cancer Research UK, 2012). Estimated prevalence in Europe has described 35 thousand diagnosed cases of melanoma and 9 thousand deaths

caused by melanoma in the year 2000. Furthermore, incidence rates for melanoma are particularly high among European migrants in Australia and non-Māori population in New Zealand, where the annual prevalence appears to be more than double the highest rates registered in Europe [Reviewed in (Boyle et al., 2004)].

1.1.2 Skin Biology and Structure

Adult human skin comprises over 300 million cells in a surface area of 21 square feet. It functions as a barrier by protecting the internal tissues from a variety of environmental insults, such as ultraviolet radiation (UVR), extreme temperatures, toxins and pathogens. Its pivotal functions also include thermoregulation, control of fluid loss, sensation, and immunologic surveillance (Nouri, 2008).

The human skin consists of two mutually dependent layers, the epidermis and the dermis, which rest on a fatty subcutaneous layer called the hypodermis (figure 1.1). The uppermost epidermis comprises mainly layers of keratinocytes scattered with other cell types, such as pigment-containing melanocytes, antigen-processing Langerhans cells, and pressure-sensing Merkel cells. It is separated from the dermis by the basement membrane. The dermis is the underlying layer, which harbours collagen, elastic fibers, blood vessels, sensory structures, and fibroblasts (Nouri, 2008).

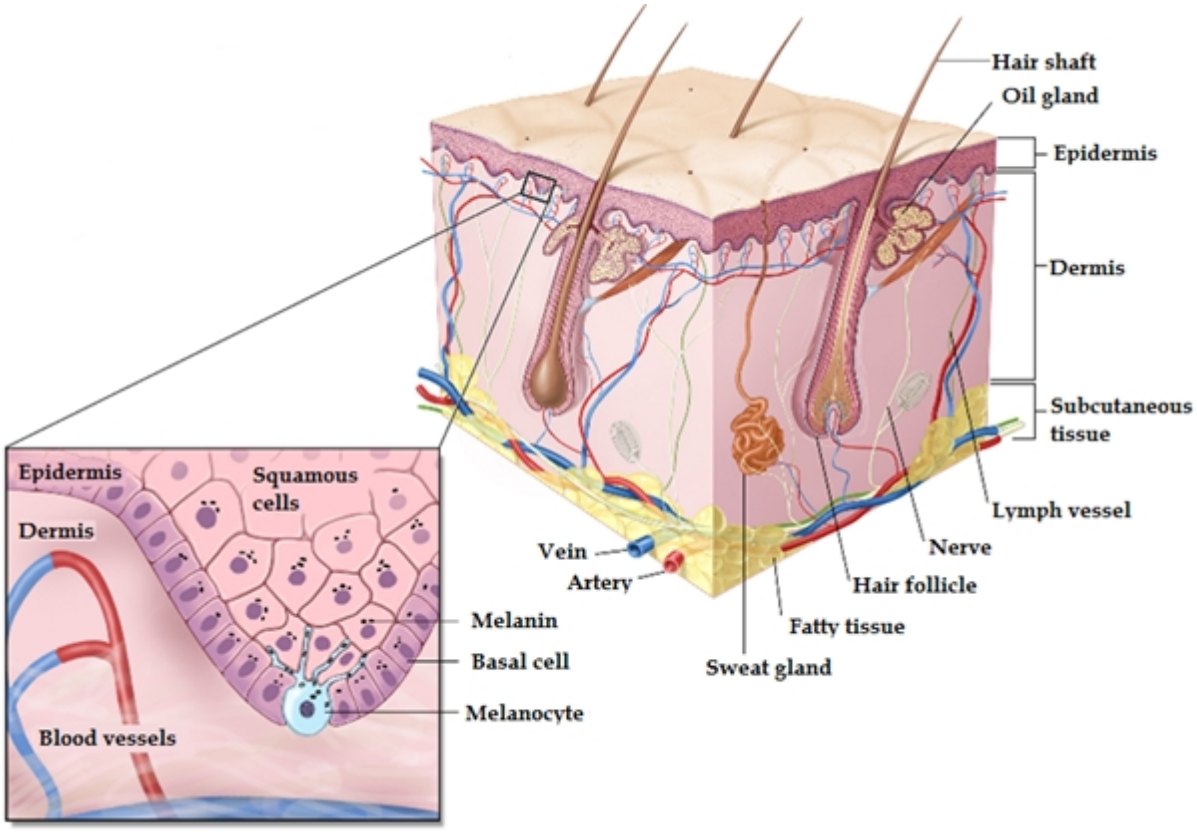

Figure 1.1: Schematic representation of normal skin architecture: The diagram displays the uppermost epidermal layer, the melanocytes that are aligned predominately in the basal layer, and the underlying dermis. Beneath these layers lies the subcutaneous tissue (The University of Chicago Medicine, 2012).

Keratinocytes and melanocytes are the main cell populations that compose the epidermis, and the main constituents that give rise to most skin tumours. For instance, actinic or solar keratoses are premalignant squamoproliferative lesions occurring on chronically sun-exposed areas of the body. These lesions arise from abnormal proliferation with loss of orderly maturation of keratinocytes. Other keratinocytic malignancies also include squamous cell carcinoma, consisting of atypical nests of abnormal squamous cells arising from the epidermis and invading the dermis [Reviewed in (Ricotti et al., 2009)].

Interspersed amongst the basal keratinocytes are the pigment-producing cells or melanocytes. Melanocytes produce melanin pigment as part of a protective mechanism to prevent the ultraviolet injurious effects on skin. However, due to various epidemiological and genetic factors, this complex pigmentary system has many potential sites for dysfunction. In fact, malignant transformation of normal melanocytes leads to progressive alterations of cell phenotype to develop melanoma (figure 1.2) [Reviewed in (Bandarchi et al., 2010)].

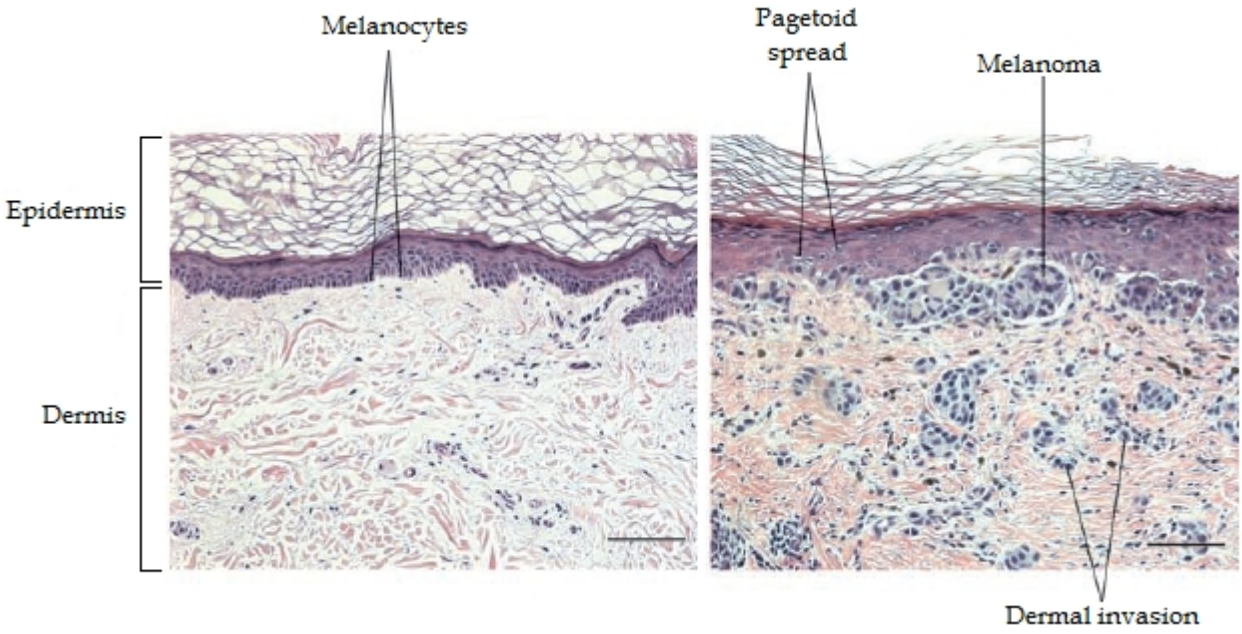

Figure 1.2: Hematoxylin and eosin (H&E) stained histological sections displaying melanocyte transformation progression. H&E staining method combines two dyes; hematoxylin stains the nucleus a shade of blue-purple colour while eosin stains the cytoplasm and connective tissue in varying shades of pink. Left| Normal skin: the melanocytes are evenly dispersed within the basal epithelial layer. Right| VGP malignant melanoma: showing melanoma cells migration into the upper epidermis (pagestoid spread) and penetration through the dermal-epidermal junction. Magnification ×20, scale bar: 20µm (Chudnovsky et al., 2005).

1.1.3 Types of Skin Cancer

Whilst there are several forms, these can be broadly categorised into three pathological types of skin cancer which are the most common. Each of these three cancers arises from different type of cells within the skin and has its own distinctive appearance. They are named after the type of cell from which they are derived from and can be subdivided into two groups: non-melanoma skin cancers and malignant melanoma skin cancers.

1.1.3.1 Non-Melanoma Skin Cancers (NMSCs)

1.1.3.1.1 Basal Cell Carcinoma (BCC):

Basal cell carcinoma (BCC) is a common skin cancer in Caucasian populations (Telfer et al., 2008). It was first described by Arthur Jacob in 1827 as a "rodent ulcer" (Jacob, 1827), and in 1900, Krompecher named it "carcinoma epitheliale adenoides" and described it as a malignant, locally invasive, and destructive cancer (Kasper et al., 2012). Three years later, Krompecher hypothesised that the tumour originated from the undifferentiated cells of the basal layer of the epidermis (Posalaky et al., 1979).

Although it is rarely metastatic, the tumour is malignant and tends to infiltrate tissues in a three-dimensional manner and the growth can be locally invasive leading to destruction particularly on sites of skin that receive the most sun exposure, such as the scalp, face and neck. Clinically, the morphological

appearance manifests itself in many forms and the lesions may be nodular, superficial, pigmented variants, cystic, morphoeic (sclerosing), or keratotic [Reviewed in (Telfer et al., 2008)].

Development of BCC has been strongly correlated with geographic latitude, with the highest incidence reported in Australia. Reports demonstrated high incidence rates in men than those in women aged > 60 (Giles et al., 1988). UV exposure is one the most significant aetiological factors, in which combination of high cumulative UVB exposure in an intermittent pattern together with reduced capacity of skin repair has been reported in the assessed BCC cases (Raasch et al., 1998). In addition to sun-exposed sites, Crowson *et al* reported that lesions can arise in sun-protected skin as well, in which the indolent-growth in these tumours was usually of superficial type (Crowson et al., 1996).

1.1.3.1.2 Squamous Cell Carcinoma (SCC):

Squamous cell carcinomas (SCC) are the second most prevalent keratinocyte-derived type of skin cancer among Caucasians (Goldman, 1998). It can also affect darkly pigmented groups and usually arises on site of pre-existing inflammatory skin conditions, burns, scars, or ulcers [Reviewed in (Diepgen and Mahler, 2002)]. SCCs are more prevalent in geographical locations near the equator, and appear in middle-aged to older individuals and are predominantly found on the head-and-neck region (Anwar et al., 2004).

Several reports associated a wide diversity of histopathological variants of SCCs with different clinical behaviours. For instance, SCCs can range from indolent, locally invasive tumours with low metastatic potential, to rapidly growing with high invasive potential [Reviewed in (Yanofsky et al., 2011)]. Invasive lesions penetrate the basement membrane and may be nodular or plaque-like, display variable keratin production, and occasionally ulcerated (Anwar et al., 2004).

Marks and colleagues reported that the majority of SCCs in light-exposed areas arise from pre-existing actinic keratosis (AK) (Marks et al., 1988). Typical AK lesions are less than 1 cm in diameter and are characterised as scaly or keratotic, ranging from erythematous to pigmented papules with discrete or diffuse borders (Rowert-Huber et al., 2007). Since AK represents the beginning of a continuum that culminates in SCC, Mortier *et al* demonstrated that neoplastic progression of AK to SCC involves a series of molecular changes leading to the inactivation of $p16^{INK4a}$ (Mortier et al., 2002). Clinically, it can be hard to distinguish between AK and SCC as they share many similarities at both molecular and histological levels (Chia et al., 2007).

Chronic exposure to solar UV radiation is the most significant predisposing factor in the development of SCC. UVR acts as a tumour promoter as it initiates carcinogenesis by damaging cellular DNA. In addition, SCC is common in oculocutaneous albinism (OCA) and xeroderma pigmentosum (XP), two conditions that are inherited in an autosomal recessive manner. The inadequate production of melanin pigment in OCA and the defect in excision repair

mechanism for UV-induced pyrimidine dimers in XP result in sever photosensitivity and a greater predisposition to SCC (Goldman, 1998). Other aetiological factors include chronic ulcers, burn scars, human papillomavirus infection, ionising radiation and exposure to chemical carcinogens— such as arsenic and tobacco [Reviewed in (Diepgen and Mahler, 2002)].

1.2. Cutaneous Malignant Melanoma

1.2.1. Epidemiology

Since the early 1960s, the annual incidence rates of melanoma have increased by 3-7% in populations of predominantly European origin (Armstrong and Kricker, 1994), with an estimated doubling of rates every 10 to 20 years (Garbe et al., 2000). In global terms, the highest incidence rates of melanoma have been observed in Australia and New Zealand (Lens and Dawes, 2004). By contrast, these rates are particularly low among indigenous population of Africa, Asia, Latin America, and southern Europe (Pearce et al., 2006). In Australia, CMM is classified as the fourth most common cancer in males and the third most common cancer in females (Lens and Dawes, 2004). In 1999, the incidence of melanoma in the Auckland Caucasian population in New Zealand was documented as the highest in the world, with the crude incidence for invasive CMM of 77,7 new cases per 100,000 population annually (Jones et al., 1999). Moreover, based on the recent cancer statistics presented by the American Cancer Society, there is an

estimate of 70,230 new cases of melanoma per 100,000 among men and women in the United States (Siegel et al., 2011).

1.2.2. History of Melanoma

In Peru, paleopathological findings of several mummies of pre-Colombian Incas, some estimated to be 2400 years old, showed diffuse melanoma metastases in the bones of the skull and extremities as well as rounded melanotic masses in the skin. The first accredited description of melanoma was by Hippocrates in the fifth century BC, followed by the annotation of the Greek physician Rufus Ephesus. However, the medical term "melanoma" was used for the first time in 1838 by Robert Caswell to designate these pigments malignant lesions of the skin. In 1858, Pemberton advocated and performed a radical excision for melanoma (Urteaga and Pack, 1966).

1.2.3. Clinical Subsets of Malignant Melanoma

While more than 95% of tumours arise within epidermal melanocytes, melanoma can also derive from non-cutaneous melanocytes. Sites of primary extra-cutaneous melanoma include ocular, mucosal, gastrointestinal, genitourinary, leptomeninges and lymph nodes (Chin et al., 2006, Markovic et al., 2007). Moreover, melanoma has been classified among the more common causes of 'metastatic cancer of unknown primary' due to its capricious behaviour, reflecting its tendencies to

arise in unexpected sites along the neural crest migratory route, or its aggressive growth of poorly differentiated lesions (Chin et al., 2006).

1.2.3.1 Superficial Spreading Melanoma (SSM):

It is the most common histologic form among Caucasians and accounts for 70% of all human cutaneous melanoma. This neoplasm is common in adults and most frequently appears on the upper back of both men and women as well as on the legs of women [Reviewed in (Volkovova et al., 2012)]. Clinically, it is characterised by an intraepidermal growth that may last 1–5 years before vertical dermal invasion occurs, and frequently the lesions are 2.5cm large by the time of detection (Briele and Das Gupta, 1979). Morphologically, the lesions are arciform in outline and sharply marginated, generally 2–4mm elevated above the surrounding skin. In addition, it is in this type of melanoma that variations in colour— from brown, grey, black, and even violaceous-pink, are noted (Clark et al., 1969).

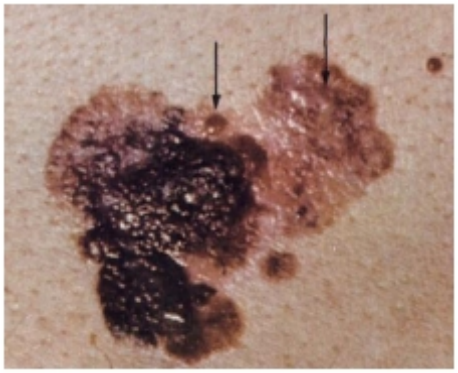

Figure 1.3: Superficial Spreading Melanoma. The picture shows a haphazard combination of the brown and pink-tan colours and two arrows pointing at discrete pink nodules (Clark et al., 1969).

1.2.3.2. Nodular Melanoma (NM):

It is the second most common subtype and accounts for 15–30% of all melanomas [Reviewed in (Volkovova et al., 2012)]. NM tends to affect more men than women, and generally, clinical presentation occurs in the fifth or sixth decade of life. The common locations are the trunk in men and the legs in women (Porras and Cockerell, 1997). This type of neoplasm evolves from an intraepithelial melanocytic proliferation (Porras and Cockerell, 1997), and is uniformly invasive extending to or into the reticular dermis or into the fat (Clark et al., 1969). Morphologically, the lesions are quite distinctive on inspection and are characterised by a relatively uniform, dark, blue-back nodule (Clark et al., 1969).

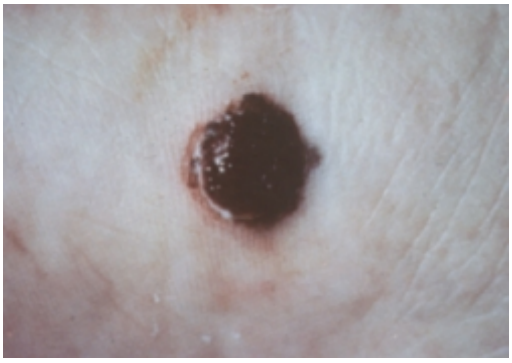

Figure 1.4: Nodular Melanoma. The picture displays a dark brown-black dome-shaped nodule. At the time of diagnosis, the size of the clinical lesion is often small in diameter (Porras and Cockerell, 1997).

1.2.3.3 Lentigo Maligna Melanoma (LMM):

Lentigo maligna melanoma originates from untreated lentigo maligna and accounts for 4–10% of all melanomas [Reviewed in (Volkovova et al., 2012)].

These tumours are characterised by their indolent-growth that may last for 10–25 years before dermal invasion occurs. In addition, they are more common in older individuals— the median age being 70 years (Briele and Das Gupta, 1979). It is occasionally confused with SSM as it shows the same colour variation, though the lesions are irregular in outline, their surface is flat, and primarily show various shades of brown rather than violaceous-pink (Clark et al., 1969). Moreover, the radial intraepidermal growth of these lesions tends to cover the largest surface area of any of the melanomas to grow to a size of 5–7cm (Briele and Das Gupta, 1979).

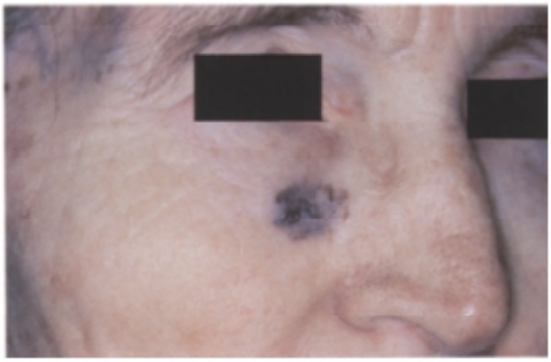

Figure 1.5: Lentigo Maligna Melanoma. This picture represents a flat, asymmetrical lesion on the face of an elderly individual. This large-sized lesion shows a combination of brown shades (Porras and Cockerell, 1997).

1.2.3.4 Acral Lentiginous Melanoma (ALM):

It is the least common form and accounts for 1–7% of all melanoma cases in Caucasians, although incidence seems significantly higher in Chinese, Japanese, Middle Eastern and African. The term was coined by Reed *et al* who described it as 'acral' because of its predilection of distal areas of the body— such as the

palmar and plantar surfaces as well as the subungual areas, and 'lentiginous' because of its distinct radial growth (Bristow and Acland, 2008). These tumours tend to have a prolonged radial growth phase and have tendencies to metastasise to regional lymph nodes, and lesions show variations in colour (Briele and Das Gupta, 1979).

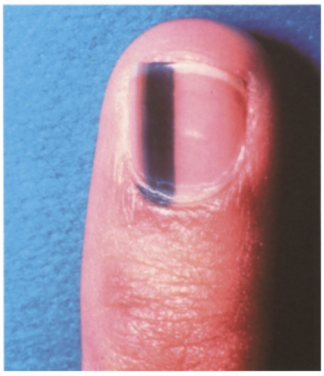

Figure 1.6: Acral Lentiginous Melanoma. The picture shows a dark longitudinal pigmented streak of the nail. The pigmentation in subungual melanomas usually spreads from the nail bed epithelium to the proximal nail fold and cuticle. These melanomas are often mistaken for a hemorrhage subungual hematoma (bruise) (Porras and Cockerell, 1997).

1.2.4 Etiologic and other Risk Factors:

Melanoma is a complex, multifactorial disease that results from the combination of the environmental influences and genetic predisposition. The aetiology of malignant melanoma has not been fully elucidated, however, it has been hypothesised that melanoma develops through divergent etiologic pathways (Cho et al., 2005).

1.2.4.1 Ultraviolet Radiation

Various environmental factors have been hypothesised to be implicated in the increased incidence of melanoma. Of these, the main factor is the increased exposure to UVR, mainly caused by the depletion of the ozone layer, and possibly attributable to behavioural changes— such as the use of sunbeds. We are daily exposed to the UV fraction of the solar radiation, however, the world's highest incidence coincides with proximity to the equator [Reviewed in (Markovic et al., 2007)]. The UVR represents a portion of the electromagnetic energy that acquires both life-giving and life-endangering effects (Hussein, 2005).

Paul Gerson Unna, in 1894, was the first to report the implication of chronic sun exposure in the pathogenesis of skin cancer, however, it was not until the 1930s that UV radiation were documented as a carcinogen (Albert and Ostheimer, 2003). Furthermore, as previously stated, UV increases DNA instability, inhibits antioxidants, and suppresses the immune system. Additionally, intermittent intense exposure to sunlight during childhood is thought to be a significant precursor to adult melanoma [Reviewed in (Sauter and Herlyn, 1998)].

According to the convention of the Commission Internationale de l'Eclairage (1987), the UVR is subdivided into three wavelength regions: UVC (200-290 nm), UVB (290-320 nm), and UVA (320-400 nm). The short waves of UVC radiation are highly mutagenic, however, they are effectively absorbed by the earth's atmosphere, and its role in the pathogenesis of skin cancer is insignificant [Reviewed in (Hussein, 2005)]. Contrariwise, the composition of solar UVR

spectrum that reaches the earth's surface is composed of 95% UVA and 5% UVB (Alapetite et al., 1996).

In human epidermal skin cells, the small amount of UVB is strongly absorbed by DNA, and is considered as the most efficient wavelength for the formation of cyclobutane pyrimidine dimers (CPDs) that leads to thymine dimer (TT) formation (Clingen et al., 1995). These dimers have been described as UVB distinct signature in DNA after they were identified in human melanoma *in situ* after exposure to UVB (Young et al., 1998). Consequently, these dimers not only affect cellular function, but they may also induce immunosuppression, and subsequently lead to tumour formation [Reviewed in (Abdulla et al., 2005)].

Atillasoy and colleagues demonstrated that chronic UVB irradiation can induce human melanocytic lesions, including melanoma. These findings were based on an experimental system that utilised full-thickness human skin — a skin graft containing both the epidermis and the dermis, xenografted to mice with severe combined immunodeficiency disease (SCID). UVB-treated xenografts at 500 J/m^2, which corresponds to approximately 2 MED (human minimal erythemal dose), three times per week, with or without an initiating carcinogen, was sufficient to induce AK and SCC within 7-month treatment/observation period, and malignant melanoma within 10 months (Atillasoy et al., 1998).

In 1989, Setlow *et al* developed a xiphophorus animal model to demonstrate the carcinogenicity of UVB absorbed by melanoma. The hybrid animals developed melanomas after repeated exposures. Although 304 nm was the lowest exposure

that induced melanomas, those wavelengths of 360 nm were also found to be important in inducing tumours (Setlow et al., 1989). The potential photocarcinogenesis of UVA has been demonstrated by Marrot and colleagues who established the induction of DNA breaks in the nucleus of Caucasian human melanocytes with 320 to 400 nm radiation (Marrot et al., 1999). Additionally, Kvam and Tyrell associated UVA exposure of tanned skin with increased mutations in melanocytes after they have demonstrated that human melanoma cells with a high melanin content accumulated larger amounts of premutagenic oxidative DNA base damage after UVA irradiation (Kvam and Tyrrell, 1999).

1.2.4.2. Skin Type

Pigmentary characteristics and host susceptibility have been reported to play a significant role in the aetiology of melanoma. For instance, pigmentary factors, such as eye colour— blue eyes compared to brown, hair colour— blond/red hair colour compared to brown/black, freckling, tendency to develop multiple moles— benign or atypical, sun sensitivity and inability to tan, have all been highly associated with melanoma risk (Titus-Ernstoff et al., 2005).

The variation in melanocortin-1 receptor (*MC1R*) gene, involved in pigmentation, was moderately associated in the increased risk of melanoma carcinogenesis. Although *MC1R* was shown to be a low-penetrance susceptibility locus, a positive association between melanoma and *MC1R* variants was duly noted (Kanetsky et al., 2006).

1.2.4.3. Family History

Patients with a familial predisposition of melanoma have approximately a 2-fold increased risk of melanoma for all body sites, except melanoma on upper extremity that was strongly associated with history of multiple sunburns (Cho et al., 2005). The initial clinical observation of familial melanoma was reported in 1951 by Cawley. The hereditary aetiology was estimated for approximately 10% of all occurrences of melanoma by Anderson in 1971. Subsequently, melanoma susceptibility locus was localised in the chromosomal region 9p21 (Meyer and Zone, 1994).

Clustering of melanoma in families has been highly associated with the presence of abnormal melanocytic naevi or moles, known as atypical mole syndrome (AMS) phenotype, inherited in an autosomal dominant pattern. Reports showed that the majority of susceptible families in the UK suffer from this phenotype, and the approximate lifetime risk is 1 in 20 (Newton, 1994). Although rare, melanoma may also develop in families with high penetrance melanoma susceptibility genes. These inherited mutations were reported in 2% of all melanomas and implicated *CDKN2A* and, rarely, *CDK4* (Thompson et al., 2005).

1.2.4.4 Melanocytic Naevi

Whether acquired, congenital or dysplastic, melanocytic naevus cells can serve as a potential precursor lesion from which melanoma may develop. The histologic presence of melanocytic naevi was found associated with 57.6% of primary SSM

and NM, supporting Clark's hypothesis of tumour progression in the melanocytic system (Sagebiel, 1993). Nevertheless, the presence of multiple naevi, atypical or non-atypical, is a strong marker for melanoma risk irrespective of family history (Thompson et al., 2005).

Several epidemiologic findings have associated the presence of large (particularly >5 mm) or giant naevi (>20 cm) with an elevated melanoma risk. Furthermore, there is a 1.5-fold increased risk in people with 11 to 25 naevi than people with ≤10 naevi, and the risk doubles with every 25 naevi [Reviewed in (Markovic et al., 2007)].

1.2.4.5. Immunosuppression

Interestingly, the immunogenic characteristics of melanoma have been associated with impairment of immune function. A number of reports documented melanoma development in immunodeficiency syndrome and transplant recipients. For instance, Smith and colleagues reported an increase in pigmented lesions in HIV-1-positive patients, clarifying that some of these were malignant melanomas (Smith et al., 1993). Likewise, renal transplantation recipients who receive long-term immunosuppression therapy have a 3.6-fold increased risk of developing melanoma than the general population (Hollenbeak et al., 2005).

1.2.5. Pathogenesis and Prognosis of Melanoma

The ABCD (Asymmetry, Border irregularity, Colour variegation, Diameter >6 mm) acronym is the standard dermoscopic terminology for melanoma screening. Devised in 1985, it has since been universally applied for appraisal of pigmented skin lesions. This acronym has been further expanded to ABCDE (a criterion for Evolving lesions), which encompasses any significant change in size, shape, shades of colour or surface features (Abbasi et al., 2004). Although this system is the main diagnostic criteria, more than 50% of melanomas are *de novo* lesions that may not have any of these characteristics (Testori et al., 2009).

In normal skin, melanocyte growth and behaviour are tightly regulated by epidermal keratinocytes. This homeostasis is exercised through a complex system of paracrine growth factors and cell–cell adhesion molecules. Divergent etiologic factors disrupt this delicate homeostatic balance, resulting in mutations in essential growth regulatory genes, the secretion of autocrine growth factors, and the loss of adhesion molecules. Consequently, this dysregulation triggers a continuous proliferation of the melanocytes, leading to a malignant phenotype (Haass et al., 2004).

In a tissue's architectural context, naevi may be defined as 'junctional'— naevus cell nests scattered at the junction of the epidermis and the underlying dermis, 'dermal'— nests of naevus cells restricted to the dermis, or 'compound'— nests of naevus cells overlapping components of both dermis and epidermis. Melanocytic naevi are commonly benign, but can progress in a radial fashion to

invade the papillary dermis (uppermost layer of the dermis). The radial-growth-phase (RGP) melanoma involves an intra-epidermal lesion that may demonstrate local microinvasion of the dermis, which is considered to be the primary malignant stage. These lesions may acquire metastatic potential and progress to the vertical-growth phase (VGP) to invade deeper into the dermis as tumourigenic nodules (figure 1.7). Nevertheless, not all melanomas behave through each of these individual phases (Gray-Schopfer et al., 2007).

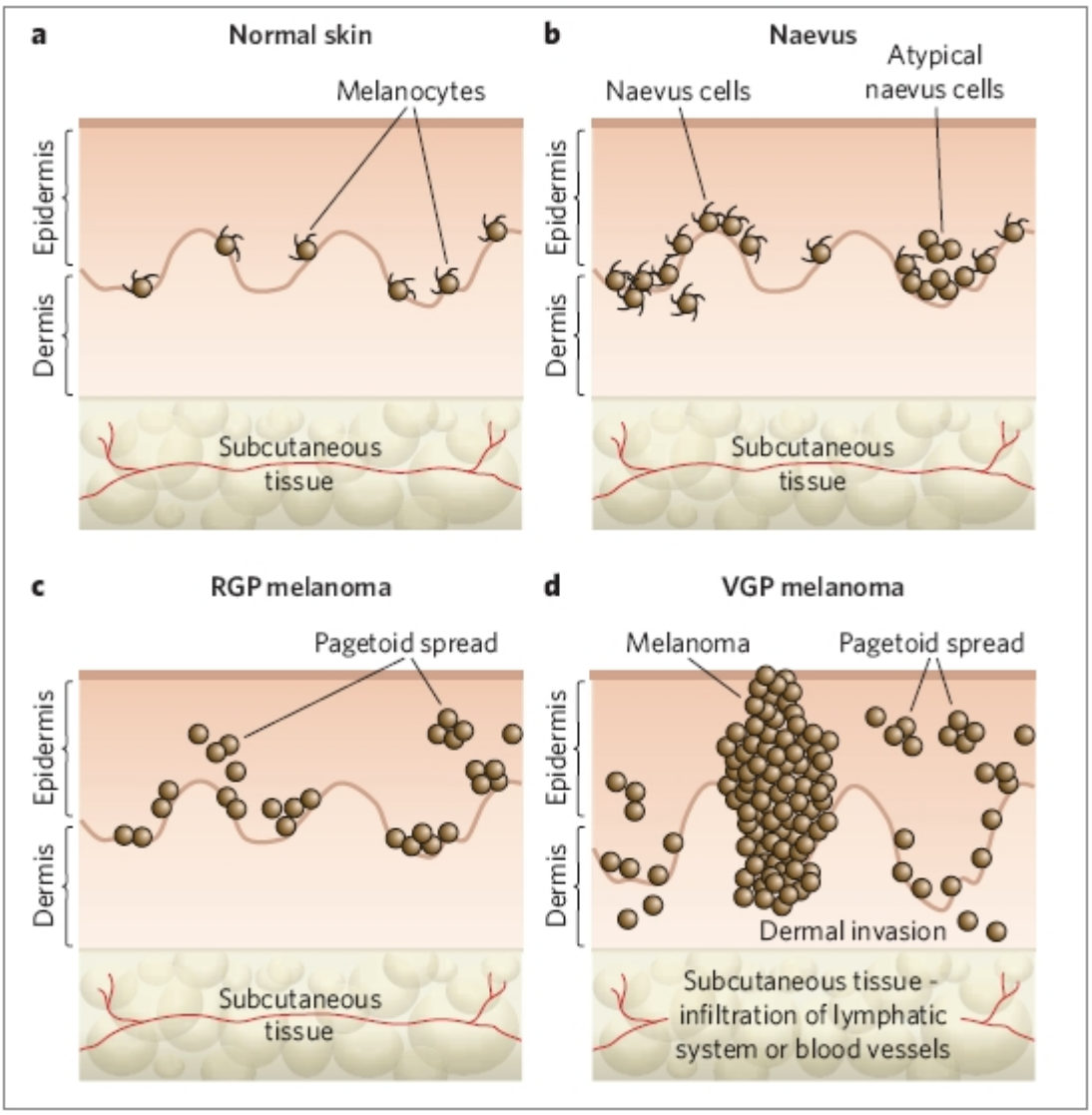

Figure 1.7: Schematic illustration of transformed melanocytes progression. A| Normal skin: showing scattered dendritic melanocytes within the basal layer of the epidermis. B| Naevus: benign melanocytic naevi appear with an increased number of dendritic melanocytes during early stage disease. C| RGP melanoma: primary malignant stage. D| VGP (vertical-growth-phase) melanoma: documented as the deadly stage, in which the lesional cells infiltrate the vascular and lymphatic system (Gray-Schopfer et al., 2007).

In 2001, the American Joint Committee on Cancer (AJCC) designated a staging system for cutaneous melanoma that estimates the survival rates at different stages

based on certain standard criteria (table 1.1). This system mainly used the TNM classification: **T** indicates the size of the primary tumour, **N** indicates number and/or extent of spread to regional lymph nodes, and **M** indicates the presence of metastasis). This staging system was largely based on data collected from melanomas with superficial spreading and nodular growth patterns (Balch et al., 2001).

	5-YEAR SURVIVAL	10-YEAR SURVIVAL
Stage I (primary tumour ≤ 1 mm)	93%	85%
Stage II (primary tumour > 1 mm)	68%	55%
Stage III (regional node metastasis)	45%	36%
Stage IV (systemic metastasis)	11%	6%

Table 1.1: Stage-specific survival estimates for melanoma patients, according to the AJCC staging system. These survival rates are based on the details of 17,600 patients from 13 melanoma treatment centers around the world (Thompson et al., 2005).

This new staging system incorporated major changes and the prognosis mainly depended on the thickness of the primary tumour and the presence or absence of metastasis to regional lymph nodes (Thompson et al., 2005).

The T category thresholds of melanoma were defined as 1.0, 2.0 and 4.0 mm in thickness in patients with stage I disease. Ulceration was frequently observed among patients in stage II disease with tumours > 1 mm in thickness. Prognosis of the N category, for patients with stage III disease, used the number of metastatic lymph nodes rather than their gross dimensions and whether they were

microscopic or macroscopic. In addition, ulceration was also defined as a criterion of this staging. Finally, the presence of an elevated serum lactic dehydrogenase and the site of distant metastases were used for the M category in stage IV disease (Balch et al., 2001).

1.3. Molecular Genetics of Cutaneous Malignant Melanoma

Prevalence differences across ethnic groups may reflect different environmental behaviours; however, the genetic backgrounds play a significant role in melanoma predisposition. The existence of familial clustering in approximately 5–12% of all melanomas, which may affect one or more first degree relatives, suggests the segregation of mutant predisposition alleles (Loo et al., 2005).

Melanoma tumourigenesis is thought to be a long-term multistep accumulation of genetic defects that disrupt normal melanocytic proliferation and differentiation (Morita et al., 1998). Analysis revealed that the earliest genetic alterations in this multistep disease appear to involve mutations in the melanocytes of the melanocytic dysplastic naevi (MDN) involving allelic loss of important tumour suppressor genes— such as *p16*, microsatellite instability (MSI), and alterations of tumour suppressor genes (TSGs) [Reviewed in (Hussein, 2004)].

Karyotypic analysis and cytogenetic studies have indicated allelic deletions at several chromosomes, including 1p, 6q, 9p or 10q, 11q and 17q. Analyses also revealed that the mutation or loss of one or more of the familial susceptibility

genes, located at 1p36, 9p21, and 12q14, which also act as TSGs, may lead to the development of melanoma [Reviewed in (Hussein, 2004)].

1.3.1. Chromosomal Aberrations in Melanoma

Certain combinations of accumulated chromosomal aberrations seem fundamental for the pathogenesis of advanced, metastatic neoplastic disease. The cytogenetic analyses of 158 metastatic malignant melanoma cases revealed clonal structural chromosomal aberrations in 80% of the cases at chromosomes 1, 6, 7, 11, 9 and 3, respectively. Chromosomal aberrations were considered as clonal if observed in at least two metaphases of the same cell line, per ISCN (International Cancer Screening Network) convention. Moreover, analysis of chromosome segment gains and losses showed frequent loss of chromosomes 6, 10 and to an equal extent, involvement of chromosomes 1, 7, and 9, respectively. Based on frequency of chromosome involvement in this study, the authors suggested that structural abnormalities of chromosome 1 and 6 and loss of chromosome 10 are important in the pathogenesis of sporadic advanced melanoma, and supported the linkage of familial melanoma to chromosome 9p (Thompson et al., 1995).

Matsuta and colleagues evaluated chromosomal aberrations in 22 malignant melanomas using the fluorescence *in situ* hybridisation (FISH) with chromosome-specific DNA probes. Quantitative hybridisation signal analysis and histological data revealed the frequent aberrations in chromosomes 6, 7, 9, and 10. Additionally, these analyses also showed gain of chromosomes 6, and 7, and monosomy of chromosomes 9 and 10, emphasising their important roles in the

tumourigenesis and development of malignant melanomas (Matsuta et al., 1997). The table below summarises some of the frequently observed chromosomal aberrations in melanoma tumourigenesis.

CHR	ABERRATIONS	CANDIDATE GENES	INVOLVEMENT
1p	Deletion; translocation; Loss of heterozygosity (LOH)		LOH in advanced melanomas
6q22-27	Deletion most common		40%-75% LOH in late stage Melanomas
7	Amplification	*EGFR*	Increased expression in melanomas; level correlates with aggressiveness
9p21	LOH; deletion; intragenic mutation	*INK4a*	Dysplastic naevus; early melanoma; hereditary predisposition
10q24-26	LOH	*PTEN*	Dysplastic naevus; early Melanoma

Table 1.2: Chromosomal aberrations in cutaneous malignant melanoma. Chromosomal aberrations in 1p36 are commonly reported in early-stage melanoma. Cytogenetic rearrangements spanning 6q22-27 have been observed in both early- and late-stage primary tumours. *EGFR* is frequently overexpressed in association with amplified copies of chromosome 7 in late-stage melanomas. The 9p21 region most commonly harbours homozygous deletions in sporadic cases and both deletions and point mutations in familial cases. LOH and chromosomal rearrangements spanning 10q24-26 have been reported in melanoma, whereby *PTEN* appears to be targeted for loss [Adapted from (Chin et al., 1998)].

1.3.2. Alterations at Chromosome 9p21 in Melanoma

Tumour suppressor genes are pivotal for regulating cellular behaviour and differentiation. Based on the classical 'two hit' hypothesis, the inactivation of a TSG requires two genetic events to lose both alleles of the gene in order to result in the uncontrolled cell growth. Loss of heterozygosity (LOH) at specific regions provided evidence for the presence of these suppressors, which could be caused by chromosomal deletion, mitotic recombination, non-dysjunction, or unbalanced translocation [Reviewed in (Hussein, 2004)].

Historically, Cowan *et al* suggested that deletion of a gene(s) on 9p could be an initial step in the malignant transformation of melanocytes (Cowan et al., 1988). LOH at 9p21 in primary melanomas, prior to the acquisition of metastatic potential, led to suspect the existence of a melanoma TSG in this region (Fountain et al., 1992). In addition, homozygous deletions on 9p21 have been frequently reported in familial melanomas (Cannon-Albright et al., 1992). Cytogenetic studies and molecular analyses of familial and sporadic melanomas presented compelling evidence that loss of suppressors harboured in the chromosomal region 9p21 represents a critical stage in the development of virtually all melanomas (Chin et al., 1998).

1.3.3. Melanoma Susceptibility Genes

The genomic complexity of familial melanoma fuelled considerable attention to study the class of genes involved in the predisposition to melanoma. These studies

have identified the existence of high-penetrance genes as well as low-penetrance genes described below.

1.3.3.1. High-Penetrance Susceptibility Genes

1.3.3.1.1. *CDKN2A* gene [location: 9p21]

Deletion mapping has identified the 9p21-encoded cyclin-dependent kinase inhibitor $p16^{INK4a}$ (*CDKN2A*) as a candidate TSG involved in both sporadic and familial melanomas. This gene was established to be homozygously deleted or frequently carried frameshift, nonsense, or missense mutations in nearly 75% of melanoma cell lines (Kamb et al., 1994).

The *CDKN2A* gene encodes the p16 protein (Kamb et al., 1994), which functions to bind to CKD4 and inhibit the catalytic activity of the CKD4/cyclin D enzymes. In addition, $p16^{INK4}$ may act as a negative regulator of cell proliferation by inhibiting the CDK4-mediated phosphorylation of the retinoblastoma (Rb) protein. Moreover, in cells lacking a functional Rb protein, there is an increased activity of $p16^{INK4}$ with a consequent inhibition of CDK4 (Serrano et al., 1993).

CDKN2A consists of 3 coding exons: exon 1 (E1) containing 125bp, exon 2 (E2) containing 305bp, which have been implicated in mutations, and exon 3 (E3) containing only 12bp (figure 1.8). Hemizygous genetic lesions in either E1 or E2 of *CDKN2* were frequently observed in primary and metastatic melanomas (Kamb et al., 1994). This gene encodes two distinct proteins translated in alternate

reading frames (ARFs), $p16^{INK4A}$ encoded by the alpha transcript— comprising exons 1α, 2, and 3, and the smaller beta transcript— comprising exons 1β, 2 and 3 specifies $p14^{ARF}$.While $p16^{INK4a}$ is central in cell-cycle control by regulating G1-phase, $p14^{ARF}$ acts via the p53 pathway to induce cell-cycle arrest or apoptosis (Kefford et al., 1999).

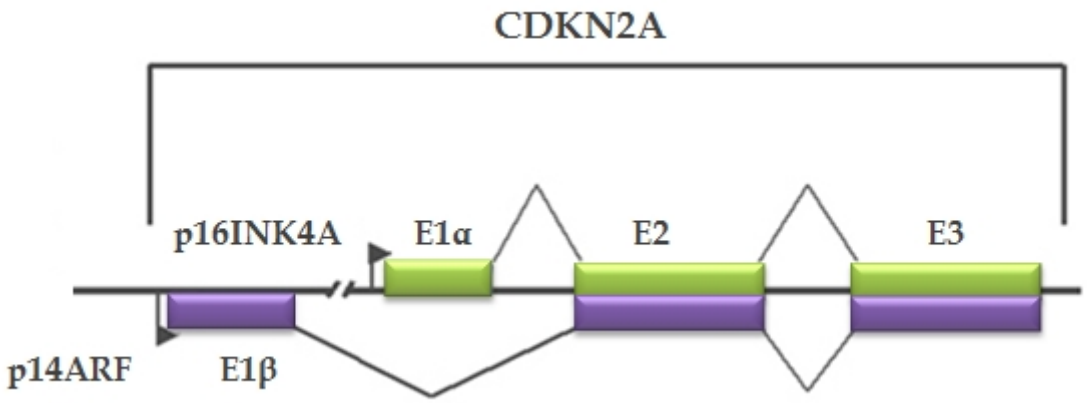

Figure 1.8: Genomic organisation of the CDKN2A locus, which encodes for two transcripts: $p16^{INK4a}$ (exons 1α, 2 and 3), coloured in green, and $p14^{ARF}$ (exons 1β, 2, and exon 3 translated in alternate reading frame), coloured in purple.

An estimate of mutation penetrance in the *CDKN2A* gene showed rates ranging between <5 to >50% of tested melanomas, subject of family and population selection (Bishop et al., 2002). This penetrance could be influenced by birth cohort, levels of sun exposure, and possibly by modified genes, which could cause multiple naevi in certain families (Kefford et al., 1999).

1.3.3.1.2. *CDK4* gene [location: 12q14]

A candidate gene search led to the identification of the second melanoma susceptibility gene, *CDK4* on chromosome 12q14, which acts as an oncogene (Zuo et al., 1996). *CDK4* mutations have been found in few families worldwide. For instance, the first germline mutation, Arg24Cys— resulting in a Cysteine substitution for an Arginine at codon 24, has been cosegregated with melanoma in two unrelated families who do not carry germline $p16^{INK4a}$ mutation. The Arg24Cys germline mutation in the $p16^{INK4a}$-binding site in CDK4 abolishes the binding of these two proteins, hence generating an oncogene that is resistant to normal physiological inhibition by $p16^{INK4a}$ (Zuo et al., 1996). The second germline mutation, Arg24His— Arginine to Histidine substitution, which occurred in the same codon as the first alteration, was reported in only one family (Soufir et al., 1998).

Although *CDK4* mutation penetrance seems low in familial melanoma, these mutations have a similar impact as those in *CDKNA2*. Families who carry *CDK4* mutations share similar phenotypic characteristics, and show high penetrance for melanoma in mutation positive family members [Reviewed in (de Snoo and Hayward, 2005)]. On the other hand, Wolfel and colleagues reported *CDK4* mutations as somatic alterations in two sporadic melanomas, describing that this mutation produced a mutated protein that has functionally prevented binding of the CDK4 protein to $p16^{INK4a}$ (Flores et al., 1997).

1.3.3.1.3. *p14^{ARF}* gene [location: 9p21]

A part of the *CDKNA2* gene is common to another transcript that encodes the human p14^{ARF} protein, with a coding sequence from exons 1β and 2 (Bressac-de-Paillerets et al., 2002). Consequently, point mutations located in exon 2 affect the impairment of p16 and p14^{ARF} proteins concurrently, confounding the role of each gene in melanoma tumourigenesis. Nevertheless, multiple cases of melanoma-prone families reported defects at the *p14^{ARF}* gene exclusively, indicating the fact that ARF locus represents a melanoma susceptibility gene in its own right [Reviewed in (de Snoo and Hayward, 2005)]. In addition, 16bp exon 1β germline insertion, described in a sporadic multiple melanoma case, was shown to specifically altering p14^{ARF}, but not p16^{INK4a}. The mutant protein was functionally impaired and showed loss of growth arrest in a p53 expressing melanoma cell line (Rizos et al., 2001).

1.3.3.2. Low-Penetrance Susceptibility Genes

1.3.3.2.1. *MC1R* gene [location: 16q24]

The melanocortin receptor-1 (*MC1R*) gene, located on chromosome 16q24.3, is one of the common low-penetrance melanoma susceptibility genes. The MC1R is ubiquitously expressed in melanocytes and keratinocytes, and functions as a receptor for alpha-melanocyte stimulating hormone (α-MSH) and adrenocorticotropic hormone (ACTH). The binding of α-MSH and MC1R

stimulates a series of events that result in the production of the brown/black eumelanin. Polymorphisms of the *MC1R* gene could be evolutionarily deleterious, and may result in diminished receptor function, which disequilibrates melanin synthesis from eumelanin to the red-yellow and potentially mutagenic pheomelanin (Stratigos et al., 2006).

In addition to being remarkably polymorphic in Caucasians, several reasons have suggested that human *MC1R* alleles may be associated with increased susceptibility to melanoma (Palmer et al., 2000). To date, three *MC1R* variants alleles also called 'red hair colour' variants, have been shown to be associated with an increased risk of melanoma, and these include Arg151Cys, Arg160Trp, and Asp294His (Stratigos et al., 2006). These variants confer about a 2.2-fold increased risk of CMM in individuals carrying one of these three 'active' variants, and the risk increases for each additional allele carried (Palmer et al., 2000).

1.3.4. A Melanoma Molecular Disease Model

Speculation that melanomas may evolve along the 'naevus' pathway and arise at different anatomical sites dependently/independently of chronic sun-exposure, postulates a 'divergent pathway' model in melanoma epidemiology (Whiteman et al., 1998). Transformation of melanocytes lies at the convergence of activated or abrogated pathways, in which oncogenic signalling network requires cooperation of tumour suppressors (Hocker et al., 2008).

The two main classes of genes that result in cancer when mutations prevent or alter their normal function are oncogenes and tumour suppressor gene. While an oncogene is a normally occurring proto-oncogene that is activated by point mutation or chromosomal rearrangement (i.e. RAS, RAF), a tumour suppressor gene, on the other hand, is a 'cell cycle' control gene that in many instances is inactivated by mutations such as deletion, frameshift, or hypermethylation (i.e. p53, Rb) (Weinberg, 1994).

Oncogenic RAS is the central piece of a complex signalling network that regulates proliferation, survival and invasion and acts through two distinct canonical effector cascades, the RAF-MAPK and the PI3K-AKT signalling streams (figure 1.9). Activating mutations that target one of the two key MAPK pathway genes, BRAF or NRAS, have been found in up to 90% of melanomas and benign melanocytic neoplasms. On the other hand, the PI3K-AKT signalling pathway is aberrantly activated in up to 70% of melanomas through loss or inactivating mutations in PTEN (Phosphatase and Tensin homolog), or though amplification of any PI3K subunit [Reviewed in (Hocker et al., 2008)].

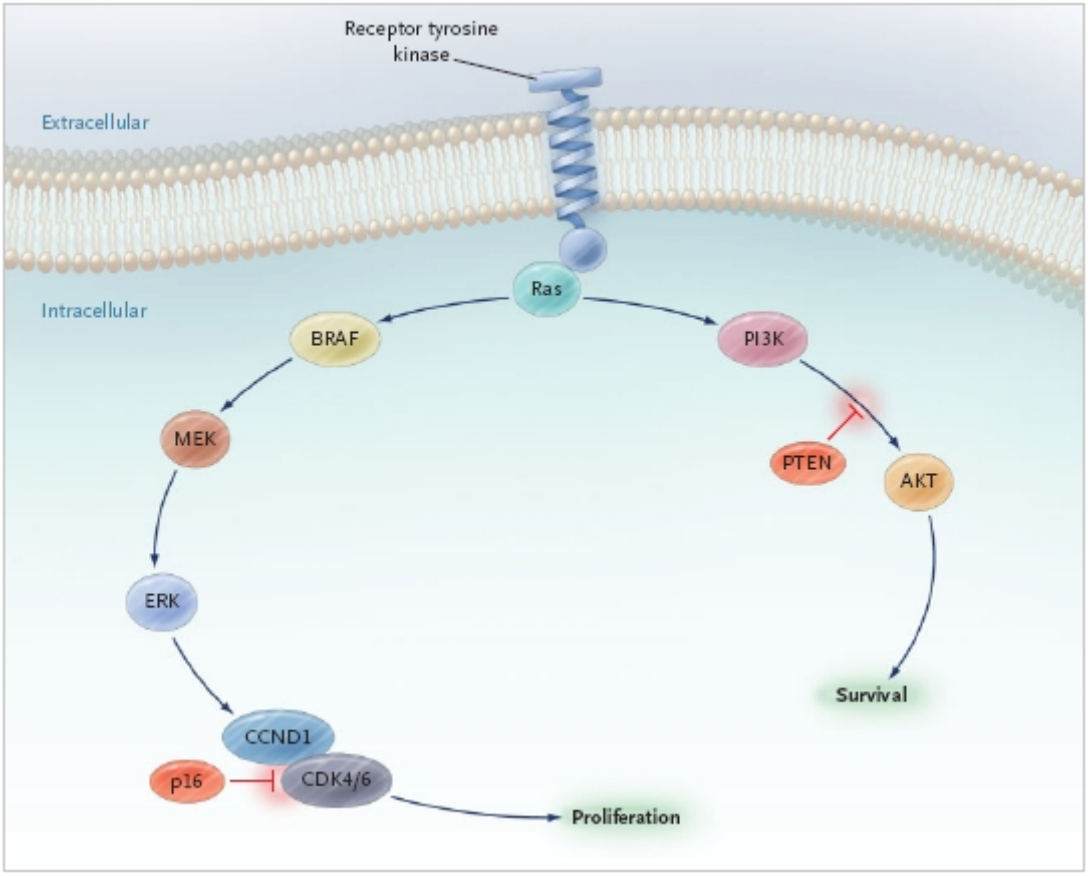

Figure 1.9: A simplified diagram of the fundamental signalling networks involved in melanoma tumourigenesis. Activation of RAS can promote proliferation through the MAPK pathway or survival through the PI3K/AKT pathway (Curtin et al., 2005).

The human RAS family consists of three proto-oncogenes that are located on different chromosomes: the *H-RAS* and *K-RAS* genes are the cellular counterparts of the viral Harvey and Kirsten genes, respectively, and the *N-RAS* gene is derived from a human neuroblastoma cell line (Bar-Sagi, 2001). Activating point mutations in the *N-RAS* gene, mostly at codon 61, have been reported in 56% of congenital naevi from patients with skin types II, III and IV (Papp et al., 1999). Given the closely related functions of NRAS and BRAF in the MAPK pathway,

Pollock and colleagues reported activating mutations in NRAS in 7 of 11 melanoma metastases carrying a wild-type BRAF (Pollock et al., 2003). Activation of senescence, by coexpression of NRAS and BRAF in the same melanoma cells, postulated an epistatic relationship of synthetic lethality between both oncogenes, leading to selection against 'double-mutant' cells (Petti et al., 2006).

A study based on genome-wide mutation detection approach has reported *BRAF* somatic missense mutations in 66% of malignant melanomas and in a number of human carcinomas at a lower frequency. About 80% of the reported changes occurred at a single codon within the kinase domain, precisely in exon 15 at T1796A, resulting to a substitution of valine by glutamic acid at position 599 (V599E) (Davies et al., 2002). This mutation is prevalent in benign naevi, which highlights the role of BRAF activation in the molecular events necessary for melanocytic proliferation (Pollock et al., 2003).

While the RAF-MAPK cascade acts as major stimulus of melanocytic proliferation, the PI3K-AKT cascade acts as a promoter of melanoma progression. RAS binds and activates PI3K, which subsequently activates the pathway's major downstream effector, Akt [Reviewed in (Hocker et al., 2008)]. Deregulated Akt activity has been shown to steadily increase during the progression from benign naevi to primary melanomas, and lastly, to metastatic. In fact, selective activation of Akt3 has been reported in 43 to 60% of sporadic melanomas, resulting from a combination of increased Akt3 expression and decreased PTEN protein activity

due to loss or haploinsufficiency of the *PTEN* gene (Stahl et al., 2004). LOH on chromosome 10q has been reported in 30 to 50% of malignant melanomas. *PTEN* is one of the genes on chromosome 10 whose mutations were reported in approximately 10% of melanomas [Reviewed in (Chudnovsky et al., 2005)]. In addition, PTEN expression has been reported lost or decreased in 15 to 50% of sporadic melanomas even in the absence of intragenic *PTEN* mutation or biallelic deletion. Therefore, an epigenetic mechanism of biallelic functional inactivation or haplotype insufficiency could account for *PTEN* dysfunction (Zhou et al., 2000). Essentially, NRAS activation and PTEN abrogation have been shown to exist in a reciprocal manner and may functionally overlap in at least a subset of cutaneous melanoma (Tsao et al., 2000).

The absence of oncogenic-induced senescence, which is primarily caused by the mutation of tumour suppressors, leaves the mechanisms that mediate senescence unimpeded. Rb (retinoblastoma) and p53 are the two main signalling pathways that characterise senescence and highly targeted in tumours (Collado and Serrano, 2006).

The *CDKN2A* (*INK4A*/*ARF*) locus encodes the $p16^{INK4a}$ and the $p14^{ARF}$ and engages both Rb and p53 anticancer pathways. Deletion of this locus has been reported in approximately 50% of primary tumours and nearly all melanoma cell lines. $p16^{INK4a}$ functions by inhibiting CDK4/6-mediated phosphorylation of the retinoblastoma tumour suppressor protein (pRb). In the hypophosphorylated state, pRb binds and represses E2F transcriptional activity and prevents the progression

through the G1-S junction. Following its localisation to the 9p21 gene, germline *INK4a* point mutations were reported to co-segregate with familial melanoma in some kindreds. On the other hand, $p14^{ARF}$ stabilises p53 by inhibiting its MDM2-mediated ubiquitinylation. Several studies reported germline mutations exclusively affecting $p14^{ARF}$ in familial melanomas [Reviewed in (Sharpless and Chin, 2003)].

Functional alteration of the p16-cyclin D/CDK4-Rb pathway is a common event in melanoma. Interconnection that exists between MAPK and Rb pathways occurs at the level of cyclin D, which functions as a regulatory subunit of CDK4/6, leading to phosphorylation of Rb and promoting entry into mitosis (Sauter et al., 2002). Interestingly, most melanoma cell lines that exhibit *PTEN* alterations, either harbour *p16*/*CDKN2A* or *CDK4* mutations, postulating that insults to both the Rb pathway and the PTEN pathway may contribute to melanoma development (Tsao et al., 1998). Furthermore, the *CD1* gene (*CCND1)* is a crucial component of the CDKs complex and a vital melanoma oncogene. The chromosomal region that encompasses the *CD1* locus demonstrated frequent amplification in acral lentiginous melanomas (44.4%). Remarkably, antisense-mediated knockdown of this gene induced apoptosis *in vitro* and led to significant regression of melanoma xenografts in immunodeficient mice (Sauter et al., 2002).

In a pivotal function study, Chin and colleagues reported that *INK4a*-deficient transgenic mice with melanocyte-specific expression of mutant H-RAS developed multiple cutaneous melanomas after a short latency and with high penetrance.

These mice harboured deletion of the wild-type *INK4a* allele and retained a wild-type *p53* gene with no observed mutation or allelic loss. Unlike most solid tumours, the relative death of *p53* mutations in melanoma postulated a possible functional overlap in tumour suppressor activity between *p53* and *INK4a*, given that the latter is a constituent of the former's anticancer pathway. The reciprocity between p53 and $p19^{ARF}$ ($p14^{ARF}$ in human) suggested that *INK4a* is a tumour suppressor gene that is strongly implicated in the genesis of melanoma, and that its loss requires concomitant activation of RAS in order to accelerate melanoma development (Chin et al., 1997).

1.4. Treatment of Cutaneous Malignant Melanoma

1.4.1. Surgical Treatment

The gold standard treatment in primary melanoma is to achieve a complete surgical resection of the tumour with margins of normal-appearing skin (Brenner and Tamir, 2002). As previously mentioned, the first surgical dissection for melanoma was performed in 1858 by Pemberton, who carried a wide excision below the underlying fascia with the removal of the implicated lymph nodes by groin dissection (Urteaga and Pack, 1966).

The current established surgical management of primary melanoma consists of excision and primary closure. It involves a diagnostic biopsy of 2 mm margin and a small amount of the underlying subcutaneous tissue. However, larger lesions (>3cm on body or >2cm on face) require a full-thickness incisional biopsy by

removing a small amount of the skin containing both the epidermis and the whole thickness of the dermis with some of the subcutaneous fat. The appropriate surgical excision is based on tumour thickness and vary from 0.5 cm for melanoma *in situ* to 2 cm margin in melanomas >2 mm. In fact, the depth of excision in all surgical trials of primary melanoma has always been to the muscle fascia, which is the recommended deep margin for eliminating any suspicious melanoma lesions. Moreover, sentinel lymph node (SLN) biopsy provides accurate staging information for patients with primary melanoma ≥1.0 mm thick and without distant metastases, or ulcerated melanomas (Testori et al., 2009).

Surgical curative treatment in melanoma is subjected to a high tendency for local, regional or distant recurrence [Reviewed in (Cobben et al., 2002)]. The phenomenon of metastatic relapse after surgical treatment of the primary lesion may take more than a decade to arise, and could be the behavioural consequence of the same quiescent cancer-initiating cell that derives cancer progression (Schlaak et al., 2012).

1.4.2. Adjuvant Therapies

Given that melanomas are prone to metastasise and the limited therapeutic options for inoperable advanced melanomas have forced the development of more adjuvant therapeutic approaches (Garbe et al., 2008). Previously, numerous randomised and nonrandomised studies have tested a range of adjuvant regimens including chemotherapy, high dose chemotherapy, isolated limb perfusion (ILP),

immunotherapy, combination chemo-immunotherapy, and radiotherapy. The agents that have been assessed include non-specific immunotherapy with levamisole, Bacillus Calmette-Guerin (BCG), megestrol acetate (Megace), transfer factor (TF), and vitamin A; however, these regimens were unequivocally unbeneficial [Reviewed in (Molife and Hancock, 2002)].

Despite inadequate response rates of 15%, which are generally incomplete and endure only a few months, Dacarbazine (DTIC) is the standard therapy for metastatic melanoma (Augustine et al., 2009). As an alkylating agent, DTIC exerts cytotoxic effects by causing DNA intrastrand cross-links. After metabolic activation, its primary mechanism of action is cell disruption by attacking DNA, causing nucleic acid alkylation ―adding an alkyl group, and hence triggering apoptosis. In addition, DTIC is a cycle-nonspecific agent, affecting melanoma cells during more than one cell-cycle, therefore preventing multiplication of rapidly growing cancer cells. However, its efficiency varies in different kinds of melanoma cells, limiting success in the treatment of melanoma (Olszewska-Slonina et al., 2005). Subsequently, Temozolomide (TMZ) was designed as a second-generation alkylating chemotherapeutic agent, however, response rates of only 13% are achieved (Augustine et al., 2009). Therefore, treatment for this group of patients required more robust curative strategies.

Ipilimumab, a monoclonal antibody directed against cytotoxic T lymphocyte-associated antigen 4 (CTLA-4) on lymphocytes, was shown to improve overall survival in patients with metastatic melanoma when used as a monotherapy in

phase II studies, as well as when combined with other agents— such as dacarbazine or Interleukin 2 (Hodi et al., 2010). On the other hand, trials on carriers of the BRAF V600E mutation have recently showed improved rates of overall and progression-free survival with the discovery of the single-agent vemurafenib, which specifically targets the V600E mutation in patients with metastatic melanoma (Chapman et al., 2011). Nonetheless, these regimens were not designed for the entire patient group due to lack of the V600E mutation, and were associated with adverse events such as toxicity and development of resistance (Engesaeter et al., 2012).

Recently, an open-label study— in which both the researchers and the patients are aware of the drug being administered, involving 247 patients, with metastatic BRAF V600 melanoma, evaluated the efficacy of a combination regimen of the BRAF-inhibitor dabrafenib and the MEK-inhibitor trametinib. The combination therapy significantly improved median progression-free survival, which was 9.4 months, as compared with 5.8 months in dabrafenib monotherapy. In addition, the combination regimen showed greater extent of tumour regression with a response rate of 76%, as compared with 54% with monotherapy regimen. Moreover, proliferative skin lesions such as cutaneous squamous-cell carcinomas, papillomas, and hyperkeratosis were commonly observed with dabrafenib monotherapy, and less frequently with the combination regimen. However, frequent adverse events were observed in patients receiving combination therapy than those in the monotherapy regimen, and that included pyrexia, fatigue, nausea, vomiting, and diarrhoea. Together, the use of MEK-inhibitor in this trial

corroborated a possible strategy to delay/suppress mechanisms of resistance in melanoma (Flaherty et al., 2012).

Observations through prospective randomised studies have shown a significant therapeutic advantage of interferon alpha (IFN-α), not only for prolonging the recurrence-free survival interval but also for total survival, wherein the risk of death was reduced by 3% after 5 year from the time of IFN administration [Reviewed in (Garbe et al., 2008)]. A meta-analysis of 14 randomised control trials (RCTs), which involved 8122 patients with high-risk cutaneous melanoma, demonstrated a statistically significant benefit of IFN-α adjuvant treatment in both disease-free survival and overall survival, with relative risk reductions of 18% and 11%, respectively (Mocellin et al., 2010). Despite the controversy on its therapeutic efficacy, a one year high-dose adjuvant IFN therapy is approved by the Food and Drug Administration (FDA) in the United States and proposed in European countries for resected melanoma at high recurrence (Grob et al., 2012).

1.5. Interferon in Human Malignant Melanoma

Karyotypic analysis of cultured melanocytes from a variety of congenital to increasingly malignant melanocytic lesions reported the loss of one copy of chromosome 9 or the loss of 9pter-p22 chromosomal region. Based on these findings and previous reports, the authors hypothesised that loss of an allele from 9p is central in the transformation of melanocytes, mapping the possible candidate genes to the interferon loci (Cowan et al., 1988). Conversely, Petty and colleagues

reported that melanoma predisposition gene locus neighbours the IFNA-D9S126 clustering (Petty et al., 1993). Further refinement of the putative TSG(s) suggested that the clustering of 31% of melanoma cases with LOH at IFNA indicated that interferon-α loci presumably harbour candidate suppressors, describing it as a 'hot spot' and a potential boundary marker of TSGs (Hussein et al., 2002).

1.5.1. Characterisation of the Type 1 Interferon Gene

The human type I interferons consist of one IFN-β and multiple IFN-α subtypes, as well as -ω and -κ subtypes. These cytokines are distinguished by their pleiotropic properties that confer capacity to exert physiological and pathological roles in infections and cancer. In fact, these characteristics made them useful therapeutic agents in clinical medicine today. The type I IFN gene cluster encompasses a region of 400kb on the short arm of *Homo sapiens* (HAS) chromosome 9p21, consisting of 26 genes— 13 *IFNAs*, a single *IFNB* and *IFNW*, and 11 *IFN* pseudogenes (Hardy et al., 2004).

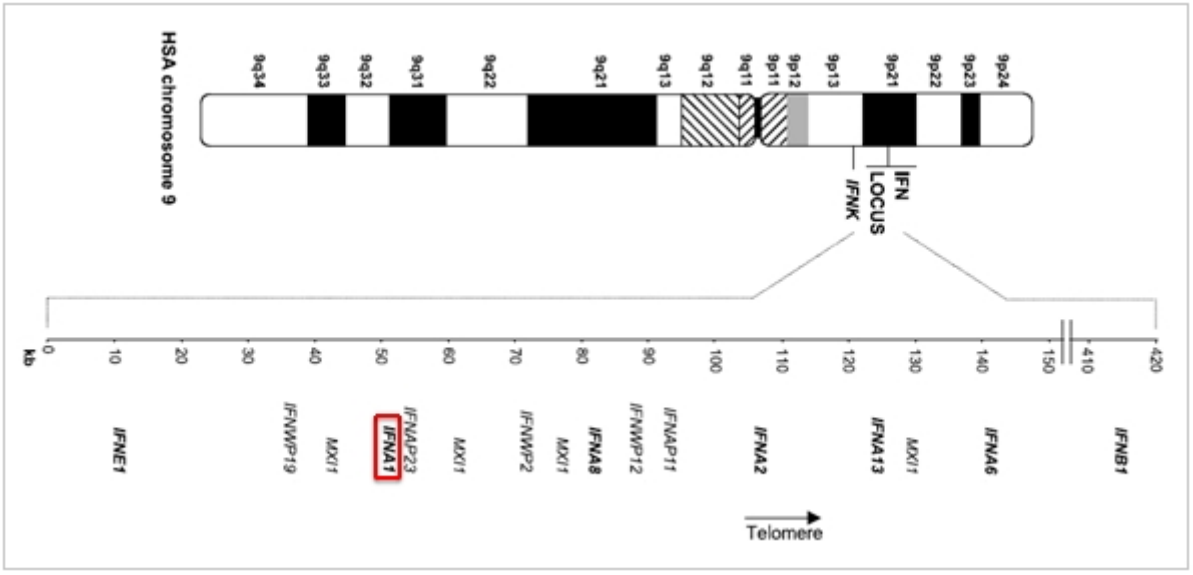

Figure 1.10: Schematic illustration of HAS chromosome 9 with an enlarged exemplification, depicting type I IFN locus genes. This schema shows the type I *IFN* genes— centromeric *IFNA1* and *IFNA8*; telomeric *IFNA2*, *IFNA6*, *IFNA13*, and *IFNB1*. Additionally, there are five α and ω *IFN* pseudogenes— *IFNAP11*, *IFNAP23*, *IFNWP2*, *IFNWP12*, and *IFNWP19*. This predicted human gene designated *MXI1*, a most possibly pseudogene, which was repeated four times throughout the cluster, as well as *IFNE1* (Hardy et al., 2004).

1.5.2. Biological Effects of Interferons

The interferons are named after their 'interference' with an antiviral activity (Pestka et al., 1987). These cytokines are endowed with compelling biological effects on cells, exerting immunomodulatory, antiproliferative, pro-apoptotic, antiangiogenic and antitumoural activities [Reviewed in (Ferrantini and Belardelli, 2000)]. To date, empirical research on the IFN-α subset has revealed its prominence in the promotion of T cells *in vivo* proliferation and survival, and monocytes differentiation into dendritic cells along with enhancing the latter's

activities. These immunomodulatory effects have been employed to apply IFN-α as a designated candidate for therapeutic efficacy *in vivo* (Arico et al., 2011).

Historically, to investigate the antitumour effects of these cytokines, a mixture of virus-induced α/β interferons was used for the treatment of mice inoculated with either IFN-sensitive or IFN-resistant syngeneic tumour cells. However, the molecular mechanisms by which interferon acts remains unclear. In the 1990s, manipulating the antitumour response through *in vitro* gene transfer was considered as an attractive prospect to generate a more effective cell-based cancer vaccine by inserting cytokine genes into tumour cells [Reviewed in (Ferrantini et al., 2007)].

1.5.3. Efficacy of IFNs in the Treatment of Melanoma

Bart and colleagues have previously demonstrated encouraging *in vitro* antitumoural effectiveness of IFN-α in murine B16 melanoma cell line, causing moderate inhibition of cell multiplication (Bart et al., 1980). The use of interferon as adjuvant treatment for high-risk melanoma is controversial in terms of therapeutic efficacy. Although some research groups stated that high-dose interferon-α for high-risk resected melanoma patients is unrivalled when compared with other adjuvant treatments, others incontrovertibly discouraged its clinical use (Wheatley et al., 2002). Despite the conflicting opinions, the FDA has previously approved high-dose IFNα-2b (HDI) adjuvant treatment for patients with stage IIB-III melanoma, as well as the recent PEGylated IFNα-2b (PEG-

IFN)— a covalent conjugate of recombinant IFNα-2b with monomethoxy polyethylene glycol (PEG), for the adjuvant treatment of stage IIIA-C melanoma with microscopic or gross nodal involvement (Rubin et al., 2012).

In the recent meta-analysis by Mocellin *et al*, dose regimens of adjuvant IFN-α varied from high dose [20 MU/m2], intermediate dose [10 MU/m2], to low dose [1–3 MU/m2]. This analysis indicated statistically significant improvement in both disease-free survival and overall survival, though no optimal IFN-α dose and/or treatment duration could be identified. Regarding the use of PEG-IFN therapy on the other hand, a recent randomised study compared the efficiency and safety of adjuvant low-dose PEG-IFN intended for 36 months and standard European low-dose IFN therapy for 18 months in an intermediate-risk melanoma population without clinically detectable nodes. The trial did not reveal superiority for prolonged adjuvant PEG-IFN over standard low-dose IFN therapy. Moreover, PEG-IFN was associated with higher rates of toxicity (47.3% versus 25.2%) and discontinuations (54.3% versus 30.4%) compared with IFN (Grob et al., 2012).

RESEARCH AIM AND OBJECTIVES

In order to provide new therapeutic targets for the treatment of advanced melanoma, it is essential to derive a full genetic model of the disease. Dissecting the genetic heterogeneity and performing comprehensive genomic characterisation will certainly aid to reveal the existence of many yet to be identified tumour suppressor genes in CMM.

Previous investigation provided evidence for the presence of additional TSG(s) on 9p that function independently of the *INK4* locus, spanning between markers D9S171 (9p21) to IFNA (9p22) (Parris et al., 1999). To examine the activity of these loci, Dr. Lylia Ouboussad, former PhD student, introduced A9HyTK9a— a variant of chromosome 9 deleted for the *INK4* locus only, into the highly tumourigenic melanoma cell line UACC-903 by microcell mediated chromosome transfer. In her study, the constructed hybrids were assessed for tumourigenicity *in vitro* by anchorage-independent growth, whereby a category of hybrids demonstrated growth suppression in soft agar (suppressors) and the other one did not **(**segregants). Gene expression of a panel of functional genes in chromosome 9p21 region was carried out by RT-PCR, followed by real-time PCR analysis. The results demonstrated significantly high expression of *IFNA1* in "suppressed" compared to "segregant" hybrids (p <0.05 students unpaired t-test) suggesting that the deletion of *IFNA1* gene might be associated with a loss of tumour suppressor activity.

The hypothesis of my research is that *IFNA1* has a tumour suppressor function and for further functional validation, I tried to investigate such tumour-suppressive activity in melanoma; therefore, the aims of this project were as follows:

1. Subcloning IFNA1 cDNA from pCR®4-TOPO® cloning vector into pcDNA3 expression vector.
2. Establish a panel of stably *IFNA1*-expressing clones.
3. Assess their tumourigenic behaviour by anchorage-independent growth in soft agar.
4. Evaluate IFNA1 expression at both post-transcriptional and translational levels.
5. Given that melanomas are highly resistant to apoptosis, I also investigated whether *IFNA1* could sensitize this resistance.

CHAPTER 2

GENERAL MATERIALS AND METHODS

2.1. Cell Lines

UACC-903: Highly tumourigenic human malignant melanoma cell line, a kind gift from Dr. J. M. Trent, National Cancer Institute, Bethesda, MD (Trent et al., 1990), was derived from a primary melanoma specimen and displays anchorage-independent growth and rapid population doubling in plastic culture. It is deleted for exons 1α and 2 of the *p16* (Parris et al., 1999), and harbours the $BRAF^{V600E}$ mutation (Esteve-Puig et al., 2009). Given that it is deleted for the *p16*, UACC-903 was an ideal model for this study to assess possible antitumour role of *IFNA1* independently of the *p16*.

Culture medium: RPMI-1640 (Sigma-Aldrich)

PC-3: Epithelial cell line from a human prostatic adenocarcinoma (Kaighn et al., 1979), which was used as a tumourigenic control in this study.

Culture medium: Ham's F12K (Gibco, Invitrogen).

NB1-Tert: This cell line was established by transfecting NB1 normal fibroblast cells with human telomerase transcriptase (hTERT) (Ulus-Senguloglu et al., 2012). hTERT-immortalised cells tend to have a relatively 'normal' phenotype. Following their immortalisation, primary human cells retain their diploid karyotype, contact-inhibition, anchorage dependency, and require growth factors for proliferation. Aside from their unlimited lifespan, they are genomically stable, remain differentiated, possess normal cell cycle checkpoints, and express functional p53, pRB, and $p16^{INK4a}$ (Lee et al., 2004). Hence, hTERT efficiently extends the cells' lifespan without changing their normal phenotypic characteristics, which makes the NB1-Tert a relatively normal cell line and an ideal control for this study.

Culture medium: Dulbecco's Modified Eagle Medium (DMEM) (Gibco, Invitrogen).

2.2. General Cell Culture Equipment

All cell culture was performed in LaminAir Class II (Heraeus Instruments) safety cabinet that had been cleaned by swabbing with 70% industrial methylated sprit (IMS) before and after any cell manipulation. Cells were cultured in fully humidified incubators (Heraeus 6000, Heraeus Instruments, Germany) that were set at either 5% or 10% and at 37°C. An inverted phase contrast microscope, Olympus CK40, was used for visualising the cells.

2.3. Cell Culture

Cells were cultured in growth medium supplemented with 10% foetal bovine serum (Gibco, Invitrogen) and 2 mM of L-Glutamine (Gibco, Invitrogen). At each subculture, the cell monolayer was washed with pre-warmed versene (0.2mg/ml EDTA in phosphate-buffered saline (PBS) (Sigma Chemicals, Dorset, UK)) and gently detached by incubation in 1 ml of 0.25% trypsin-EDTA (Sigma-Aldrich) for 1-2 minutes. To neutralize the trypsin, the cells were resuspended in 9 ml of pre-warmed complete growth medium. The cell suspension was then transferred into a 15 ml conical tube (Sarstedt) and spun down in a centrifuge (Megafuge 1.0, Heraeus Instruments) at 1200rpm for 5 minutes— the relationship between revolutions per minute (RPM) and relative centrifugal force (RCF) or g-force (×g) is: $RCF = 1.118 \times 10^{-5} \times R \times N^2$ where R is the radius of the rotor in centimetres, and N is the speed in RPM (Kahn et al., 1976). After centrifugation, the supernatant was aspirated and the cells were resuspended in 10 ml of complete growth medium and subcultured in 1:3 or 1:4 at a seeding density of 5×10^5 to 1×10^6 cells/ml to reach confluence within 48 to 72 hours.

2.4. Cryopreservation of cells

Healthy log phase cells were fed with fresh medium one day before freezing them down. On the following day, the cells were visualised under an inverted microscope in order to confirm the absence of contamination and to assess cell density. After detaching, spinning down the cells and aspirating off the

supernatant, the cell pellet was gently flicked and resuspended in freezing medium consisting of 90% of foetal bovine serum (Gibco, Invitrogen) and 10% DMSO (Dimethyl Sulfoxide) (Fisher). Aliquots of 0.5 or 1.0 ml of cells were transferred into cryogenic vials (Sarstedt) and kept in a Nalge Nunc Cooler filled with isopropyl alcohol for 24 hours prior to storing them in liquid nitrogen.

2.5. Recovery of Cells from Cryopreservation

Vials of cells were recovered from liquid nitrogen and swabbed with 70% IMS. Prior to thawing the cells at 37°C, caps were loosened to release the pressure. Cells were transferred into 10 ml of pre-warmed complete growth medium and centrifuged at 1200rpm for 5 minutes. The supernatant was aspirated off and the pellet was gently flicked and resuspended in the appropriate volume of complete medium. After 24 hours, complete growth medium was replenished to remove any residual DMSO.

2.6. RNA Extraction Using Trizol® Reagent

TRIzol (Invitrogen) is a ready-to-use reagent for isolating total RNA from cells and tissues. The reagent combines phenol and guanidine isothiocyanate in a monophasic solution that maintains the integrity of RNA while disrupting cells and dissolving cell components during sample homogenisation or lysis.

2.6.1. Cell Homogenisation

Monolayer of cells at 80-90% confluence was washed twice with 10 ml of cold PBS. Two millilitres of TRIzol reagent (Invitrogen) was added and left for at least 1 minute at room temperature. The cell lysate was gently retropipetted for homogenisation, transferred into a 1.5 ml sterile Eppendorf tube and incubated for 5 minutes at room temperature to allow the complete dissociation of the nucleoprotein complex.

2.6.2. Phase Separation

After incubating the homogenised samples, 200µl of chloroform (per ml of initial TRIzol) was added to the samples and the tubes were shaken vigorously for at least 15 seconds. The samples were then incubated for 3 minutes at room temperature prior to spinning them at 13000rpm for 30min at 4°C in a bench centrifuge (Eppendorf centrifuge 5414R). Following centrifugation, the mixture is separated into a clear upper aqueous phase that contains RNA, and lower red phenol/chloroform phase.

2.6.3. RNA Precipitation, Wash and Redissolving

The aqueous phase was carefully pipetted into a sterile Eppendorf tube. A total of 500µl of isopropyl alcohol was added to each sample and mixed gently for 15 seconds prior to incubation for 10 minutes at room temperature. Samples were

centrifuged at 13000rpm for 20 minutes at 4°C. After the centrifugation, the RNA precipitate formed a gel-like pellet on the side and bottom of the tube. The supernatant was decanted and the RNA pellets were washed with 1 ml of 75% ethanol, per ml of initial TRIzol. The samples were mixed by vortexing for 5 to 10 seconds prior to centrifugation at 8000rpm for 5 minutes at 4°C. The ethanol was decanted and the RNA pellets were air-dried at room temperature for 5 to 10 minutes. RNA was dissolved in 20µl of diethyl pyrocarbonate (DEPC)-treated water (Fisher Scientific) and incubated at 55 to 60°C for 10 minutes the stored at –80°C.

2.6.4. Quality Control

RNA concentration and purity was determined by spectrophotometry using NanoDrop 2000c spectrophotometer (Thermo Fisher Scientific, Wilmington, USA). UV absorbance was measured at 260ηm and the quality was determined by using A_{260}/A_{280} ratio.

2.7. Standard Polymerase Chain Reaction (PCR)

PCR is an enzyme-mediated-reaction that enables selective amplification of a specific DNA sequence. A basic PCR set up requires DNA polymerase, a DNA template to be amplified, and a designed pair of primers of approximately 20 bases that are complementary to the template in 5' to 3' direction in order to initiate the synthesis of the new DNA strands.

The basis of PCR amplification of DNA consists of a series of 20 to 40 repeated cycles of three temperature dependent steps, which can sometimes be preceded by a hot start step if the polymerase requires thermoactivation, thereby avoiding nonspecific amplification products resulting from mispriming. Elevated temperature (>90°C) is held anywhere between 1 to 10 minutes.

Initially, the denaturation of DNA, which consists of heating the reaction to >90°C for 20 to 40 seconds, separates the double strands by disrupting the hydrogen bonds between the complementary bases. In the next step, DNA annealing, the primers are allowed to anneal to the DNA template. However, an optimisation must be performed to find the correct annealing for each primer set and to reduce any unspecific binding, such as primer dimer. Note also, that during this step the temperature is usually lowered to 50-65°C for 20 to 40 seconds. This is followed by the extension/elongation step at 72°C for 30 to 40 seconds, in which the DNA polymerase synthesises a new complementary DNA strand to the DNA template. A final extension is given at 72°C for 5 to 10 minutes to ensure the completion of any truncated products.

2.8. Agarose Gel Electrophoresis

Agarose gel electrophoresis is a method used to separate negatively charged DNA or RNA fragments by forcing them to move through a gel matrix in response to an electric current. These fragments are separated by size with the smaller ones migrating faster and farther through the pores of the gel.

The preparation of 1% horizontal agarose gel consisted of dissolving 1g of agarose (Fisher Scientific) in 100 ml of 1X TBE buffer (Tris/Borate/EDTA) (Fisher Scientific), and heated in a microwave for 2 to 3 minutes until the agarose has completely dissolved and formed a transparent homogenised mixture. After cooling the latter, 5µl of EtBr (10 mg/ml) was added— EtBr is the most commonly used dye to visualise DNA and RNA in gels during exposure to the UV light. After gently swirling the mixture, it was poured into a casting tray (Bio-Rad) containing sample combs and allowed to solidify at room temperature. The solidified gel was then submerged in TBE/EtBr buffer until the level was about 5mm above the surface of the gel and the combs were carefully removed. About 5–8µl of 1 Kb plus ladder (1µg/µl) (Invitrogen) was loaded to estimate the molecular weight of the samples. The test samples were mixed with the appropriate amount of 6X loading buffer (Thermo Scientific) —containing orange G dye for visual tracking of DNA migration during electrophoresis, and slowly loaded into each well. Electrophoresis was carried out at 60 to 70 Volts until the fastest dye had moved ¾ of the gel length. Upon completion, gels were visualised under a UV transilluminator which causes EtBr bound to DNA to fluoresce, and pictures were taken using an Alpha Imager 2200 (Alpha Innotech Corporation).

2.9 Statistical Analysis

Statistical analyses were carried out using Microsoft Excel 2010 software. All *t*-tests were done at 95 percent significance with α set at 0.05.

CHAPTER 3

SUBCLONING AND CHARACTERISATION OF *IFNA1* GENE

3.1. INTRODUCTION

To evaluate the anti-tumourigenic effect(s) of *IFNA1* in human melanoma, IFNA1 cDNA fragment of 691bp in size was subcloned into pcDNA3 expression vector at EcoRI restriction site, under the control of cytomegalovirus (CMV) promoter. The expression of this plasmid construct was assessed in UACC-903 cell line to further assess its tumourigenic behaviour by anchorage independent growth in soft agar and evaluate its expression at post-transcriptional and translational levels.

DNA cloning is the process of generating multiple copies of a particular sequence of DNA by inserting it into a plasmid vector. These plasmids are double-stranded molecules that carry a cloning site, a drug-resistance gene, and a replication origin within bacterial cells that have been specifically constructed for recombinant cloning technology. Their frequent use in modern recombinant DNA methods is due to the fact that they can propagate and are inherited autonomously of the bacterial chromosome (Lodish H, 2000).

To assess the tumour suppressor potential of any gene, it is essential to be able to control its expression before any further manipulations. pcDNA3 is a 5.4 kb expression vector (figure 3.1) that utilises a CMV promoter, which drives high transcriptional activity of the gene of interest in transfected cells. This expression vector harbours multiple cloning sites located downstream of the CMV promoter, ampicillin and neomycin resistance genes, and an SV40 (Simian Virus 40) early promoter — providing neomycin resistance gene expression for selecting stably transfected mammalian cells using G418 (Mammalian Expression Vectors Guide, Invitrogen).

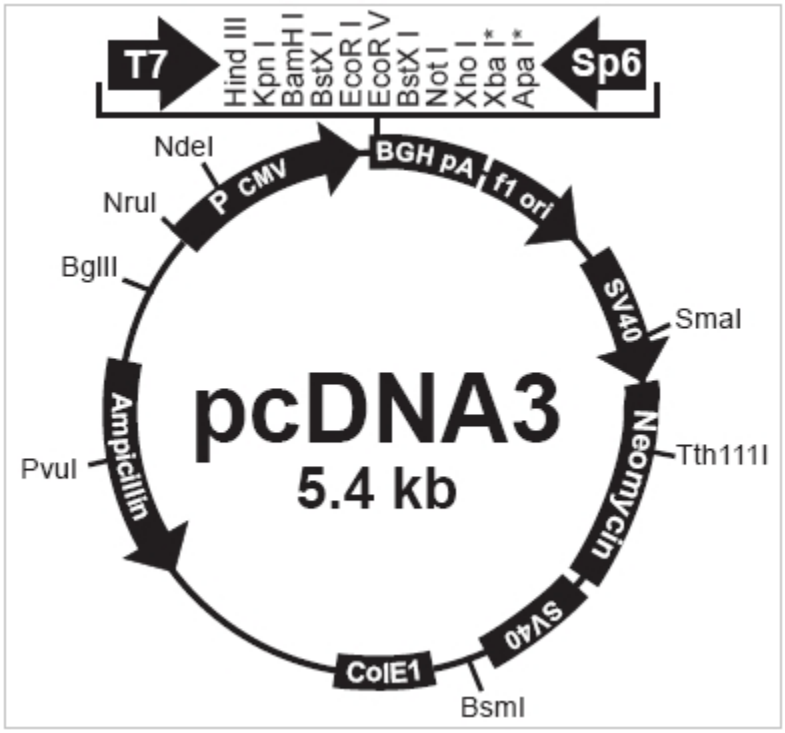

Figure 3.1: Schematic representation of the pcDNA3 expression vector. The diagram displays the multiple cloning sites located downstream of the CMV promoter, the different restriction enzyme sites (such as EcoRI, Hind III, SmaI, etc), as well as ampicillin and neomycin resistance genes (www.invitrogen.com).

The notion of IFN-α antiproliferative and pro-apoptotic effects has had a big impact in the treatment of advanced melanoma. This cytokine can directly inhibit the proliferation of tumour cells by delaying their progression through the S and into the G2/M phases. Moreover, high concentrations of IFN-α in the microenvironment have been demonstrated to induce apoptosis, however, this effect seems transient and greatly depends on cell sensitivity to the expression of interferon alpha receptor and genes. Although IFN-α antitumour effects have been widely documented, the precise mechanisms that trigger and potentiate this behaviour are yet to be defined (Maellaro et al., 2003).

3.2. MATERIALS AND METHODS

From our previous research study, conducted by Dr. Lylia Ouboussad, IFNA1 PCR product was directly inserted into a sequencing vector using the TOPO TA cloning® kit (Invitrogen, UK) (figure 3.2). Formerly, PCR product, resulting from the amplification of IFNA1 cDNA, was ligated into pCR®4-TOPO® cloning vector. Transformation in competent *E.coli* cells resulted in 8 colonies that have had their plasmid DNA isolated and purified using Miniprep kit (Qiagen). To confirm the presence of IFNA1, all 8 DNA plasmid products were treated with EcoRI and their sequencing (Cogenics, UK) revealed that clone number 3 displays 100% similarity to *IFNA1* gene. Subsequently, clone number 3 has been used for the current study.

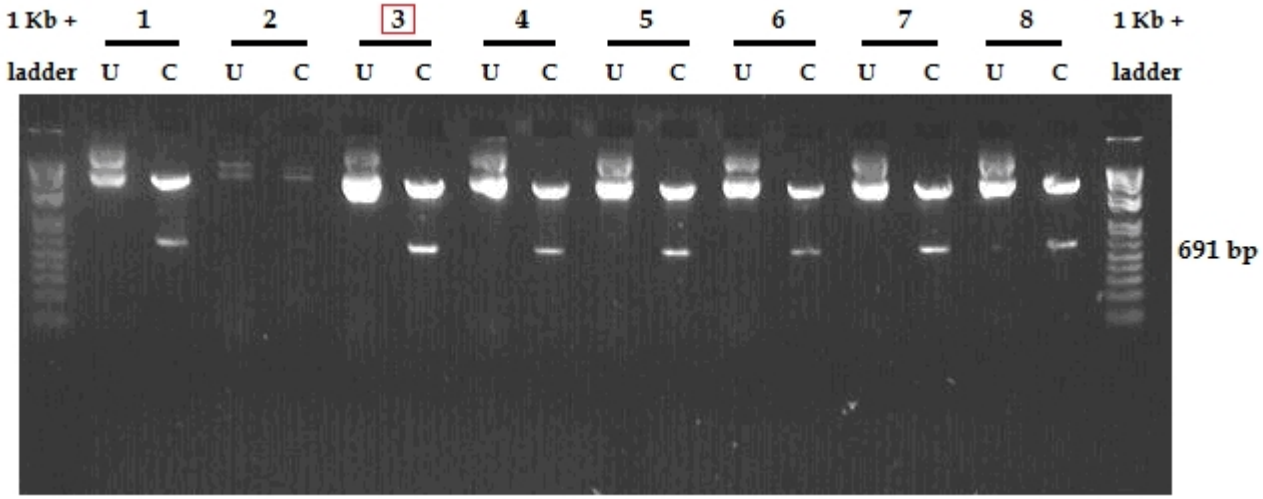

Figure 3.2: Agarose gel image of plasmid cDNA treated with ECORI enzyme. U (Uncut) are the control samples, where no enzyme was added, and C (Cut) are the cDNA samples digested with EcoRI resulting in 2 bands: the upper one corresponds to plasmid DNA and the bottom one to IFNA1 cDNA with a size of 691 bp. A 1 Kb+ ladder was used to determine the size of the insert.

3.2.1. EcoRI Restriction Enzyme Digestion

In order to release IFNA1 from the pCR®4-TOPO® cloning vector, 2µl of EcoRI restriction enzyme (10 units/ µl) (New England Biolabs) was used to digest 10µl of plasmid DNA in a total volume of 50µl including 5µl of 10X restriction buffer (New England Biolabs) and 33µl of DEPC treated water. The reaction was incubated at 37°C for 2 hours and the final product was electrophoresed on a 1% EtBr-stained agarose gel. The size of the digests was determined by using 1 Kb plus ladder (Invitrogen, UK) as shown in the figure below.

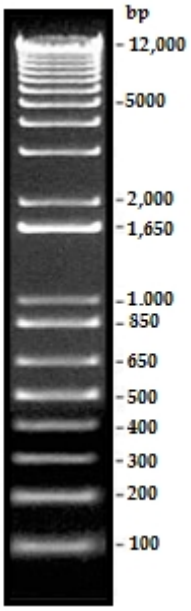

Figure 3.3: 1 KB plus ladder is used to estimate the molecular weight of double-stranded DNA fragments from 100bp to 12 kb (http://www.lifetechnologies.com)

Preparation of 1% TBE agarose gel, containing EtBr at a final concentration of 0.5µg/ ml, was carried out by loading the digested DNA sample, which contained 7µl of 6X loading buffer. Electrophoresis was carried out at 35 volts for 45

minutes. Subsequently, the final product was visualised under a UV illuminator and a picture (figure 3.3) was taken by Alpha Imager 2200 (Alpha Innotech Corporation, USA).

3.2.2. Geneclean– Purifying DNA Fragments from TBE Agarose Gel

GENECLEAN® Kit III (Qbiogene) was used to purify the band of interest by excising the lower band of approximately 691bp from the former agarose gel. The DNA band was excised with a sterile scalpel blade using long wavelength UV light (362ηm) and placed into a tube. To the excised gel slice, 50µl of TBE modifier, which facilitates dissolving the gel, and 450µl of NaI solution were added to the tube. The agarose blocks were completely dissolved by incubation in a 55°C water bath for 5 minutes while frequently flicking the contents gently. Once dissolved, 10µl of GLASSMILK® was added to the DNA/NaI solution. The sample was gently vortexed and incubated for 5 minutes at room temperature with gentle mixing every 1 minute to ensure that GLASSMILK® stays in suspension. The sample was then centrifuged at 14000×g for 30 seconds. Once centrifuged, the supernatant was discarded and the GLASSMILK®/DNA pellet was washed 3× by adding 250µl of NEW Wash solution, followed by vortexing and brief centrifugation. The pellet was air-dried at room temperature and re-suspended in 15µl of dH_2O. The DNA was eluted from the GLASSMILK® by gentle vortexing and centrifugation at 14000×g for 30 seconds. Finally, the supernatant containing the eluted DNA was carefully removed and transferred into a new tube, and stored at -20°C until further manipulations.

3.2.3. Preparation of LB Agar Plates

Luria-Bertani (LB) agar plates were prepared by weighing out 10g of bacto tryptone, 5g of bacto yeast extract, 10g of sodium chloride, and 15g of bacto agar. These reagents were dissolved in 950 ml of distilled water and autoclaved at 121°C for 20 minutes. After allowing the agar to equilibrate in a water bath at 55°C, 100µg of ampicillin per ml of agar solution was added. The agar solution was poured into 100-mm petri dishes (Corning, Fisher Scientific) and the top of each plate was flamed with a Bunsen burner to prevent the development of bubbles on the surface of the agar. Each plate was partially covered with its lid and allowed to set for 30 minutes at room temperature. Finally, the plates were wrapped and stored at 4°C for no longer than one month.

3.2.4. Ligation of cDNA into Expression Vector and Transformation

3.2.4.1. Preparative Restriction Enzyme Digests

For further cloning steps, pcDNA3 vector was linearized in a final volume of 20µl containing 3µl of pcDNA3 (1µg/ µl), 2µl of 10X restriction buffer, 1µl of EcoRI and 14µl of DEPC treated water.

3.2.4.2. Ligation of Plasmid Vector and Insert

IFNA1 cDNA was cloned into the linearized pcDNA3 vector. A ligation reaction was set up in a final volume of 20µl using T4 DNA ligase (New England

Biolabs). The reaction consisted of 1µl of 150ηg plasmid vector, 10µl of purified DNA (29.2ηg/µl), 2µl of 10X buffer (New England Biolabs), 1µl of T4 DNA ligase (0.4 unit/ µl), and finally 6µl of DEPC treated water was added to make up the final volume to 20µl. The contents were briefly centrifuged and incubated at room temperature for 10 minutes prior to incubation overnight at 4°C.

3.2.4.3. Transformation of Competent *E.coli* (DH5α) cells

A total of 2µl ligation reaction was taken and added into 50µl of competent *E.coli* cells (DH5α) (Invitrogen) that were previously thawed on ice. The contents were flicked gently and the tube was placed on ice for 30 minutes. Heat-shock was carried out in a water bath at 42°C for 45 seconds, and then the tube was immediately placed on ice for 2 minutes. Prior to incubation, 900µl of pre-warmed SOC medium (Super Optimal broth with Catabolic repressor) (Invitrogen) was added to the mixture and the tube was placed horizontally in a rotary shaking incubator at 37°C for 1 hour at 225rpm. Cells were spread on LB agar plates with 100µg/ml ampicillin by using the L-shaped plastic spreader. Once dried, plates were inverted and placed in a 37°C incubator overnight. The colonies were observed on the following day and a total of 12 individual colonies were picked and inoculated in 5 ml of LB medium containing 100µg/ml ampicillin (selective LB medium). An additional control tube that does not contain cells was used to confirm the absence of contamination. The tubes were incubated overnight at 37°C with shaking at 225rpm. On the following day, the bacterial cultures became very turbid except the control tube. These cultures were re-inoculated by

diluting 1ml of the starter culture in 500mL of selective LB medium and further incubated overnight at 37°C with shaking at 225rpm. Aliquots of each clone were stored at -80°C by taking 750µl of bacterial culture into an Eppendorf tube and adding 250µl of warm glycerol (Sigma-Aldrich).

QIAGEN® plasmid Midi purification kit, purchased from QIAGEN, was used to extract and purify plasmid DNA from the overnight cultures of the selected colonies.

3.2.4.3.1. Harvesting and lysis of bacterial cells

The 500mL overnight cultures were harvested by centrifugation in Sigma 6K10 centrifuge at 6000×g for 15 minutes at 4°C. After removing the supernatant, the pellet was homogeneously re-suspended in 4ml of re-suspension buffer P1 (50 mM Tris·Cl; pH 8.0; 10 mM EDTA, 100 µg/ml RNase A).

After harvesting and re-suspension, the bacterial cells were lysed in 4 ml of lysis buffer P2 (200 mM NaOH; 1% SDS (w/v), in which NaOH lysis the cells and SDS solubilises phospholipids and DNA as well as proteins. The contents were mixed thoroughly by vigorously inverting the capped tubes 5 times and were then incubated for 5 minutes at room temperature.

3.2.4.3.2. Neutralisation and clearing of lysates

The lysed cells were then neutralised by adding 4ml of chilled neutralisation buffer P3 (3.0 M potassium acetate; pH 5.5) and were immediately mixed by inverting the tubes until the solution was homogeneous, and were incubated on ice

for 15 minutes. The lysates were centrifuged at 16000 ×g for 30 minutes at 4°C. The supernatant containing plasmid DNA was transferred to a sterile tube and re-centrifuged for 15 minutes. The clear supernatant was transferred to a new tube

3.2.4.3.3. Bind, wash and elute plasmid DNA on QIAGEN-tip

The QIAGEN-tip 100 was equilibrated by applying 4 ml of buffer QBT (750 mM NaCl; 50 mM MOPS, pH 7.0; 15% isopropanol (v/v); 0.15% Triton® X-100 (v/v)) and allowed to drain into a waste tube by gravity flow. The supernatant containing plasmid DNA was applied to the equilibrated QIAGEN-tip and allowed to enter the resin by gravity flow. After discarding the flow-through, the QIAGEN-tip was washed twice with 10ml of buffer QC (1.0 M NaCl; 50 mM MOPS, pH 7.0; 15% isopropanol (v/v)) by allowing the buffer to move through by gravity flow. After discarding the flow-through, the DNA was eluted with 5ml of elution buffer QF (1.25 M NaCl; 50 mM Tris·Cl, pH 8.5; 15% isopropanol (v/v)) into a clean 15ml vessel.

3.2.4.3.4. Precipitating, washing and re-dissolving plasmid DNA

The DNA was precipitated by adding 3.5ml of room-temperature isopropanol to the eluted DNA, followed by centrifugation at 16,000 ×g for 30 minutes in 4°C. Once centrifuged, the supernatant was carefully discarded, and the DNA pellet was washed with 2ml of room-temperature 70% ethanol to remove any precipitated salt. Another centrifugation was carried out for 10 minutes at 16,000 ×g. The supernatant was carefully discarded and the pellet was air-dried for 5

minutes. The purified plasmid DNA was re-dissolved in 250µl of TE buffer (10 mM Tris·Cl, pH 8.0; 1 mM EDTA) and was then stored at -20°C.

3.2.4.4. Isolating Colonies with Construct Plasmid

Having a large number of colonies in which some of them are likely to harbour the plasmid with the insert and some might contain the re-ligated plasmid only, it was important to conduct a simplified and rapid protocol for screening the bacterial colonies with cloned constructs by digesting them with EcoRI. Restriction digests were set up in a total volume of 20µl by using 5µl of each plasmid DNA, 1µl EcoRI, 2µl 10X buffer, and 12µl of DEPC treated water. A total of 24 samples have been run on a 1% agarose gel electrophoresis to confirm the EcoRI treatment, in which 12 of them consisted of 2µl of uncut (undigested) plasmid DNA, 2µl of 6X buffer and 4µl DEPC treated water; the other 12 consisted of 2µl cut (digested) DNA, 5µl 6X buffer and 2µl DEPC treated water. Plasmids were then electrophoresed on a 1% agarose gel and visualised using Alpha Imager (figure 3.4).

To confirm the presence and the right insertion of the fragment of interest, an aliquot of 100ηg/µl of the positive clone and the sequencing primers were sent to Cogenics (Essex, UK). The sequencing primers consisted of CMV forward 5'CGCAAATGGGCGGTAGGCGTG (Invitrogen) and IFNA1 reverse 5'ATGAAAGCGTGACCTGGTGT (Invitrogen).

The following is the FASTA sequence of IFNA1, downloaded from National Center for Biotechnology Information (NCBI reference sequence: NM_024013.2), showing the IFNA1 reverse primer.

AGAACCTAGAGCCCAAGGTTCAGAGTCACCCATCTCAGCAAGCCCAGAAGTATCTGCAAT
ATCTACGATGGCCTCGCCCTTTGCTTTACTGATGGTCCTGGTGGTGCTCAGCTGCAAGTCAA
GCTGCTCTCTGGGCTGTGATCTCCCTGAGACCCACAGCCTGGATAACAGGAGGACCTTGAT
GCTCCTGGCACAAATGAGCAGAATCTCTCCTTCCTCCTGTCTGATGGACAGACATGACTTT
GGATTTCCCCAGGAGGAGTTTGATGGCAACCAGTTCCAGAAGGCTCCAGCCATCTCTGTCC
TCCATGAGCTGATCCAGCAGATCTTCAACCTCTTTACCACAAAAGATTCATCTGCTGCTTG
GGATGAGGACCTCCTAGACAAATTCTGCACCGAACTCTACCAGCAGCTGAATGACTTGGA
AGCCTGTGTGATGCAGGAGGAGAGGGTGGGAGAAACTCCCCTGATGAATGCGGACTCCAT
CTTGGCTGTGAAGAAATACTTCCGAAGAATCACTCTCTATCTGACAGAGAAGAAATACAG
CCCTTGTGCCTGGGAGGTTGTCAGAGCAGAAATCATGAGATCCCTCTCTTTATCAACAAAC
TTGCAAGAAAGATTAAGGAGGAAGGAATAACATCTGGTCCAACATGAAAACAATTCTTAT
TGACTCATACACCAGGTCACGCTTTCATGAATTCTGTCATTTCAAAGACTCTCACCCCTG
3’-TGTGGTCCAGTGCGAAAGTA-5’ IFNA1 Reverse
CTATAACTATGACCATGCTGATAAACTGATTTATCTATTTAAATATTTATTTAACTATTCAT
AAGATTTAAATTATTTTTGTTCATATAACGTCATGTGCACCTTTACACTGTGGTTAGTGTAA
TAAAACATGTTCCTTATATTTACTC

3.3. RESULTS

The GENECLEAN procedure was successfully prepared by formerly electrophoresing the digested DNA fragment. The band of interest was carefully excised from the gel as small as possible, and the DNA was finally eluted for further use.

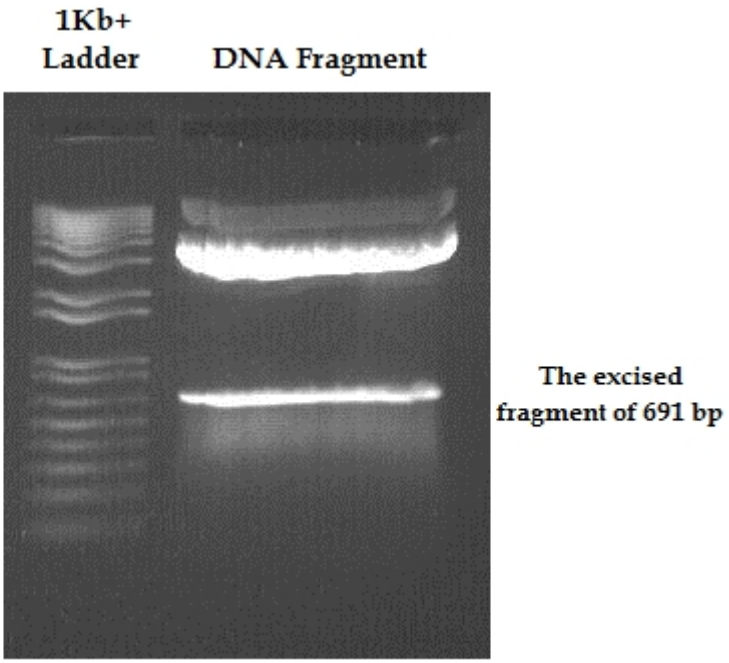

Figure 3.4: A picture of 1% agarose gel showing the treated plasmid DNA with EcoRI restriction enzyme. This plasmid was electrophoresed for 45 minutes at 35 volts. The upper band corresponds to the plasmid vector, whereas the lower one corresponds to IFNA1 cDNA with a size of 691 bp. The latter was carefully excised and eluted using GENECLEAN®

EcoRI digestion of the 12 isolated colonies has been performed to verify which of the latter has the band of interest. From the 12 plasmids, the IFNA1 cDNA of 691bp was exclusively seen in clone number 1 as displayed below. The other 11 plasmid digests did not display a lower band, signifying that the insertion was unsuccessful.

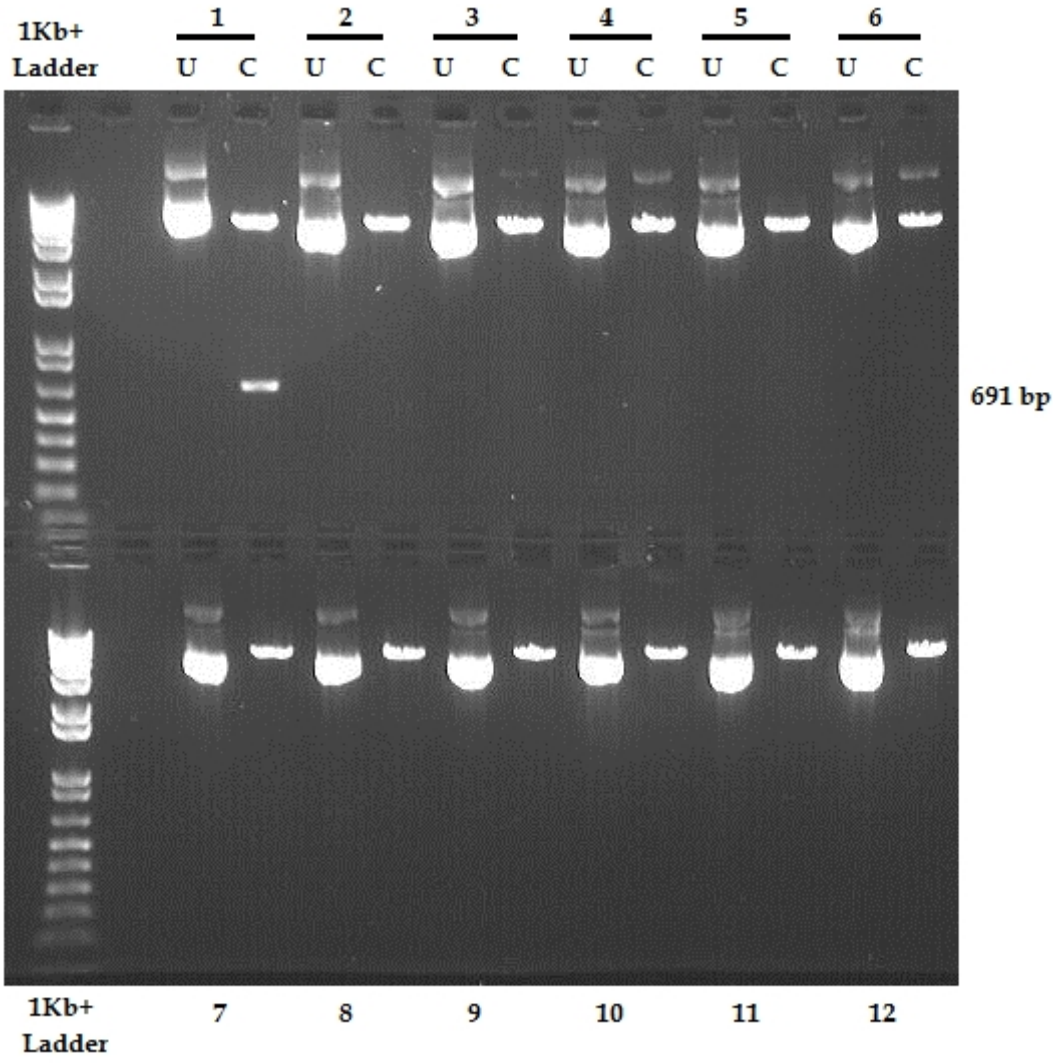

Figure 3.5: A picture of 1% agarose gel showing the 12 treated colonies with EcoRI. The gel was run for 35 minutes at 60 volts. U| uncut or control samples where no enzyme was added; C| cut or digested DNA plasmids with EcoRI. The upper band corresponds to the plasmid vector and the lower one to IFNA1 cDNA with a size of 691bp.

The sequencing results from Cogenics, which have been analysed using SnapGene viewer (figure 3.6), showed a 100% compatibility of the sequence (clone number 1) to *IFNA1* gene. This indicates the absence of mutations in the

sequence and that the PCR product was ligated into the pcDNA3 expression vector in the correct orientation.

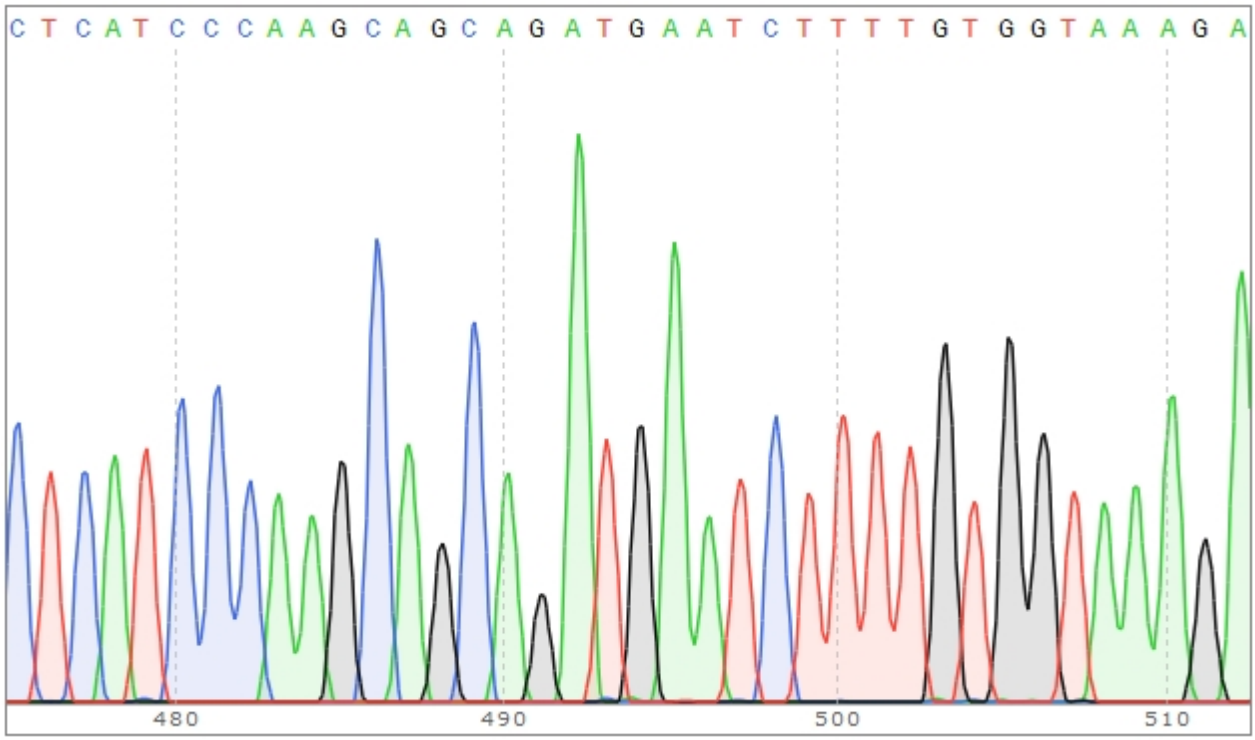

Figure 3.6: SnapGene analysis of IFNA1 cDNA sequencing. The picture illustrates a region of the sequenced IFNA1 in the pcDNA3 expression vector. The analysis generated a four-colour chromatogram— blue, black, green, red peaks in sequences indicate C, G, A and T bases, respectively. The nucleotide peaks seem evenly-spaced and vary in height. The real peaks are easily distinguished from the baseline noise peaks, which seem very minimal. In addition, sequence analysis of the clone revealed a full length IFNA1 cDNA without errors, hence, a fully functional pcDNA3-IFNA1 expression construct.

3.4. DISCUSSION

Our previous research group study pursued the identification of novel TSG(s) in melanoma and has provided experimental evidence that supports the candidacy of *IFNA1* as a tumour suppressor gene. The basic logic behind any genetic manipulation is to assess the expression of the gene of interest. Accordingly, the first step toward compiling sufficient data to validate this hypothesis was to be able to express this gene in melanoma cells.

IFNA1 PCR product that was previously cloned into pCR®4-TOPO® cloning vector has been subcloned into pcDNA3 expression vector. Initially, after digestion with EcoRI, IFNA1 PCR product was isolated from a 1% agarose gel using the GENECLEAN kit. As depicted in figure 3.4, the gel displays three bands. The high-molecular-weight band, which appears faint, could be the result of nicked or relaxed circular plasmid DNA that has not been completely digested. The second band represents the supercoiled plasmid, linearized by EcoRI digestion. Finally, the third band, which migrated through the gel at about twice the rate of the supercoiled plasmid, represents the desired IFNA1 PCR product of 691bp that has been successfully isolated and eluted. The isolated fragment was then ligated into the digested pcDNA3 and transformed into competent *E.coli* DH5α.

The protocol used to extract and purify plasmid DNA from bacterial cell suspensions is based on the alkaline lysis method of Birnboim and Doly, 1979. During the procedure, sodium hydroxide (NaOH) denatures both chromosomal

and plasmid DNAs to single strands by disrupting the hydrogen bonds between base pairs. Upon neutralisation by the addition of potassium acetate (CH_3CO_2K), the large chromosomal DNA precipitates, while the small plasmid DNA renatures correctly and stays in solution. However, prolonged exposure to alkaline conditions causes the plasmid DNA to entre an irreversibly denatured state. The resulting closed circular plasmid DNA is refractory to restriction enzyme digestion and runs faster on agarose gels (Adapted from QIAprep® Miniprep Handbook).

Plasmid vectors that are used to clone DNA inserts tend to be circular and genetically engineered. Plasmids exist in a highly supercoiled state *in vivo*. Such covalently closed circular-DNA molecules would maintain their supercoiled conformation after plasmid isolation and downstream processing; however, a certain amount will sustain single- or double-stranded nicks that result in nicked-circular (open-circular) or linear plasmid forms, respectively (Balagurumoorthy et al., 2008).

The electrophoretic mobility of these three topological forms differs in an agarose gel. The supercoiled DNA has a tighter conformation and a more entangled shape than the other two and migrates faster through the pores of the agarose matrix than its linear form, and the linear DNA migrates faster than its nicked-circular form (Restriction Enzyme Cleavage of DNA, EDVO kit #102 Manual, EDVOTEK®). Figure 3.5 exemplifies all these three conformations. For example, lane (10 U), in the lower part of the gel, displays three bands produced by separating uncut plasmid DNA: the upper nicked-circular, the middle band of linear DNA, and the

thick band of supercoiled DNA at the bottom. Although the supercoiled structure is the desired form of plasmid DNA and normally the predominant species, a small portion of this form becomes nicked, which is a common event during the plasmid preparation.

The pure plasmid DNA in figure 3.5 shows no contamination with other nucleic acids, such as degraded RNase A-resistant RNA, but a sharp band of 691bp. However, the subcloning efficiency is notably low since only one insert was successfully ligated in the expression vector. When digests are performed with the same endonuclease enzyme to generate compatible ends, ligation then simply involves the joining of two linear DNA fragments. DNA ligase catalyses the formation of a phosphodiester bond between juxtaposed 5'-phosphate and 3'-hydroxyl termini. However, DNA ligase can join cohesive/blunt end termini before the desired ligation can take place. This phenomenon is described as re-circularisation of plasmid DNA and it can be minimised by removing the 5'-phosphate residues from both termini of the plasmid DNA with alkaline phosphatase. The 5'-dephosphorylation reaction would eventually suppress self-ligation of the plasmid vector and efficiently decrease the number of empty vectors. However, a foreign DNA segment with intact 5'-terminal phosphate residues can be ligated efficiently into the dephosphorylated vector (Green and Sambrook, 2012). Therefore, this step was not performed in order to eliminate undesired ligation products. Although only one IFNA1 cDNA fragment was ligated into pcDNA3, the sequencing results of the plasmid DNA displayed effective insertion.

CHAPTER 4

EVALUATING THE TUMOURIGENICITY OF IFNA1-TRANSFECTED UACC-903 CLONES FOR ANCHORAGE-INDEPENDENT GROWTH IN SOFT AGAR ASSAY

4.1. INTRODUCTION

In attempt to exploit the tumour-suppressive potential of *IFNA1* in the development of melanoma, as previously suggested by our research group, UACC-903 melanoma cell line was stably transfected with IFNA1. Subsequently, to assess the effect of *IFNA1* gene expression on the malignant behaviour of this cell line, I have monitored and measured the colony-forming ability of each transfected clone by assessing their tumourigenicity in soft agar. Clonogenicity in soft agar of the highly tumourigenic UACC-903 cell line has been demonstrated in numerous studies (Church et al., 1993, Robertson et al., 1996, Parris et al., 1999).

Mammalian cells are able to take up and recombine exogenous DNA into the nucleus to generate expression of genes of interest. The delivery of intact DNA

across the enzymatic and membrane barriers, however, is not a spontaneous phenomenon, mainly because of the size and charge of DNA. Thereafter, a number of chemical, lipid and physical approaches— such as calcium phosphate, liposome fusion, microinjection, and electroporation, have been developed to facilitate and offer enhanced efficiency of the so-called 'transfection' process (Felgner et al., 1987). Although certain viruses can also be used as highly efficient delivery vectors, this method can be associated with non-specific inflammations or an unexpected immune response *in vivo* (Khalil et al., 2006).

Transfections are fundamentally characterised as transient or stable. The transfected genetic material can be expressed in a transient fashion, whereby the foreign DNA is able to be transcribed but cannot be copied and, consequently, will be degraded and diluted during mitosis (Stuchbury and Munch, 2010). Therefore, gene expression could be analysed for a period of 24 to 96 hours following introduction. Alternatively, analysing the long-term impact of gene expression requires establishing stably transfected subpopulations. The introduced genetic material would integrate into the target cell genome to persist only in the presence of a selecting agent [reviewed in (Grimm, 2004)].

Stable transfection of tumour cells with expression plasmids containing IFN-α genes has been reported to result in abrogation of tumour growth and establishment, and induction of antitumour immunity in several murine tumour model systems (Tuting et al., 1997). For instance, the murine B16 melanoma cells, characterised by very low immunogenicity and high tumourigenicity, were

transfected with mouse *IFN-α1* gene and tested for their ability to grow by injecting them in syngeneic and allogeneic mice. Interestingly, while IFN-α1-B16 transfectants showed decreased tumourigenicity in syngeneic mice, these clones were totally rejected by allogeneic mice. Furthermore, immunisation of the latter with irradiated IFN-α1 cells exhibited long-lasting tumour-specific immunity with parental B16 cells (Kaido et al., 1995).

The loss of anchorage dependence phenomenon is a hallmark of neoplastic transformation that was first described in 1964 by MacPherson and Montagnier who used growth in soft agar for selecting transformed cells from polyoma-infected baby hamster kidney cells (Peehl and Stanbridge, 1981). Further studies have demonstrated a strong correlation between the tumourigenicity in immunodeficient nude mouse and the anchorage-independence *in vitro* (Shin et al., 1975). Subsequently, this correlation has been further established as a quantitative marker for tumourigenicity *in vitro* (Jones et al., 1976, Howell and Sager, 1978).

Deprivation to substratum adhesion triggers cell cycle arrest which causes normal epithelial cells to undergo programmed cell death (apoptosis) in a phenomenon referred to as anoikis (Frisch and Ruoslahti, 1997). Acquisition of apoptosis resistance by loss of anchorage is believed to be a critical step during tumour progression and metastasis (Kantak and Kramer, 1998).

Oncogenic transformation is commonly accompanied by a variety of cellular changes, which include deregulated growth control, alterations in adhesiveness, motility, morphology and organisation of the cytoskeleton. Neoplastically transformed cells exhibit pronounced morphological changes, characterised by rounded cell shape with poorly organised microfilament bundles, as previously illustrated in a study by Pollack and colleagues (1975). The organisation of microfilaments has been demonstrated to be highly correlated with anchorage-independent growth and cellular tumourigenicity, emphasizing the pivotal role of microfilament alteration in oncogenic transformation (Gimona et al., 1996). Furthermore, several studies have reported that many microfilament associated proteins — such as α-actinin, gelsolin, vinculin and tropomyosins, are down-regulated to varying levels in various neoplastic cells; thus they are considered to contribute to the deterioration of the microfilament system, and their restoration inhibits the malignant phenotype. Altogether, this signifies that cytoskeletal organisation is central in maintaining a normal phenotype (Shah et al., 2001).

Maintaining cell-cell and/or cell-ECM (extracellular matrix) interactions is what supports the cell to function. The ECM is produced by collaboration between epithelial cells and stromal fibroblasts to form a dynamic complex architecture of glycoproteins, collagens, glycosaminoglycans and proteoglycans. This macromolecular array of proteins not only provides structural support for the cell and its biological functions, but can also determine the cell behaviour, polarity, migration, differentiation, proliferation and survival. These behaviours are

determined by communicating with the intracellular cytoskeleton and transmission of growth signals [reviewed in (Kim et al., 2011)].

Neoplastic transformation is the product of the tissue microenvironment. Altered expression of soluble factors and ECM components are the unequivocal characteristics distinguishing tumour microenvironments from normal tissue counterparts. While tumourigenic cells are capable to thrive independently from ECM survival cues, different stages of cancer development have been modulated by abnormal ECM dynamics [reviewed in (Schooley et al., 2012)].

The soft agar colony formation assay is a convenient method to monitor and assess anchorage-independent growth in a semi-solid media agar. MacPherson and Montagnier initially introduced this assay for selecting transformed cells from polyoma-infected baby hamster kidney cells (Peehl and Stanbridge, 1981). This assay was further refined by Hamburger and Salmon who developed anchorage-independent growth for the detection of colony-forming human myeloma stem cells *in vitro*. Growth was induced in a conditioned medium prepared from adherent spleen cells of BALB/c mice (inbred albino strain developed by H.J. Bagg), which has been previously primed with 0.2ml of mineral oil. Bone marrow cells derived from myeloma patients were suspended in 0.3% agar in a supplemented growth medium to yield a final concentration of 5×10^5 cells/ml. Cultures were incubated at 37°C in a 5% humidified incubator. Final colony counts were made 2 to 3 weeks later, when the colonies consisted of 40 to several hundred round cells of >20 μm diameter. Cells derived from bone marrows of

untreated patients or those in relapse could easily thrive, and the number of colonies was proportional to the number of cells plated, however, cells derived from normal volunteers failed to form colonies (Hamburger and Salmon, 1977). These results presented a normal population that could not grow in soft agar and a tumourigenic population that displayed anchorage-independent growth *in vitro*.

Anchorage-independent growth in soft agar has been previously correlated to the ability of transformed cells to form tumours in nude mice (Freedman and Shin, 1974, Shin et al., 1975). Furthermore, a study conducted by Cifone and Fidler correlated the pattern of *in vitro* anchorage-independent growth of tumour cells with their ability to produce metastases *in vivo*. Generally, when the semi-solid agar layer concentration was increased from standard 0.3% to 0.6%, highly metastatic cells were distinguished from cells of low metastatic potential by the ability of the former to multiply and develop larger tumour colonies at a faster rate than the latter (Cifone and Fidler, 1980).

4.2. MATERIALS AND METHODS

4.2.1. Selection with Geneticin®

The bacterial Neomycin phosphotransferase gene is one of the most commonly used selectable markers in mammalian cell culture. Geneticin® or G418 is an aminoglycoside antibiotic similar in structure to gentamicin, neomycin, and kanamycin. Since Neomycin sulphate does not cross the cellular membrane of mammalian cells, G418 is an alternative antibiotic for selection of cells stably transfected with Neomycin resistance gene (*neo*). Expression of the *neo* gene confers resistance to G418 sulphate by blocking polypeptide synthesis through interference with ribosomal function and inhibiting protein elongation (G418, Sigma-Aldrich).

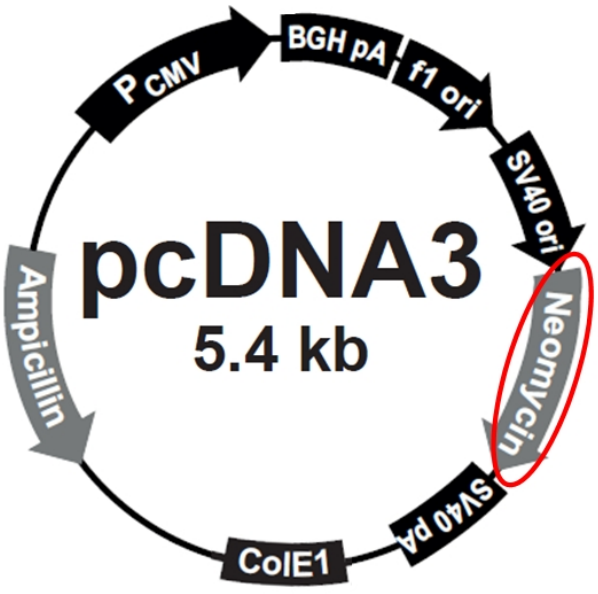

Figure 4.1: Schematic representation of the pcDNA3 vector showing multiple cloning sites and 'ampicillin' and 'neomycin' drug resistance genes (Mammalian Expression Vectors Guide, Invitrogen)

Selection with G418 would enable the subpopulation of cells, where the exogenous IFNA1 has been incorporated into the genome, to persist while the non-transfected cells undergo selection. However, since cells differ in their susceptibility to G418, determination of the optimal antibiotic dosing was very critical. The stock solution consisted of dissolving 1g of G418 (PAA) in 10 ml of DEPC treated water to optimise a final concentration of 100 mg/ml, filtered using a 0.22 micron filter, and stored at -20°C. Thereafter, a dose response curve protocol was applied on the parental UACC-903 to determine the minimum antibiotic concentration that will result in approximately 50% of cell death in about 5 days and kills all the cells over the course of two weeks.

In 6-well cell culture plates, cells were seeded to achieve a cell density of 70-80% needed for the multi-titration. The following day, the culture medium was substituted with complete growth medium containing varying concentrations of G418 (0, 50, 100, 200, 300, 400, 500, 600, 700, 800µg/ml). The plates were then incubated at 37°C in a humidified atmosphere of 10% CO_2 air. Each well was examined for viable cells regularly, and the selective medium was replenished every three days until the optimal concentration was determined. After two weeks, the cells were washed with PBS and visualised under an inverted microscope and the lowest dose that killed the cells was used for the selection.

Choosing a transfection reagent could be very challenging as most of the previously listed methods tend to exhibit high cellular toxicity or poor reproducibility. GeneJuice® transfection reagent (Novagen, UK) is composed of

histone, a nontoxic cellular protein, and a small amount of polyamine (manufacturer's description). The formula of histone and the polyamine neutralises the negative charge on the DNA molecules, making it easy to traverse the negatively charged cellular membrane. Thereafter, DNA entry is thought to be followed by endocytosis, in which the highly cationic polyamine enhances the DNA–GeneJuice complex fusion by promoting endosomal escape (Reagents for Transfection Guide, Merck Millipore).

In order to test the efficiency of this reagent, UACC-903 cells were transiently transfected with pEGFP-C1 (Clontech) expression plasmid. Green fluorescence protein (GFP) distribution was verified 24h post-transfection by a fluorescent cell analyser (figure 4.2).

4.2.1.1 Preparation of Cells for Transfection

Prior to transfection, 2×10^6 cells/ ml were seeded in complete growth medium per 100-mm petri dish and left to proliferate overnight at 37°C (10% CO_2) to reach 70-80% confluence. In a sterile Eppendorf tube, 18µl of GeneJuice® transfection reagent was added drop-wise to 800µl of serum-free RPMI 1640 medium, briefly vortexed and left to incubate for 5 minutes at room temperature. For each dish to be transfected, 6 µg of circular DNA was added to the GeneJuice®–serum-free medium complex. Mixed by gently retropipetting, the mixture complex was incubated for 10 minutes at room temperature and then entirely added drop-wise

to the cells in complete growth medium. The dishes were gently rocked to ensure even distribution and returned to the incubator. After 5 hours of incubation, the transfection mixture was replaced with 15 ml of complete growth medium. After 48h, cells were harvested by trypsinisation and subcultured at 1:5 split ratio in complete growth medium containing 700 µg/ml of G418. For 2 weeks, cells were treated every 3-4 days with selective medium until distinct colonies were visualised.

4.2.1.2. Isolation of Drug Resistant Clones

Once the resistant cells formed distinct colonies, they were circled with a marker on the underside of the petri dish. Culture medium was aspirated off and with a pair of sterile forceps, an appropriate sized cloning cylinder was drawn on autoclaved Vaseline and carefully lowered onto the colony and pressed down firmly. Depending on the size of the cylinder being used, 50-100µl of trypsin-EDTA was pipetted and cells were left to incubate for 2 minutes. Once detached, the cells were retropipetted, diluted into 5 ml of selective medium and transferred into a 60-mm petri dish. Subsequently, individual cells that further survived the selection, expanded into propagated and characterised clonal groups.

4.2.2. Soft Agar Assay

In this study, anchorage-independence assays were performed by seeding exponentially dividing cells in a semi-solid agar using the same complete growth medium to culture the cells. This assay consisted of the preparation of two types of layer, a 0.33% agar layer where cells are seeded on top of a previously hardened 0.6% agar layer, which prevents the attachment and subsequent growth of cells on the surface of the plate.

Preparation of the 6% agar base layer was prepared by incorporating 6g of Agar Noble (Sigma) with 1g of Bacto-Peptone (BD Biosciences) in a final volume of 100 ml of double distilled water. The 3.3% top layer consisted of mixing 3.3g of Agar Noble with 1g of Bacto-Peptone in a total volume of 100 ml of ddH_2O. Finally, both agar stock solutions were sterilised by autoclaving at 121°C (15lb/sq inch) for 15 minutes.

To prepare the 0.6% agar base layer, 9 ml of culture medium supplemented with 10% (v/v) foetal bovine serum and 2 mM of L-Glutamine were mixed thoroughly with 1 ml of 6% molten agar and rapidly dispensed by pouring 4ml of aliquots into each well of a 6-well plate (Sarstedt). After that, the agar was allowed to set inside the biosafety cabinet for 10 to 15 minutes.

Cells were detached with trypsin/EDTA, re-suspended in a complete culture medium and counted to derive a final density of 5×10^3 cells/ 4ml (per well). Subsequently, 1.6 ml of the 3.3% molten agar has been diluted to 0.33% by

mixing it with 13.4 ml of complete growth medium and 1 ml of 5×10^3 cells, to reach a final volume of 16 ml of 0.33% top layer. Lastly, 4ml of the latter mix has been rapidly dispensed on top of the base layer, making sure that there are no air bubbles. The assays were conducted with at least two technical replicates per clone and repeated with at least four biological replicates. The 6-well plates were incubated for 3 weeks in humidified incubators at 37°C with 10% CO_2 (UACC-903 parental cells and transfected clones), and 5% CO_2 (PC-3 control cell line). After the incubation period, the plates were stained with 0.005% (w/v) crystal violet (Sigma-Aldrich) for 30 minutes and counted under an inverted microscope, in which only colonies that formed more than 50 cells were counted.

4.3. RESULTS

Optimisation for stable transfection begins with successful transient transfection. For this reason, GFP was used to monitor and develop an efficient transfection protocol by testing the expression of transfected cDNA using a 1:3 ratio, cDNA(µg):GeneJuice®(µl). Cellular imaging of GFP transfection into UACC-903 parental cells gave an estimated transfection efficiency of approximately 50% as shown below.

(A) **(B)**

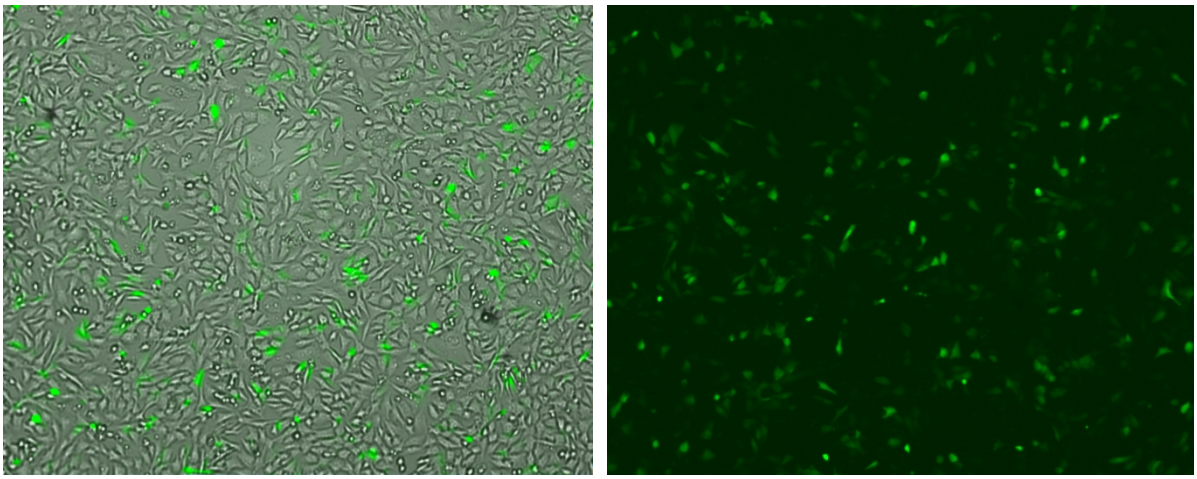

Figure 4.2: UACC-903 cells transiently transfected with GFP. These pictures were captured after transfection using Juli® smart fluorescent cell analyser by Digital Bio. A| Represents a merged image of UACC-903 cells in brightfield and GFP in fluorescent field; B| Image of GFP in fluorescent field. EGFP has an excitation peak at about 488ηm with an emission peak wavelength of 509ηm.

Subsequently, the cloned IFNA1 cDNA into pcDNA3 expression vector under the control of the CMV promoter was then transfected into UACC-903 cells. Ten

clones (C1 to C10) were established to stably express *IFNA1* together with two additional clones transfected with empty vector pcDNA3 (clone1 and clone2 pcDNA3) as controls.

Colony-forming ability was expressed as a percentage by dividing the number of counted colonies by the number of cells seeded. The number of colonies was proportional to the initial number of cells seeded, signifying that these colonies were derived from single cells, as previously described by Hamburger and Salmon (1977). The colony efficiency of the parental tumourigenic UACC-903 together with PC-3 prostate cancer cell line— which previously showed anchorage-independent growth in soft agar and produced tumours in nude mice (Kaighn et al., 1979), and both empty vector pcDNA3 clones, were used as controls and produced more than 50% colony-forming ability.

The ability to thrive in soft agar was rather variable in the transfected clones, in which two types have been observed; (*a*) clones that preserved their tumourigenic phenotype and demonstrated a high number of large colonies (figure 4.3), and (*b*) clones that displayed a reduced ability for anchorage-independence in soft agar, demonstrating few and small-sized colonies, or clones that failed to grow (figure 4.3). The results are summarised in figure 4.4 by plotting the mean percentage and comparing it to the parental UACC-903 cells.

Figure 4.3: Representative images of soft agar colony formation at day 21

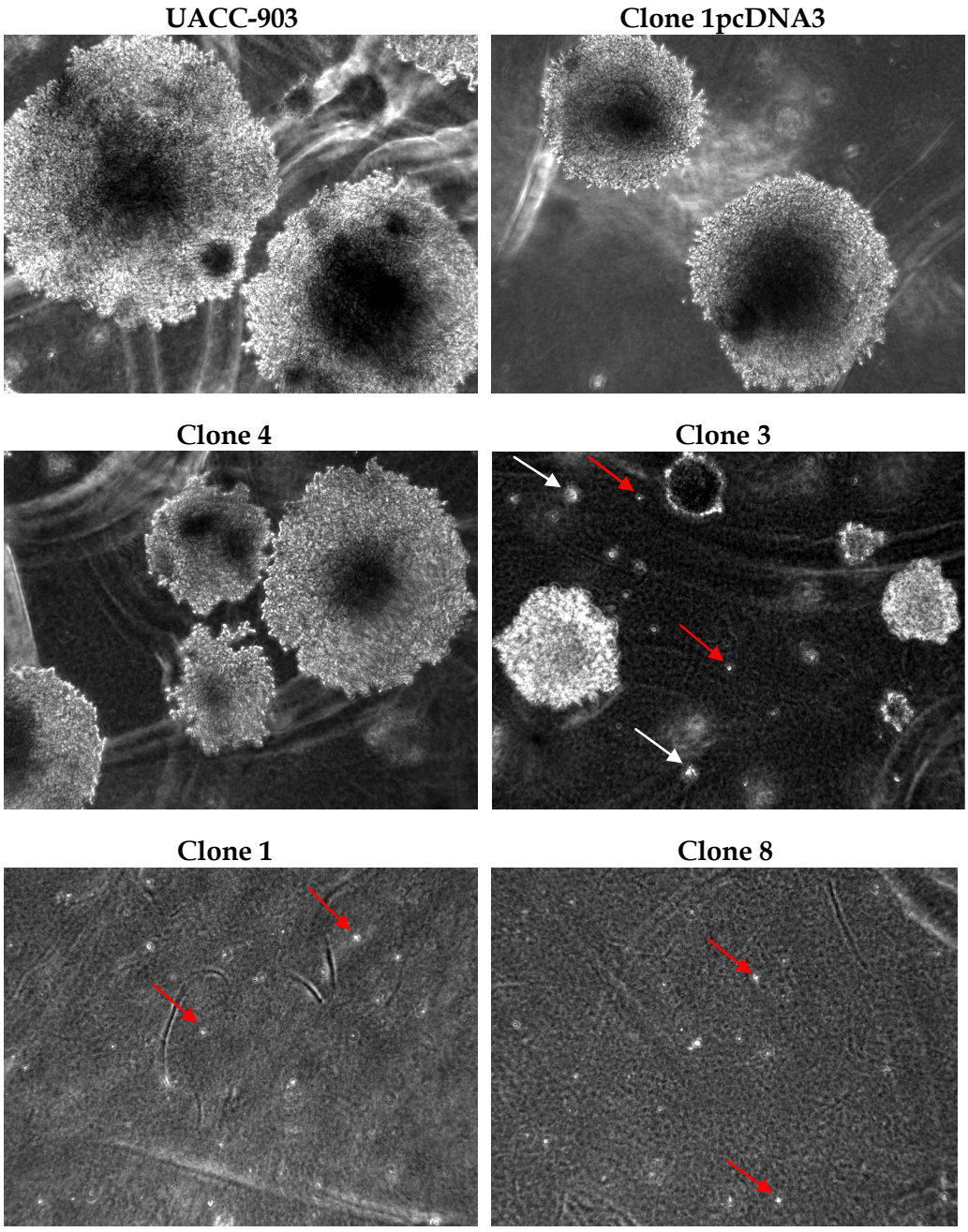

Photomicrographs of soft agar colonies captured under ×100 magnification using an Olympus IX71 inverted microscope attached to a CoolSNAP-cf camera (Photometrics). The growth of these colonies was measured in 35mm diameter dishes with a lower layer of 0.6% agar solution and an upper layer of 0.33% agar solution, in which 5×10^3 cells/well were re-suspended. The first 4 images display large colonies that vary in size, and were counted as tumourigenic. The white arrows indicate small-sized colonies that formed <50 cells and were not counted as tumorigenic, while the red ones indicate single cells that have failed to form colonies.

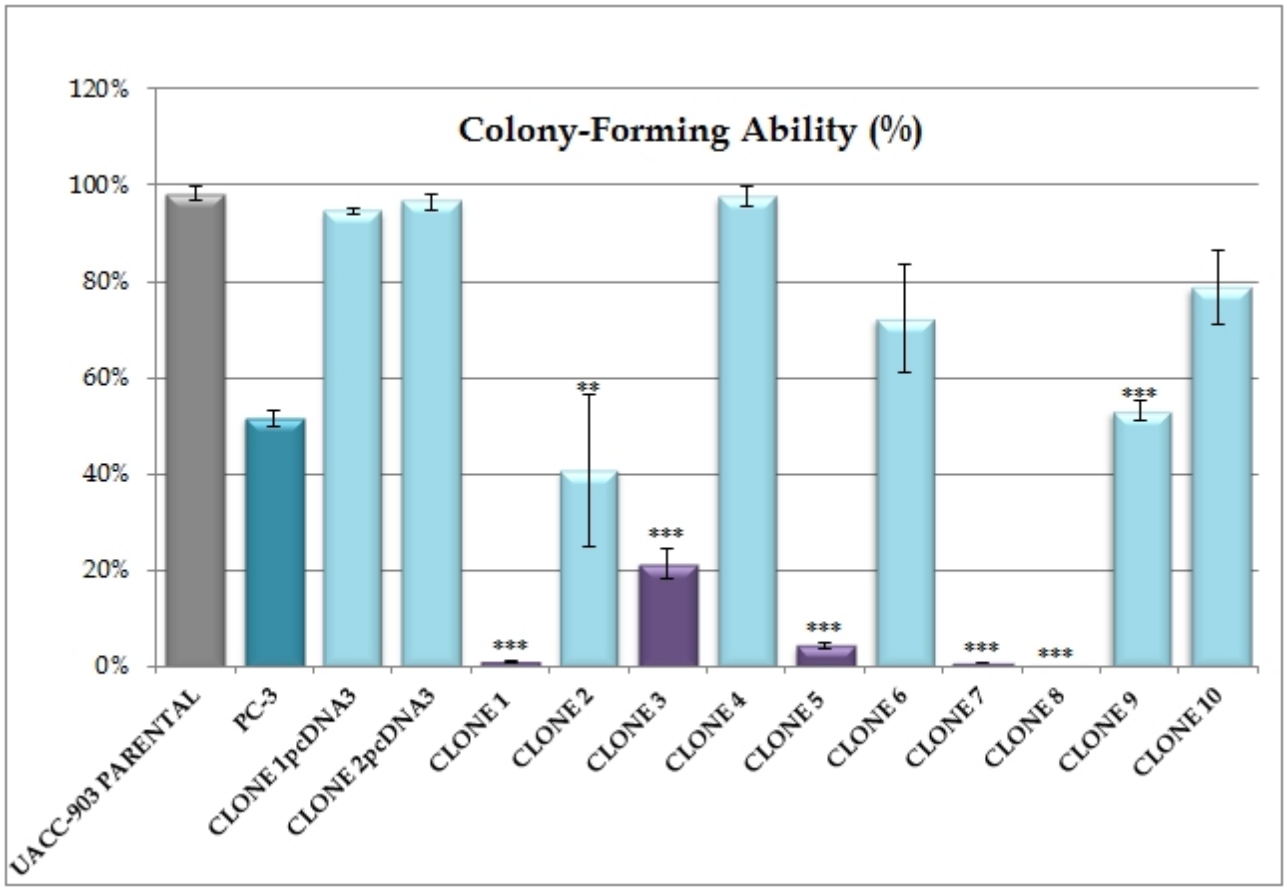

Figure 4.4: Average colony-forming ability of the transfected clones against parental tumourigenic UACC-903. Clone 2, 4, 6, 9 and 10, coloured in light blue, showing high growth ability varying from 41 to 98%, whereas the clones in purple showing significantly reduced capacity of 21% and 4% for anchorage independence in clone 3 and clone 5, respectively, or no growth (≤1%) in soft agar as seen in clone 1, 7, and 8. Error bars indicate standard error of the mean. Asterisk (*) indicates statistically significant differences between the control (UACC-903) and the transfected clones (*p < 0.05 (significant); **p < 0.01 (very significant); ***p < 0.001 (highly significant)).

4.4. DISCUSSION

The ability to undergo proliferation and to differentiate *in vitro* in the absence of cell-substratum adhesion is thought to be the critical growth precondition of neoplastically transformed cells. Soft agar assay of the stably transfected clones with *IFNA1* cDNA generated two populations. The first population preserved its tumourigenic phenotype by exhibiting high efficiency of anchorage-independence characteristics similar to the parental UACC-903 and PC-3 prostate cancer cells. Conversely, the other population displayed a significantly decreased colony-forming efficiency or even failed to grow in soft agar, a rather reversed tumourigenic phenotype. Colony-forming ability of ≤1% compared to parental UACC-903 would categorise the clones that failed to form colonies as suppressors (Parris et al., 1999).

Previous investigations have provided evidence of tumour suppression activity after the introduction of two chromosome 9 derivatives into UACC-903 cells; (9a) contained locus-specific deletions of *INK4*, and (9b) harboured a microdeletion spanning between D9S171 (9p21) to IFNA (9p22). Tumourigenicity assessment of these microcell hybrids showed that chromosome 9a variant demonstrated an increased ability to suppress growth in soft agar and suppressed both tumour formation and metastasis in athymic *nu*/*nu* immune-deficient mice to a greater extent than chromosome 9b variant (figure 4.5). These results suggested the presence of tumour suppressor gene(s) on 9p21 that function independently of *INK4* locus (Parris et al., 1999).

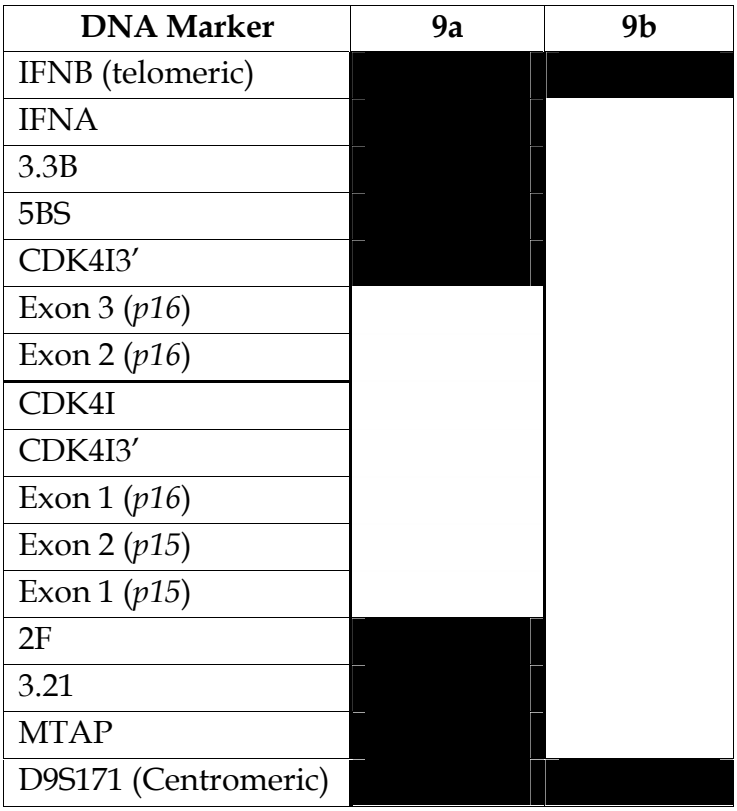

Figure 4.5: Chromosomal region 9p21-22 showing deletions in the two variants of chromosome 9 transferred to UACC-903 cell line. 9a| a variant of chromosome 9 harbouring exon-specific deletions of the $p15^{INK4B}$ and $p16^{INK4a}$ genes; 9b| a variant of chromosome 9 harbouring a microdeletion of ~30cM from markers D9S171 to IFNA. ■ present markers, □ deleted markers (Parris et al., 1999).

Given that UACC-903 parental cells are deleted for the *p16* and that the introduction of hybrids microdeleted for the *INK4* locus would still cause growth suppression implies compelling evidence that the region between IFNA (telomeric) to D9S171 (centromeric) harbours suppressor(s) that would confer tumourigenicity if deleted, as observed in the hybrids constructed with chromosome 9b variant. In parallel, transfection of *IFNA1* abrogated the growth of some of the clones or reduced their tumourigenicity, to a certain extent.

Altogether, this would clearly suggest a possible suppression activity of *IFNA1* in UACC-903 cells, and raises the question of whether the introduction of *IFNA1* restores the normal phenotype. Nevertheless, the fact that some of the clones could still display their tumourigenicity in soft agar could be because of the disintegration of exogenous IFNA1 during the process of transfection.

The use of cationic polyamine to facilitate the insertion of plasmid DNA has been documented to operate by binding and condensing plasmid DNA into confined structures of approximately 100–200ηm. However, the topology of plasmid DNA has an impact on transfection efficiency in mammalian cells. The supercoiled and open-circular DNA have been shown to provide greater efficiency than the linear counterparts, in which more compact vectors form more nuclease resistant polyplexes with comparatively more transgene expression (Dhanoya et al., 2011). Although the uptake of DNA polyplexes is dependent upon topology, the transfected circular plasmid will be linearized by a random cut in the course of integration, in which parts of the plasmid such as the resistance gene or the gene of interest could be destroyed upon linearization (Stuchbury and Munch, 2010).

CHAPTER 5

DETERMINATION OF *IFNA1* GENE EXPRESSION LEVELS USING REAL-TIME QUANTITATIVE REVERSE TRANSCRIPTION PCR

5.1. INTRODUCTION

In this section of the study, the expression levels of *IFNA1* were measured using the real-time qRT-PCR relative quantification method. This method was used to analyse the variation in gene expression in the stably transfected clones. This method compares the C_t value of *IFNA1* gene with an internal housekeeping gene, which was *GAPDH*, in each tested sample.

The reverse transcription polymerase chain reaction (RT-PCR), established by Kary Mullis and colleagues in the mid-1980s, has been the preferred method for the detection and amplification of mRNA in a cyclic process, generating a large number of essentially identical copies. However, in spite of its sensitivity, the standard PCR had some limitations. In 1992 Higuchi *et al*. refined the original PCR method and developed the revolutionary real-time PCR [Reviewed in

(Kubista et al., 2006)]. While the preceding era of quantitating nucleic acids involved densitometric scanning (Piechaczyk et al., 1984), Southern and Northern blotting, quantitative PCR has become, par excellence, the method of choice (Ferre, 1992).

Analysis of PCR kinetics was established by Higuchi *et al*. who initially constructed a real-time system that visualises and amplifies PCR products by adding an intercalator, in this case, ethidium bromide (Higuchi et al., 1992). This system used a thermal cycler with a UV source and a CCD camera. As the PCR products accumulate and the intercalator binds to the newly synthesised double-stranded DNA, it generated a plot of increased fluorescence signal against the cycle number. However, as revolutionary as this method was, it still lacked specificity (Higuchi et al., 1993).

The advent of real-time PCR alleviated the lack of detection and quantification within the amplification phase, which was previously associated with the traditional quantitative or semi-quantitative PCR. Hydrolysis probes (TaqMan), hairpin probes (molecular beacons, scorpions), fluorescent-labelled hybridisation probes (Light Cycler), and DNA-binding agents (SYBR Green), are the four fluorescence-based approaches which have been commonly used for quantitative detection in real-time PCR. These chemistries offer an accurate determination of the accumulated newly amplified DNA by detecting the fluorescence signal which increases proportionally with the cycle number, combining amplification and detection into a single step [Reviewed in (Chao, 2008)].

While PCR technology enabled the amplification, sequencing, and analysis of the genome, real-time PCR offers a greater number of advantages, and thus, proves to be valuable in a wide variety of diagnostic applications. These include pathogen detection, single nucleotide polymorphism (SNP) analysis, analysis of chromosome aberrations, protein detection by immuno-PCR, and gene expression analysis (Jain, 2010).

Tartour *et al*. highlighted the role of Interleukin 6 (IL-6), the multifunctional cytokine, in the pathogenesis of carcinoma of the uterine cervix using quantitative PCR assay to measure the variation from sample-to-sample. They presented the first report of quantitative gene expression of this cytokine in tumour tissue (Tartour et al., 1994). Furthermore, Bieche *et al*. developed a quantitative real-time PCR assay (qRT-PCR) to quantify the *MYC* gene expression in a series of 134 unilateral invasive primary breast tumours. They confirmed that gene expression dysregulation of this proto-oncogene is potentially involved in breast tumourigenesis (Bieche et al., 1999).

Koyanagi and colleagues expanded the usage of this technology and developed a multimarker real-time PCR assay to detect melanoma cells in patients' blood and assess tumour progression. Their objective was to develop a method that would successfully detect metastasis and monitor treatment response of melanoma patients (Koyanagi et al., 2005). Latterly, Arenberger *et al*. supported this "staging" method by describing it as a disease progression predictor in melanoma patients highlighting the usefulness of real-time PCR in enabling efficient screening of a large number of samples (Arenberger et al., 2008).

This technology consists of a PCR reaction that generates copies of a DNA template in a logarithmic manner. In other words, the amplification increases exponentially and eventually reaches a 'plateau phase' where the reaction is no longer in log-linear growth. As a result, some reactions will generate more end product than others, emphasising the predominant reason for why "traditional" end point quantification of PCR products is so unreliable. The ability to measure the kinetics of the reaction as the PCR products accumulate, in a real time range, provides a distinct advantage of measuring the amount of PCR products at a point in which the reaction amplifies exponentially. During the exponential growth phase in real-time PCR, mathematical extrapolation takes place to determine the starting amount of template (Ginzinger, 2002).

The two common approaches used to quantify mRNA transcription in real-time PCR are absolute quantification and relative quantification. Absolute quantification of transcription, as the name implies, determines the absolute amount of target sequence– expressed as copy number per cell or total RNA concentration. To ensure accurate reverse transcription and PCR amplification, this quantification assay uses an absolute standard curve to quantify the amount of target sequence of unknown samples by interpolation. In contrast, relative quantification analyses changes in target gene expression in a given sample relative to a calibrator, which could be an untreated control sample with a known concentration (Bustin, 2000).

Two derived approaches are used for relative quantification: standard curve and comparative C_t. The standard curve approach determines the quantity of target DNA in the test sample from a standard curve and then divides it by the quantity of the same target DNA in the control sample. The threshold cycle (C_t) value represents the fractional PCR cycle number required for the sample fluorescence to rise above the threshold setting. In the comparative C_t approach, the C_t values of test samples are compared with the C_t value of a control sample, which have already been normalised to an endogenous housekeeping gene. This approach is also known as the $2^{-\Delta\Delta Ct}$ method, in which $\Delta\Delta C_t = \Delta C_{t,\ test} - \Delta C_{t,\ control}$. The fold difference in gene expression between control and test sample is calculated by using the resulting difference in cycle number (ΔC_t) as the exponent of base 2 due to the doubling function of PCR product after each amplification cycle (Chao, 2008).

5.2. MATERIALS AND METHODS

5.2.1. Nucleic Acid Purification and cDNA Synthesis

As previously described in the general materials and methods, TRIzol® reagent has been used to conduct total RNA extractions. The purity of the extracted nucleic acid used in this study was critical for generating reproducible data. Following RNA isolation, concentration and purity of each sample was determined by using NanoDrop 2000c.

5.2.1.1. Deoxyribonuclease I, Amplification Grade Treatment of RNA

For the quantification of mRNA copy number, it was important to eliminate any contaminating DNA that might have occurred during RNA extractions. To avoid the inaccurate quantification, all the RNA samples were subjected to DNase I, amplification grade treatment (Invitrogen, UK).

In an RNase free pre-chilled 0.2ml PCR tube, 1µg of total RNA was treated with 1µl 10X DNase I reaction buffer, 1µl DNase I, amp grade 1U/µl. The reaction volume was made up to 10µl with DEPC-treated water. The samples were incubated for 15 minutes at room temperature to digest any single- or double-stranded DNA. The DNase I was then inactivated by the addition of 1µl of 25 mM EDTA solution to the reaction mixture followed by incubation at 65°C for 10 minutes in a PCR machine. The samples were then chilled on ice.

5.2.1.2. Synthesis of First Strand cDNA

The first strand complementary DNA (cDNA) was synthesised by using SuperScript™ III Reverse Transcriptase kit (Invitrogen, UK). In a pre-chilled nuclease-free PCR tube, 10µl of 1µg DNase treated total RNA were mixed with 1µl of 250ηg of random primers, 1µl 10 mM dNTP Mix (10 mM each of dATP, dGTP, dCTP, and dTTP at neutral pH) (Invitrogen). The reaction volume was made up to 13µl with DEPC-treated water.

The reaction was incubated at 65°C for 5 minutes in a PCR machine. The tubes were chilled on ice for 5 minutes and briefly centrifuged prior to adding the following to the reaction; 4µl 5X First-Strand buffer, 1µl 0.1 M DTT, 1µl RNase OUT™ recombinant RNase inhibitor 40 U/µl (Invitrogen), and finally 1µl of SuperScript III™ RT (200 U/µl). In a PCR machine, the reaction was incubated at 25°C for 5 minutes, and then at 50°C for 50 minutes, and finally inactivated at 70°C for 15 minutes after which the resulting cDNA could be stored at -20°C. The quality of the synthesised cDNA samples was tested using a set of GAPH primers— details of the method used are given below. One microlitre of each cDNA sample was visualised by electrophoresis in a 2% agarose gel stained with EtBr (figure 5.1). At this stage, the cDNA could then be used as a template for amplification by RT-PCR.

5.2.2. Primer Design

The optimal primer design and optimisation are aimed at obtaining a balance between specificity and efficiency in a PCR experiment. Therefore, it is fundamental to achieve proper priming between an oligonucleotide primer and the nucleic acid template. Efficiency of a primer's functionality ensures the exponential amplification of the desired product after each PCR cycle.

The functionality of the oligonucleotides is strongly dependent on their melting temperatures (Tm), the necessary temperature to unwind the dsDNA to form ssDNA, as well as possible homology among primers. Their specificity is controlled by the length of the primer, which is between 18 and 24 bases, as well as the annealing temperature (Ta) of the PCR reaction, which should be set few degrees below the primer Tm. If lacking specificity, mispriming eventually occurs during amplification, resulting in unrelated and undesirable amplicons. It is also important to take into consideration that the primers are not self-complementary, specifically at their 3' ends, as this will encourage formation of primer dimers. Another important parameter is maintaining a reasonable GC content. In fact, primers with a 50% G + C content generally have Tm values in the range of 56-62°C, which provides efficient annealing condition (Dieffenbach et al., 1993).

For this study, the Primer Express Software v2.0 from Applied Biosystems (California, USA) was used to design the primer sequences for SYBR® Green assays. The FASTA sequence of gene of interest was downloaded from NCBI and loaded into the software by inserting the sense strand 5'–3' of the gene. This

software designs a list of oligonucleotide primers displaying the forward and the reverse primers, length, Tm and %GC. The primer sets are listed in the table below.

Gene Name	Orientation	Sequence	
GAPDH	Forward	5' GAAGGTGAAGGTCGGAGT 3'	Set 1
	Reverse	5' GAAGATGGTGATGGGATTTC 3'	
IFNA1	Forward	5' CCTCCTGTCTGATGGACAGACA 3'	Set 2
	Reverse	5' CAGCTCATGGAGGACAGAGATG 3'	
	Forward	5' TGCTTTACTGATGGTCCTGGTG 3'	Set 3
	Reverse	5' TTTGTCCCAGGAGCATCAAG 3'	
	Forward	5' GAGACCCACAGCCTGGATAACA 3'	Set 4
	Reverse	5' TGGAGCCTTCTGGAACTGGTT 3'	

Table 5.1: Primer sequences (Sigma-Aldrich) for RT-PCR and qRT-PCR. The parameters were set as the following: primer Tm: min (57°C) – max (63°c), optimum (60°C); primer length: min (18bp) – max (22) bp; primer GC% content: min (45%) – max (55%); amplicon product size: min (100bp) – max (200bp).

5.2.3. Reverse-Transcription PCR

5.2.3.1. PCR Amplification of GAPDH to check the quality of the cDNA

RT-PCR is a sensitive method for enzymatically amplifying and quantifying mRNA transcription levels. The DNA molecules are amplified exponentially via DNA polymerase and the process usually involves 20 to 35 thermal cycles. At this stage of the study, it was important to test the cDNA for an endogenous control.

Glyceraldehyde 3-phosphate dehydrogenase (GAPDH), a so-called housekeeping gene, is one of the most commonly used reference genes and a relatively stable glycolytic enzyme that catalyses the sixth step of glycolysis, a process in which glucose is converted into pyruvate (Rebouças et al., 2013). Because it is constitutively expressed, GAPDH was used as an endogenous control to compensate intra- and inter-kinetic qRT-PCR variations, such as sample-to-sample and run-to-run variations (Pfaffl and Hageleit, 2001).

The process of amplifying the newly synthesised cDNA fragments depends on the addition of primers, and for this purpose, a set of the previously designed primers for GAPDH gene were used. One microlitre of cDNA template was added to 1µl of 10µM of forward primer (5'GAAGGTGAAGGTCGGAGT 3'), 1µl of 10µM of reverse primer (5'GAAGATGGTGATGGGATTTC 3'). The final volume was made up to 30µl with 1.1X ReddyMix^{TM} PCR Master Mix (Thermo Scientific). The samples were mixed by gentle pipetting, briefly centrifuged, and placed into a PCR machine (Tetrad, Peltier Thermal Cycler PTC-225) configured with the following settings:

	Temperature	Time	Number of Cycles
Initial Denaturation	94°C	5 minutes	1 Cycle
Denaturation	94°C	45 seconds	
Annealing	60°C	45 seconds	35 Cycles
Extension	72°C	45 seconds	
Final Extension	72°C	10 minutes	1 Cycle

Ten microlitres product of the PCR reaction were loaded into 2% agarose gel stained with EtBr (Figure 5.1). Further optimisation was performed to find the correct molarity of the primers to avoid the chances of developing primer dimer (figure 5.2).

5.2.3.2. RT-PCR Amplification of IFNA1

Limiting the variations in the applied conditions on both *GAPDH* and *IFNA1* genes was one of my objectives in this study. Real-time PCR application requires running the gene of interest in parallel with an endogenous control, while both are being amplified in an automated fluorometer and under the same conditions. For this purpose, the preparations for RT-PCR were similar to the ones applied on GAPDH, and specifically applying the same annealing temperature on the three designed primer sets for IFNA1 (mentioned in table 5.1), which was set at 60°C (figures 5.3, 5.4, and 5.5).

Four controls have been used for the gene expression analysis— NB1-Tert immortalised fibroblast cell line with a relatively 'normal' phenotype, PC-3 prostate cancer cell line, and two transfected UACC-903 cell lines with empty vector: Clone 1pcDNA3, and Clone 2pcDNA3.

5.2.4. Quantitative real-time PCR (qRT-PCR)

SYBR® green I is a dsDNA-specific fluorogenic dye that gives a stronger signal with DNA than excitation of EtBr with visible light, emitting 1000-fold greater fluorescence signal upon binding to double-stranded DNA (Wittwer et al., 1997, Morrison et al., 1998). SYBR® Green PCR master mix (Applied Biosystems) used in this study contains SYBR® green I dye, AmpliTaq Gold® Polymerase, dNTPs with dUTP, Passive Reference (ROX– a dye that provides fluorescence reference to which the SYBR Green/dsDNA complex signal can be normalised during analysis), and optimised buffer components. This master mix was used for the direct detection of amplified PCR product on an ABI PRISM® 7900HT Sequence Detection System (Applied Biosystems). These amplicons are monitored in real time by measuring the increase in fluorescence caused by the binding of SYBR Green dye to dsDNA.

Following the same principle of standard RT-PCR, the samples were prepared and pipetted into a chilled MicroAmp™ Fast Optical 96-Well Reaction Plate with barcode, 0.1 ml (Applied Biosystems). Reactions were performed in triplicates and consisted on mixing the following:

- 1µl of 10µM of forward primer
- 1µl of 10µM of reverse primer
- 10µl of SYBR Green (diluting the original 2X concentration of SYBR Green to 1X concentration)

- 1µl of cDNA diluted in 7µl of DEPC-treated water giving a final volume of 20µl.

Two triplicates were used for non-template control (NTC) to check for non-specific signal arising from contamination or primer dimer formation, by adding 1µl of DEPC-treated water instead of the cDNA. After pipetting each sample in the corresponding well, the plate was covered with a MicroAmp™ optical adhesive film (Applied Biosystems) and sealed tightly over every well. The plate was briefly centrifuged and loaded into the real-time PCR instrument (ABI PRISM® 7900HT).

5.2.4.1. ABI PRISM® 7900HT Program Set-Up

GAPDH detector was assigned as 'Endogenous control' for normalisation, and IFNA1 detector was assigned as 'Target'. Thermal cycling conditions were performed with the following thermal profile steps.

STEP	***AmpliTaq Gold® Polymerase Activation***	***PCR***	
	HOLD	CYCLE (40 cycles)	
		Denature	Anneal/Extend
Temperature	95°C	95°C	60°C
Time	10 min	15 sec	1 min
Volume	20µl		

Table 5.2: Thermal Cycling Parameters for the qRT-PCR reaction

The instrument plotted the cycle number at which the product is above the threshold (C_t) on a logarithmic scale. The amplification lasted for approximately 45 minutes.

SYBR Green chemistry is designed to generate fluorescent signal upon binding to any double-stranded DNA molecule including primer dimers which might interfere with the target molecules, and consequently affect the quality of the data. For this purpose, it is important to perform a dissociation curve analysis immediately after the run. These analyses will display dissociation data from the PCR products, and any changes in fluorescence will be plotted against temperature. The dissociation curve consists of increasing the temperature progressively from 60 to 95°C.

5.2.4.2. Optimising Primer Concentration for qRT-PCR

The purpose of this procedure was to determine the forward and reverse primer concentrations that yielded the lowest threshold cycle (C_t) and maximum ΔRn while minimising non-specific amplification. Three different concentrations of forward and reverse primers were tested for optimisation using real-time PCR shown in figure 5.6, along with the dissociation curve as displayed in figure 5.7.

5.3. RESULTS

After RNA extraction with TRIzol®, the samples were quantitated using NanoDrop 2000c and electrophoresed on an agarose gel.

Sample Name	$A_{260/280ηm}$ Ratio	RNA concentration (ηg/μl)	RNA concentration (μg/μl)
UACC-903	1.89	4122.1	4.1221
PC-3	1.94	1837.5	1.8375
NB1-Tert	1.97	5642.3	5.6423
Clone 1pcDNA3	1.88	4246.8	4.2468
Clone 2pcDNA3	1.90	4055.5	4.0555
Clone 1	1.95	3319.4	3.3194
Clone 2	1.89	4060.1	4.0601
Clone 3	1.80	3809.2	3.8092
Clone 4	1.91	6147.9	6.1479
Clone 5	1.91	4027.2	4.0272
Clone 6	1.90	4352.1	4.3521
Clone 7	1.91	3941.2	3.9412
Clone 8	1.94	3957.3	3.9573
Clone 9	1.91	4550.8	4.5508
Clone 10	1.94	6115.0	6.1150

Table 5.3: Sample readings from total RNA extraction. RNA concentration and purity was measured using Nanodrop™ 2000c spectrophotometer by measuring the absorption (A) of UV light at 260ηm and 280ηm. An $A_{260/A280}$ ratio of 1.8-2.1 is indicative of highly purified RNA.

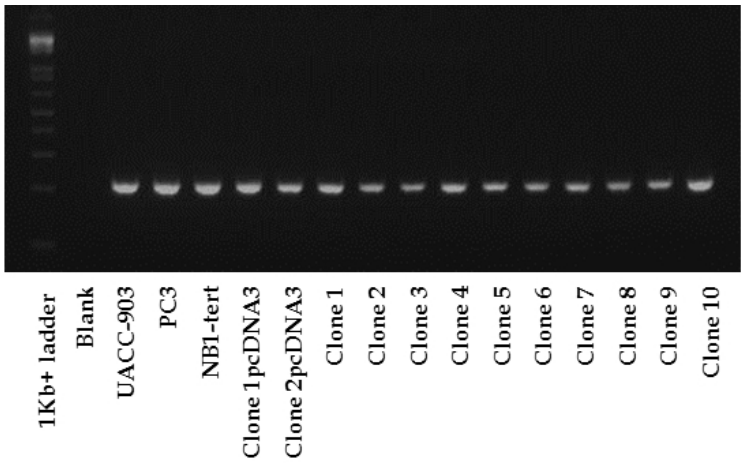

Figure 5.1: RT-PCR control gel demonstrating the quality of cDNA samples using "Set 1" GAPDH primers. The amplified products of 226bp were electrophoresed in a 2% agarose gel at 80V. The cDNA samples are of good quality as they show no sign of degradation or contamination.

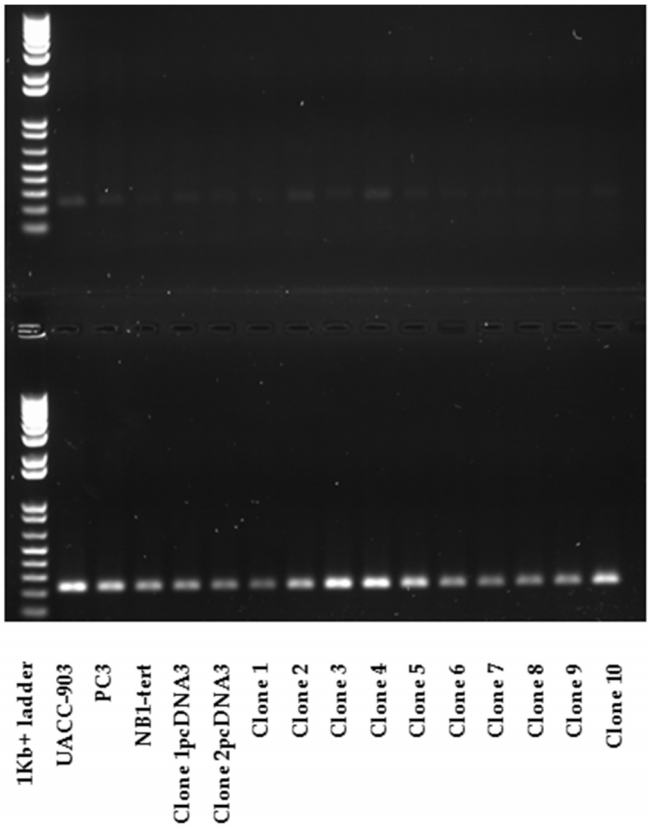

Figure 5.2: GAPDH primer optimisation. RT-PCR gel demonstrating GAPDH primer optimisation by setting the annealing temperature at 60°C. The gels represent the amplified RT-PCR products using 5µM of primers (upper) and 10µM (lower).

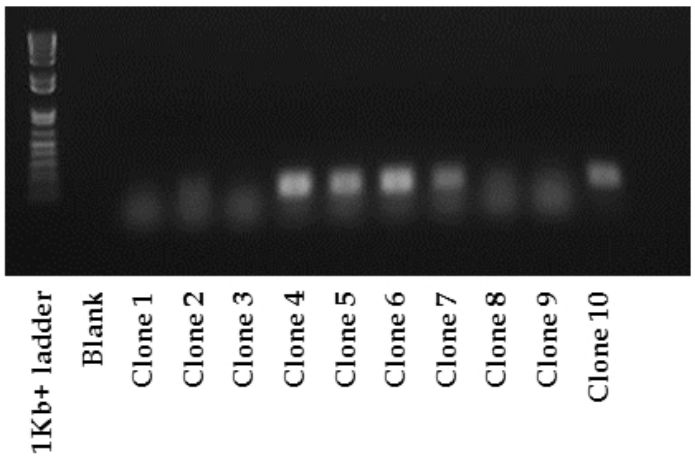

Figure 5.3: IFNA1 primer optimisation using Set 2. The gel displays RT-PCR products of the 10 transfected clones using 10µM of "Set 2" IFNA1 primers by setting Ta at 60°C. Five indistinct bands of 101bp amplicon size and some unspecific binding showing in this gel, which suggested further optimisation with the other set of primers.

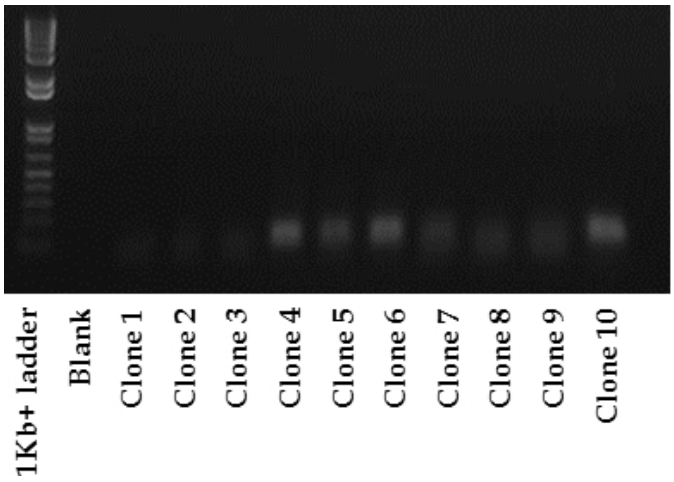

Figure 5.4: IFNA1 primer optimisation using Set 3. RT-PCR products using 10µM of "Set 3" of IFNA1 primers. The amplicon size of this set of primer is of 116bp. However, the gel shows unspecific binding of the primers.

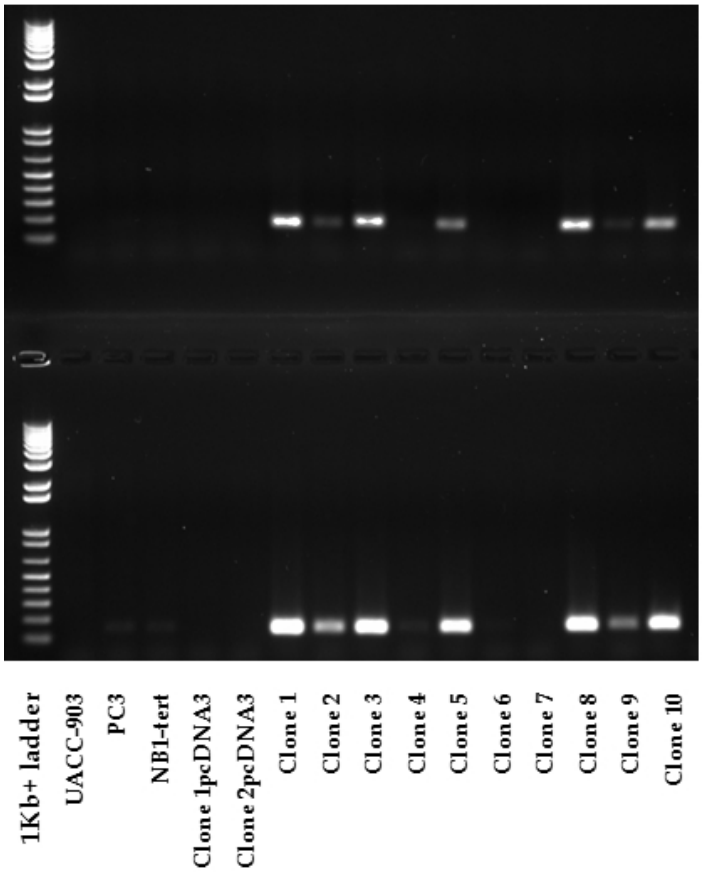

Figure 5.5: IFNA1 primer optimisation using Set 4. RT-PCR gel demonstrating IFNA1 primer optimisation using "Set 4" by setting the annealing temperature at 60°C. The gels display the amplified RT-PCR products of 144bp using 5µM of primers (upper) and 10µM (lower). The bands seem sharp and specific, especially in the lower gel.

Figure 5.6: IFNA1 primer "set 4" optimisation using qRT-PCR amplification curve

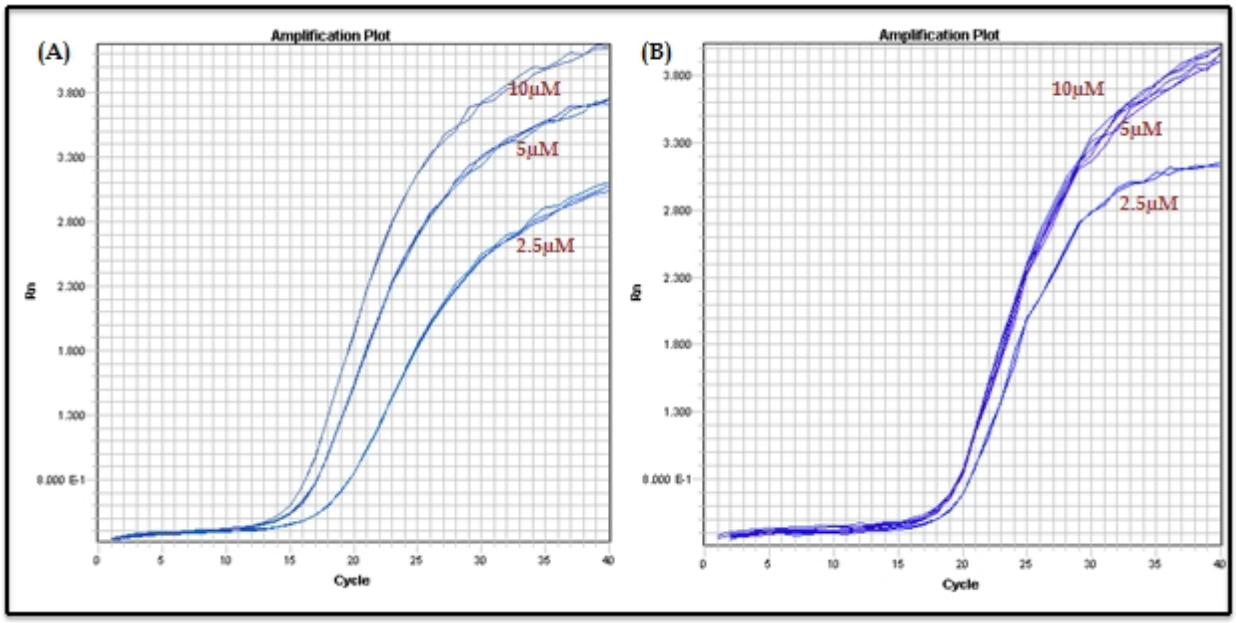

Real-time PCR amplification curves using Clone 1. **A|** Amplification curve for GAPDH primers at different concentrations. 10µM of primers generated the highest amplification efficiency of GAPDH with the lowest Ct value of 15.8. **B|** Amplification curve for IFNA1 using primer set 4 showing the highest amplification efficiency at 5µM and 10µM with a Ct value of 18.9. Despite the indifference between both concentrations, we have proceeded with using 10µM as it showed sharper bands in figure 5.5.

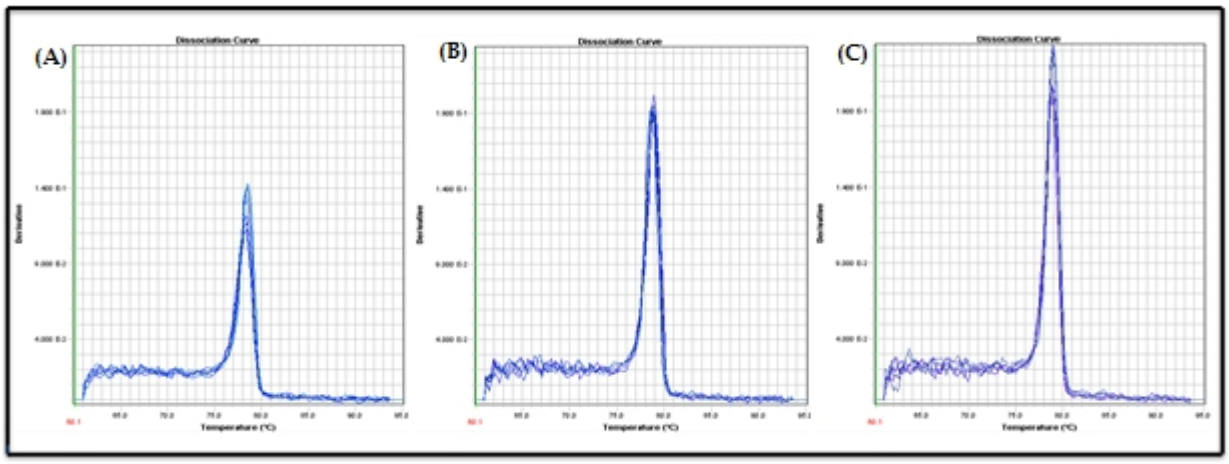

Figure 5.7: Post-amplification dissociation curves. Each curve displays both GAPDH and IFNA1 primers at different concentrations: A| at 2.5µM, B| at 5µM, C| at 10µM. These curves show a clean PCR product amplified under real-time conditions and display no sign of secondary product formation.

Designing a qRT-PCR experiment to measure the variation in gene expression is attributable to biological variability and experimental error, such as sample-to-sample variations, variation in RNA quality, sample loading, etc. Therefore, we implemented a normalisation with an invariant endogenous control, which has been previously established (Pfaffl, 2001). Performing a normalisation against an endogenous control circumvents the need of accurate quantification of the starting material, and uses a calibrator.

In this study, each sample was assayed in triplicate and the levels of IFNA1 mRNA were normalised against endogenous *GAPDH* and quantified using qRT-PCR. After amplification, the data were collected and analysed by relative quantification ΔΔCt study assay using the SDS 2.4 software tool. The amplification plot displayed in figure 5.8 represents the measurement of the fluorescent signal of each sample versus the cycle number.

Figure 5.8: Quantification of relative IFNA1 mRNA expression levels

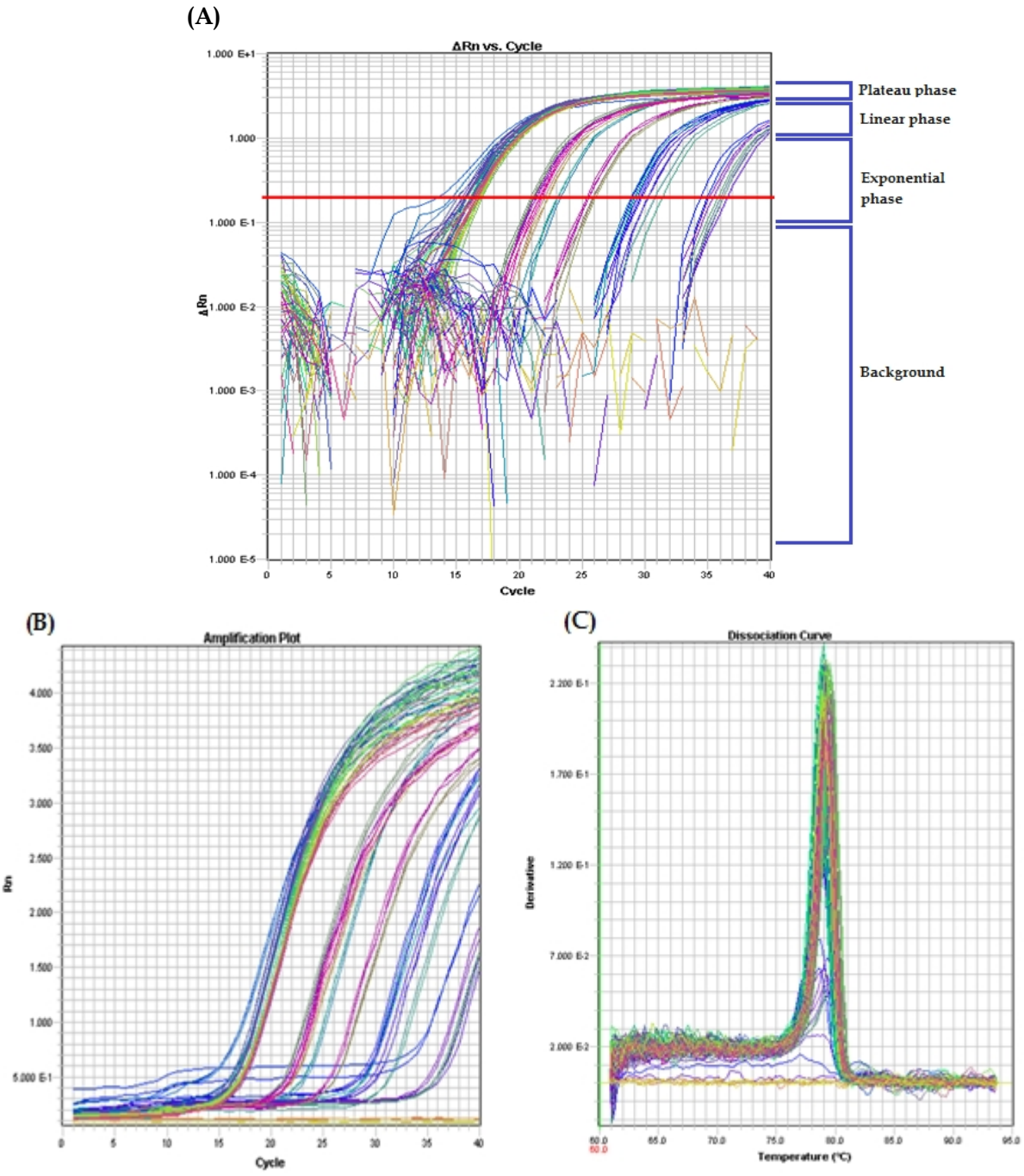

A| A logarithmic view displaying dye fluorescence (ΔRn) as a function of cycle number, demonstrating three phases of a typical amplification curve B| A linear scale of the amplification plotted as Rn vs cycle number, displaying normalised reporter dye fluorescence (Rn) as a function of cycle. The amplification curve shows different levels of *IFNA1*, which have been normalised to *GAPDH*. C| Post-amplification dissociation curve displaying the fluorescence vs temperature, and showing no secondary product formation.

The amplification plot is characterised by three distinct phases. Initially, the fluorescent signal is below the threshold of the sequence detector. A straight line with a slope occurs as the fluorescent signal increases proportionally to the amount of specific amplified product during the exponential phase. Gradually, a decrease in the slope appears during the linear phase indicating a decrease in the amplification efficiency, and as a consequence, the amplification curves exhibit low precision. Eventually, the amplification plot reaches the plateau phase displaying a steady Rn signal, where the PCR reaction is no longer generating template (Theory of Operation, ABI PRISM® 7900HT User Guide, Applied Biosystems).

The SDS software analyses the raw fluorescent data to establish C_t values for each sample. As shown in figure 5.8 (B), the average C_t values for each triplicate reaction tested for the GAPDH is ranged from 15 to 17 cycles and from 20 to 36 cycles for the samples tested for IFNA1. These C_t values reflect on the low abundance of nucleic acid levels for *IFNA1*, which were relatively compared to the abundant *GAPDH*, the constitutively expressed housekeeping gene. As for verifying the absence of contamination, amplifications were performed with a systematic negative control, containing no cDNA, illustrated in figure 5.8 (A) as background under the threshold, marked with a red line, and in (B) these NTC samples appeared as a flat mustard line below the plot of fluorescent signal.

In this analysis, quantity of each test sample is expressed relative to a calibrator cDNA sample. In this context, the calibrator is used as a reference sample to

estimate the relative-fold changes in the analysis of gene expression, and it is set to 1 and all other quantities are expressed as relative-fold difference to the calibrator. Thus, the gene expression in test samples (PC-3, NB1-Tert, both transfected clones with empty vector pcDNA3, as well as the transfected clones with IFNA1 cDNA) was relatively compared to the expression levels in the parental UACC-903 (calibrator) by measuring individual relative quantification (RQ) values. The fold-change of IFNA1 (target) expression level in the test samples was plotted relatively to the levels measured in the tumourigenic UACC-903, using GAPDH as an endogenous reference gene. All statistical tests were two-sided with α set at 0.05, and p-values < 0.05 were considered statistically significant. The results obtained were plotted in figure 5.9.

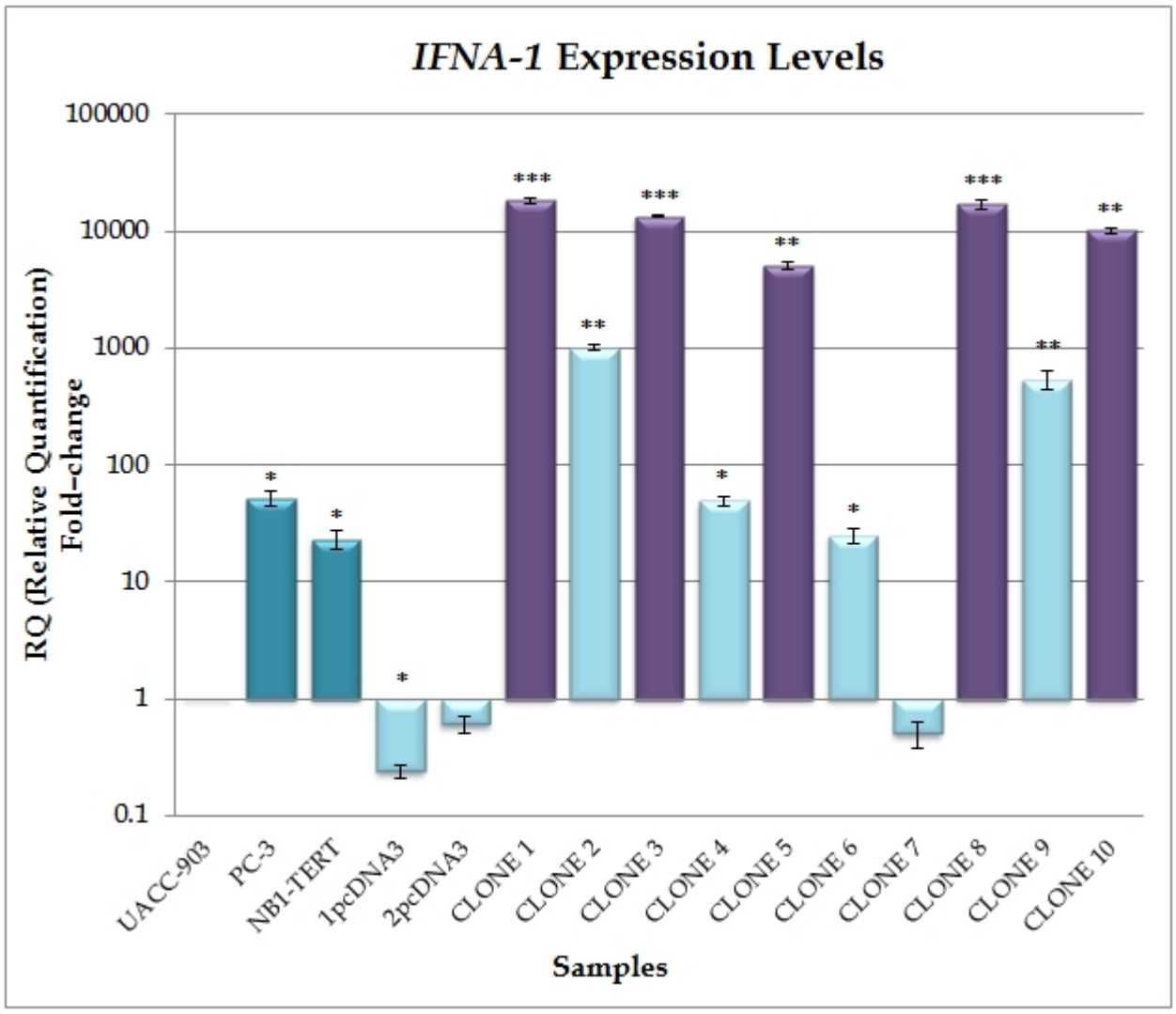

Figure 5.9: Relative quantification analysis showing the fold-change of *IFNA1* transcript abundance in test samples relative to UACC-903. *IFNA1* expression values were first normalised to *GAPDH* and then calibrated to parental tumourigenic UACC-903. Data shown is the representative of three independent experiments, in which each qRT-PCR was done in triplicates. Error bars indicate standard error of the mean. Differences in expression were evaluated with *Student's* two sample test (two-tailed, with unequal variances). Asterisk (*) indicates statistically significant differences between the calibrator (UACC-903) and the test samples where *$p < 0.05$ (significant); **$p < 0.01$ (very significant); ***$p < 0.001$ (highly significant).

5.4. DISCUSSION

The findings from the soft agar colony formation assay led us to hypothesise that *IFNA1* has a tumour suppressor function. In support of this hypothesis, qRT-PCR was used to assess *IFNA1* expression levels among the transfected clones since it provides sufficient sensitivity and specificity in detecting and comparing minute amounts of nucleic acids in a range of samples.

Relative *IFNA1* expression determinations were made with the comparative Ct method. In brief, the $2^{-\Delta\Delta Ct}$ method— where $\Delta\Delta C_t = \Delta C_{t,\ test} - \Delta C_{t,\ UACC\text{-}903}$, involves comparing the normalised Ct value of the test sample ($\Delta C_{t,\ test}$) with the normalised Ct value of the calibrator ($\Delta C_{t,\ UACC\text{-}903}$). The SDS software calculates the RQ values to establish a comparative relationship between the changes in the fluorescence signals, hence, it allows us to compare the spectral changes in the expression of the target gene. Consequently, target abundance was given by calculating RQ values for all samples relative to the calibrator, which was set to 1, and *IFNA1* expression was assessed as an increase or decrease relative to the parental UACC-903.

The expression analysis presented in figure 5.9 clearly shows a difference in gene expression profiles among the ten clones. As illustrated in figure 5.8 (B), the exponential phase of some of these clones occurs later than others, signifying a difference in mRNA expression levels between both sets. In correlation with figure 5.8 (B), the clones expressing lower levels of *IFNA1*, highlighted in light blue in figure 5.9, showed weak fluorescence signals in the amplification plot and

yielded the highest Ct values— varying from 27 to 36. These results signify that these clones express low copy number of the target *IFNA1* mRNA sequence, indicating a down-regulation of the target gene. Conversely, the high expressed clones chart highlighted in purple showed high fluorescence signal amplification peaks and yielded the lowest Ct values— varying from 20 to 23, implying a significant up-regulation of the target gene.

The relative fold-change between clone 1 and the calibrator showed more than 18,000-fold up-regulation of *IFNA1* transcription. The other highest expression was seen in clone 8, which was up-regulated by more than 17,000-fold.

The cloning of IFNA1 cDNA into pcDNA3 expression vector, which contains the CMV promoter that drives high level expression of transgenes while the BGH polyadenylation signal enhances mRNA longevity, resulted in more than 18,000-fold increase in *IFNA1* transcription, which might seem extremely high. However, Tencomnao and colleagues reported that transient transfections of pGL3-CMV reporter construct, which contains the CMV enhancer and early promoter elements, into the UACC-903 cell line yielded a high transcriptional potency, which was about 4,260-fold higher than that of the parent pGL3-Basic vector (Tencomnao et al., 2008).

Expressions of ≤ 1000-fold were considered as down-regulated, as displayed in both PC-3 and NB1-Tert, both clones transfected with empty pcDNA3, clones 2, 4, 6, and 7. Interestingly, clone 7 displayed suppression in soft agar; however, it showed a 0.5-fold down-regulation of *IFNA1* transcription.

CHAPTER 6

ASSESSMENT OF IFNA1 PROTEIN EXPRESSION

6.1. INTRODUCTION

In the previous chapters, I investigated whether *IFNA1* gene expression alters the tumourigenic behaviour of the transfected clones by analysing the variation in mRNA expression levels. Given that protein expression is a subcomponent of gene expression, this section of the study aimed at detecting and localising IFNA1 protein abundance in the transfected clones by means of ELISA's sensitivity and the detailed morphometric cellular analysis of the ImageStream^{x}.

Interferons represent a distinctive class of inducible cellular proteins. Unless stimulated, their concentrations are below detectable levels in most organs and cells in culture (Lengyel, 1982). IFNs are extracellular signalling cytokines that produce antiviral and immunological responses by activating a cascade of intracellular pathways (Gutterman, 1994). Among the interferons, IFN-α, product of leukocytes, is an important group of cytokines that vary in molecular mass and is encoded by several genes clustered in chromosome 9p [reviewed in (Feghali

and Wright, 1997)]. Early characterisation studies, using sodium dodecyl sulphate- polyacrylamide gel electrophoresis (SDS-PAGE), suggested that human IFN-α consisted of multiple protein species with molecular weights ranging between 16 and 27 kDa (Stewart, 1974).

Essentially, there are 14 nonallelic genes ―genes that are located at different loci on the same chromosome and encoding differing proteins (Redei, 2008)― that comprise the human IFN-α gene family. The amino acid sequences they encode encompass one or two base differences, which account for the multiple alleles. Apart from the pseudogene IFNAP22, there are 13 functional genes that express 12 different functional protein subtypes, in which IFNA13 and IFNA1 have identical protein sequences. Predominantly, only recombinant Hu-IFNα2 protein is used therapeutically in a variety of cancer [reviewed in (Pestka, 2007)]. The IFNA-α proteins comprise a hydrophobic, 23-amino-acid signal peptide plus a 166-amino-acid mature peptide sequence, except IFN-α2 which encodes a 165-amino-acid protein (Capon et al., 1985).

Enzyme-linked immunosorbent assay (ELISA) uses antibodies as specific analytic reagents to detect and spectrophotometrically quantitate, by a colour change, the amount of an antigen or protein *in vitro*. The sandwich ELISA confers high sensitivity and specificity, whereby it measures the amount of antigen concentration in an unknown sample between two layers of antibodies, thus resembling a 'sandwich'. However, the antigen to be measured must contain at least two antigenic sites, since at least two antibodies act in the sandwich. The

'capture' antibody is first coated on the microtiter plate. Next, the antigen is added and captured by the antibody on the well. Finally, the bound antigen is detected by adding an enzyme linked 'detection' antibody, whereby the extent of reaction is proportional to the amount of antigen present (Berg et al., 2002).

The ImageStream^{x} system (Amnis Inc., Seattle, WA, USA) is a novel approach that combines the capacities of flow cytometry and fluorescence microscopy in a single platform, providing multi-spectral imaging of heterogeneous cell populations. This technology provides quantitative analysis of cellular populations combining morphological patterns with immunofluorescence staining (Bourton et al., 2012). This rapid and technically simple method permits cell populations to be quantitatively assessed for abundance and localisation of target proteins.

6.2. MATERIALS AND METHODS

6.2.1. Sandwich ELISA

A commercially available ELISA kit for human-IFNα multi-subtypes (PBL InteferonSource, Thermo Scientific) was used for this study to quantify IFNA1 in media using a sandwich immunoassay. This kit detects 14 out of 15 known human IFNα subtypes (**IFN-α1**, IFN-αD, IFN-α2, IFN-α4a, IFN-α4b, IFN-αA, IFN-αB2, IFN-αC, IFN-αG, IFN-αH, IFN-αI, IFN-αJ1, IFN-αK, and IFN-αWA) with a lower limit of detection of 156 pg/ mL. It is based on the international reference standard for human IFN-α, which is provided by the National Institute of Health.

Exponentially growing cells were seeded at a density of 1×10^6 cells/ml. After 72 hours, 1 ml of each cell culture supernatant was collected and transferred into a sterile Eppendorf tube and stored at -20°C until further analysis.

6.2.1.1. Preparation of reagents

- Wash buffer (stored at 4°C)
  50 ml of the wash buffer concentrate
  dH_2O to 1L

- Human IFN-α solution (10,000 pg/ml)
  An extended range standard curve (156–5000 pg/ml) was constructed by conducting the following serial dilution (figure 6.1).

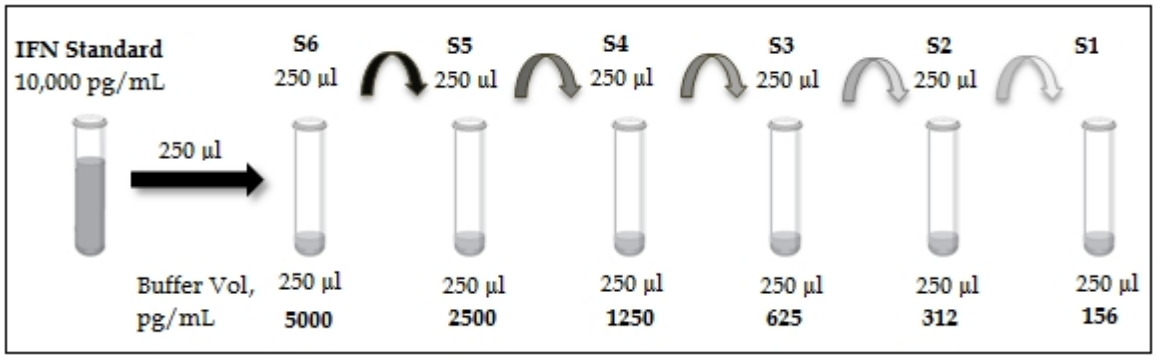

Figure 6.1: Extended range serial dilution (156-5000 pg/mL) of human IFN-α (PBL Interferon Source protocol)

- IFNα detection antibody
  20µl of antibody concentrate
  6 ml of dilution buffer

- Secondary antibody conjugated
  27µl of HRP conjugated concentrate
  8 ml of concentrate diluent

6.2.1.2. Coating with antigen

Following the manufacturer's protocol, cell culture supernatants were loaded to the designated wells by pipetting 100µl of each tested sample, in triplicate, in a pre-coated microtiter plate with the capture antibody. In parallel, 6 wells were designated for IFN-α standard and 3 wells were used for blanks containing sample diluent only. The plate was then incubated overnight at 4°C. The following day, the contents were emptied and the plate was washed once by filling the wells with 250µl of wash solution. The plate was left on a shaker for 5 minutes. The washes

were removed by flicking the plate over a sink and patting the plate on a clean paper towel.

6.2.1.3. Incubation with antibodies

A total of 100µl of diluted detection antibody was added per well, thereby forming a 'sandwich' consisting of capture antibody–IFNα–detection antibody. The plate was sealed with adhesive plastic and incubated for 1 hour at room temperature. At this stage, the detection antibody identified a different epitope on the IFN-α protein than that of the coating antibody. Following incubation, the plate was washed 3 times with 250µl of wash buffer for 5 minutes each with shaking.

Following this step, 100µl of diluted HRP conjugated secondary antibody was added in each well. The plate was sealed and incubated for 1 hour at room temperature. After 4 washes, 100µl of tetramethylbenzidine (TMB) substrate solution was added in each well and incubated in the dark for 15 minutes at room temperature. After incubation, an equal volume of stop solution (2N H_2SO_4) was added to each well. Absorbance was measured on a microplate reader at a wavelength of 450 nm.

6.2.2. Quantitation of intracellular IFNA1 Protein Expression Using the ImageStream^{x}

This cytometric approach was used to analyse the intracellular IFNA1 protein synthesis in the parental UACC-903 cells and the following transfected clones: clone 1pcDNA3 empty vector, clone 4 and clone 8.

6.2.2.1. Cell Fixation

A monolayer of cells at 80-90% confluence was washed with 10 ml of cold PBS. Cells were gently detached by trypsinisation with 1 ml of 0.25% trypsin-EDTA and pelleted by centrifugation. In an Eppendorf, cells were washed twice with 1ml of cold PBS before fixation in cold (-20°C) methanol:acetone (50:50% v/v) for 5 minutes at 4°C.

6.2.2.2. Antibodies Staining

Fixed cells were rehydrated with three washes of cold PBS and subsequently permeabilised for 5 minutes at room temperature in PBS containing 0.1% Triton X-100 (Sigma-Aldrich). In order to detect intracellular or intraorganellar antigens, permeabilisation is required to give cell-impermeable antibodies access through the plasma membrane, while maintaining the morphological characteristics of cells (Jamur and Oliver, 2010).

After blocking the cells in PBS containing 0.1% Triton X-100 and 5% goat serum for 1 hour at room temperature, cells were incubated at 4°C overnight in 200µl IFNA1 mouse monoclonal antibody (Santa Cruz Biotech) diluted to 1:500 in blocking solution. The following day, cells were washed with wash buffer made up of PBS containing 0.1% Triton X-100. Following three washes, cells were incubated for 1 hour at room temperature in the dark in 200 µl Alexa Fluor® (AF) 488 goat anti-mouse IgG (Invitrogen, UK) diluted to 1:1000 in blocking solution. Following antibody staining, cells were washed three times with 1 ml of wash buffer and once with 1 ml of PBS, then re-suspended in 100µl of Accumax flow cytometry buffer (PAA Laboratories Ltd.) containing 5µM of Draq5 (Biostatus Ltd.). For fluorescence compensation, samples were prepared by either omitting the secondary antibody (AF488) or Draq5 from the procedure.

6.2.2.3. Imaging Flow Cytometry

Data acquisition was performed using the Inspire™ software (Amnis Inc., Seattle, Washington), which enables images of individual cells in flow to be captured using a maximum of six optical channels. Cells were captured on channel 1 for brightfield (BF), which shows cell size and morphology; on channel 2 for AF488 green staining of IFNA1 protein; and on channel 5 for Draq5 red staining of the nuclear region of each cell. Cell classifiers— an instrument threshold that classifies obtained cellular images and differentiates them from objects that fall outside the cell classification parameters such as debris and cell clumps— were applied to all three channels to capture objects that range between 50 and 300

units. This classifier range was empirically determined from previous experimentations to capture primarily single cell images. Following excitation with a 488nm laser set at 40mW, a total of approximately 10,000 cells were captured at 40× magnification at a rate of ~150-200 cell images per second.

Images of 500 positively stained cells from each fluorochrome, AF488 and Draq5, were collected without BF illumination —since it is critical to capture fluorescence intensity with a single source of illumination (40 mW 488 nm laser).

6.2.2.4. Image Compensation

To ensure accurate representation of fluorescence for each captured cell, the compensation files were digitally calculated and used to create a compensation matrix, which subtracts fluorescence signal that leaked into adjacent channels. After selecting the control files created from the AF488 and Draq5 samples, the Ideas™ compensation wizard generated a table of coefficients to place the detected light displayed by each image into the corresponding channel on a pixel-by-pixel basis. Calculated compensation values were then applied to the subsequent analysis.

6.2.2.5. Analysis using Ideas™ Software

The analysis is a multistep process that comprises a series of predefined 'Building Blocks'. These tools generate a series of scatter and histograms plots that allow the identification of single, focused and double-fluorescent positive cells (figure 6.2).

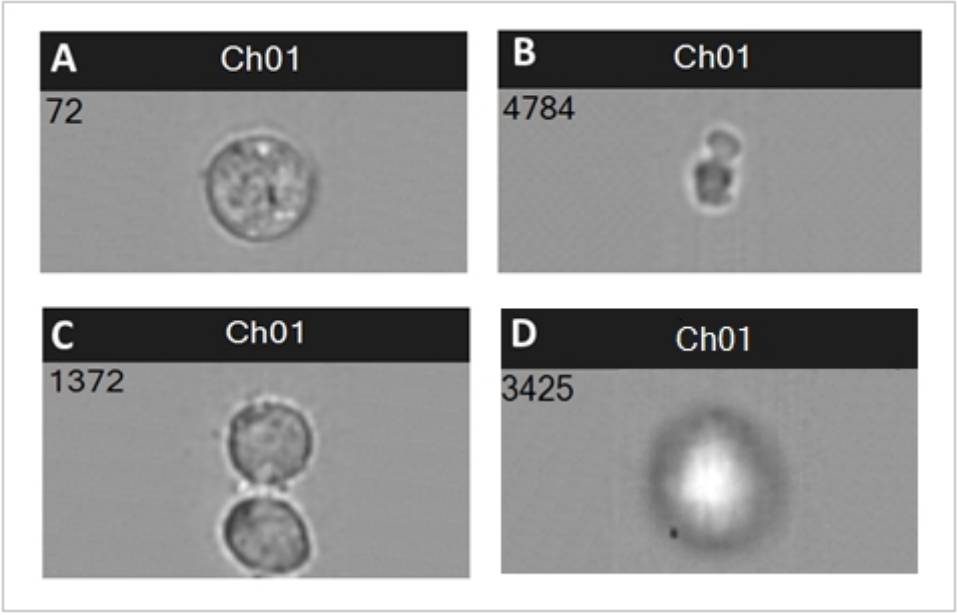

Figure 6.2: Snapshots of different objects that were captured in brightfield. Heterogeneous cell populations from the BF displaying: A| single cell in focus, B| debris, C| doublet cells and D| single cell out of focus. Debris, doublet cells, and cells out of focus have all been excluded before further analysis.

6.2.2.5.1. Single Cells

A population of single cells from the BF images was visually defined and gated using the polygon region tool, once debris and doublet cells have been excluded.

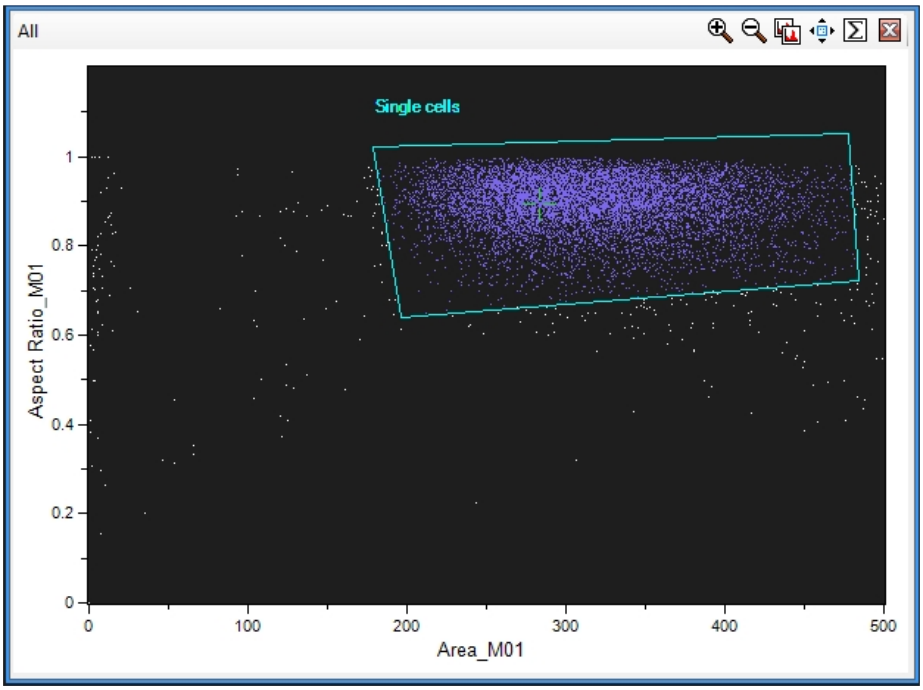

Figure 6.3: A building block tool showing a scatter plot of a defined single cell population. Each dot within the polygon region represents a single cell. Events corresponding to debris and cell clusters, such as doublets, were eliminated. Single cells are shown within the polygonal region.

6.2.2.5.2. Cells in Focus

The 'Focus' tool was then used to distribute the single cell population in histogram 'bins' based on the calculated focus of the BF images. The cells in focus were visually defined by clicking on each individual histogram bin and were selected using the line region tool.

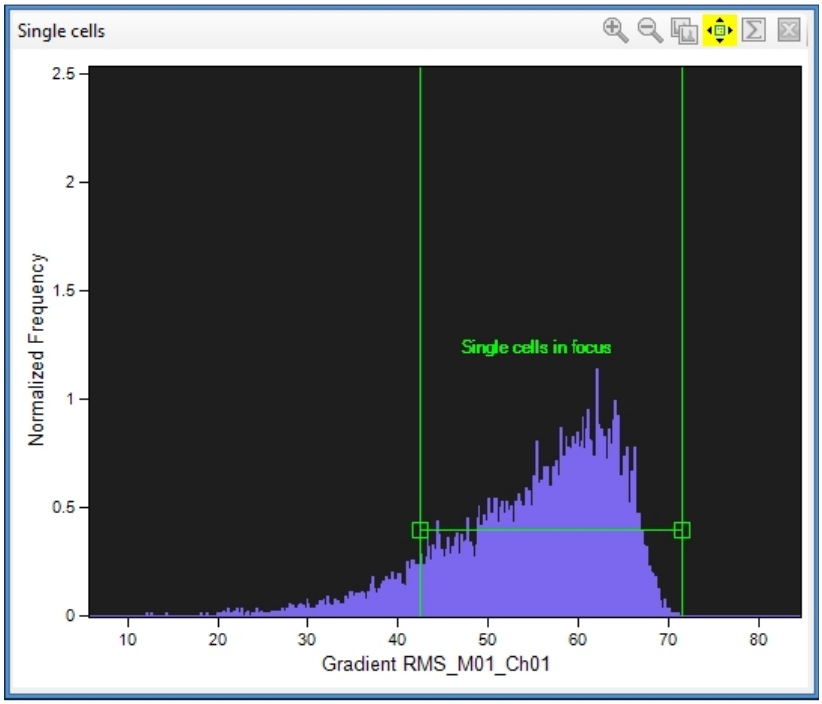

Figure 6.4: A predefined building block tool showing single cells distributed in histogram bins. Single cells in focus were defined by using the line region tool highlighted in purple. The histogram bins outside the highlighted region define the cells out of focus.

6.2.2.5.3. Double Stained Cells

Finally, using the 'Fluorescence Positive Two Colours' tool, a scatter plot of single cells in focus that stained for both AF488 and Draq5 were gated and enumerated utilising a polygon tool.

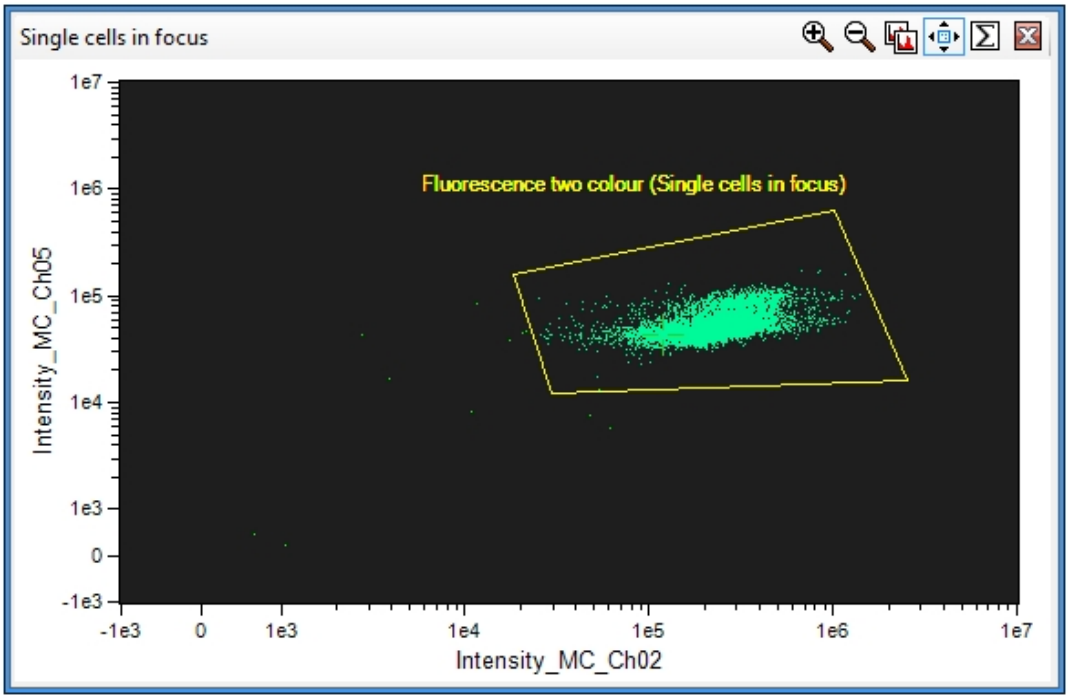

Figure 6.5: A scatter of single cells in focus that have been stained with both AF488 and Draq5. Positively stained cells were gated using the polygon tool. The x-axis plots the fluorescence intensity of green AF488 (480-560nm) in channel 2, while the y-axis plots the fluorescence intensity of red Draq5 (642-745nm) in channel 5.

6.3. RESULTS

6.3.1. ELISA Analysis

Given that interferons are extracellular signalling cytokines, ELISA was ideal for assessing IFNA1 production in the transfected clones culture media.

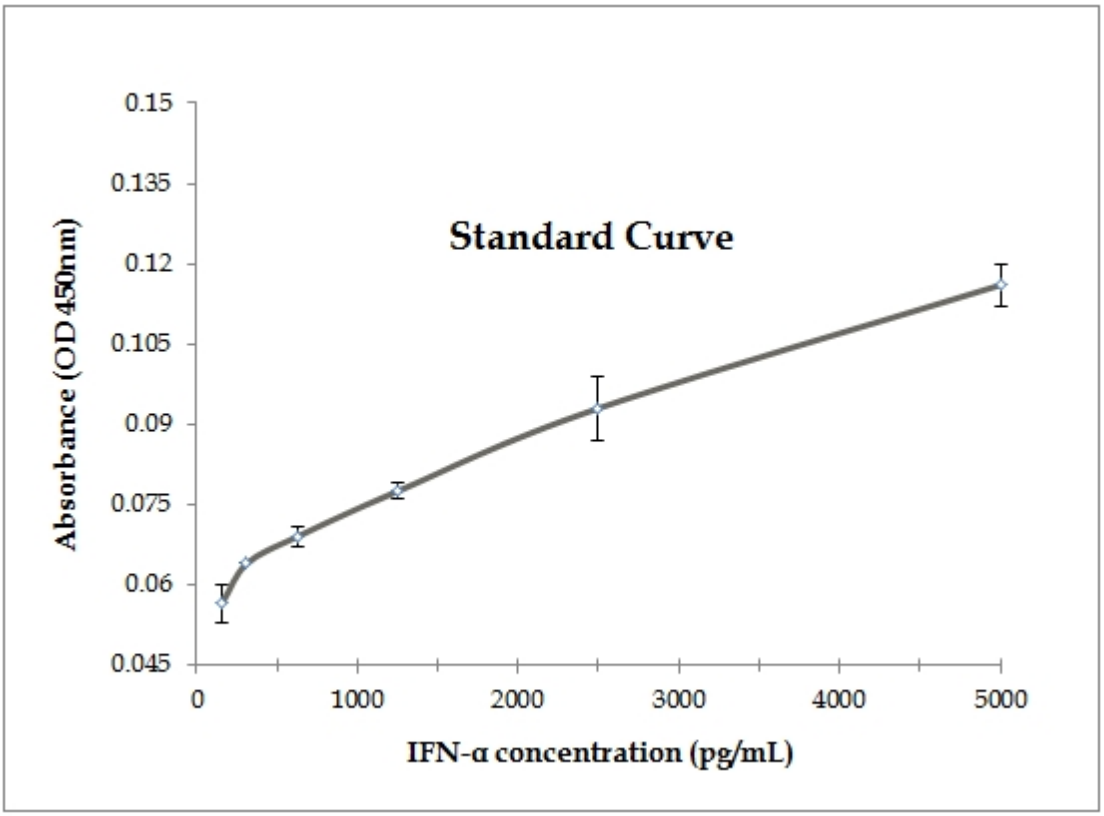

Figure 6.6: ELISA standard curve using extended range serial dilution of the IFN-α standard. This assay was performed using extended range protocol, in which the standard curve concentrations used for the sandwich ELISA were 5000 pg/mL, 2500 pg/mL, 1250 pg/mL, 625 pg/mL, 312 pg/mL, 156 pg/mL.

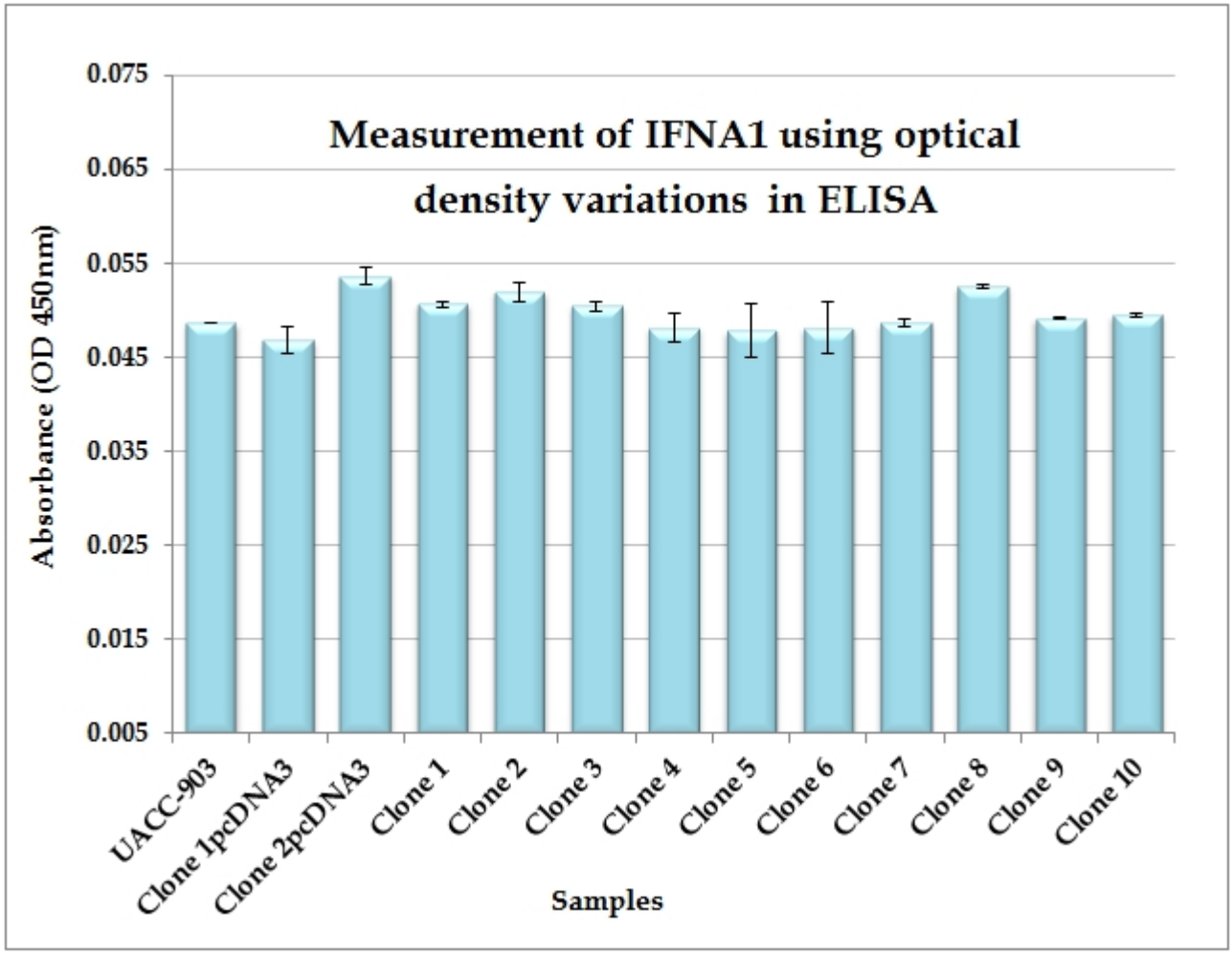

Figure 6.7: Quantitative measurement of IFNA1 production in culture media using sandwich ELISA. The optical density (OD) or fluorescent units of the samples was determined within 5 minutes and read at a wavelength of 450nm. The results show no significant difference between all tested samples. Error bars represent standard deviations from the mean values. Data shown is the representative of two independent experiments.

After testing the supernatant of each transfected clone, the analysis revealed a reading ranging from 0.48 to 0.54 OD 450nm— equivalent to 132.5pg/mL to 148pg/mL, which implies that IFNA1 levels were below 156 pg/ mL, the detection limit of this ELISA kit.

Since we could not detect high circulating levels of this cytokine, imaging flow cytometry was the ultimate method to localise IFNA1. This technology allows different cell populations to be quantitatively assessed for differences in sub-cellular localisation of target proteins.

6.3.2. Analysis of protein levels using the ImageStream^x

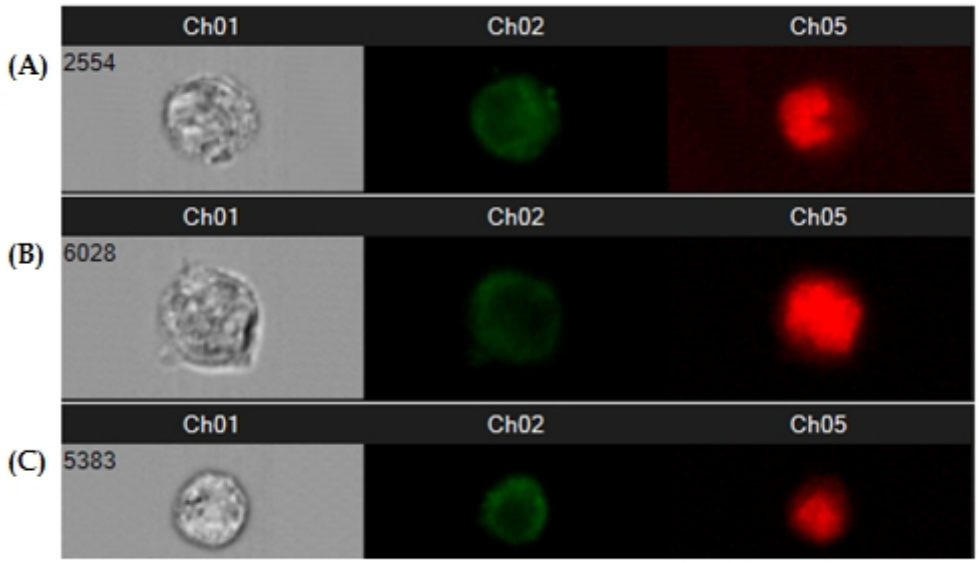

Figure 6.8: Representative images derived from imagining flow cytometry displaying brightfield images along with AF488 and Draq5 staining. The above images have been depicted in the first column for BF (Ch01) to display cell morphology, the second column (Ch02) for AF488 stained UACC-903 cell variants, and finally the third column (Ch05) for Draq5 staining of the nuclear region. Row (A) represents parental UACC-903; row (B) shows Clone 1pcDNA3; and row (C) represents Clone 4. While Draq 5 clearly stains the nuclei in red, IFNA1-AF488 immunoreactivity seems weak, resulting in poorly stained cells.

Figure 6.9: Representative ImageStream flow cytometry images showing IFNA1 protein expression in clone 8. The captured images, taken from different enumerated cells of clone 8, were stained with anti-IFNA1 antibody conjugated with AF488 (green) to identify the target protein, and Draq 5 (red) to identify the nucleus. While the nuclei are clearly stained in red, the observed green fluorescence vividly appears in the cellular membrane, suggesting the localisation of IFNA1.

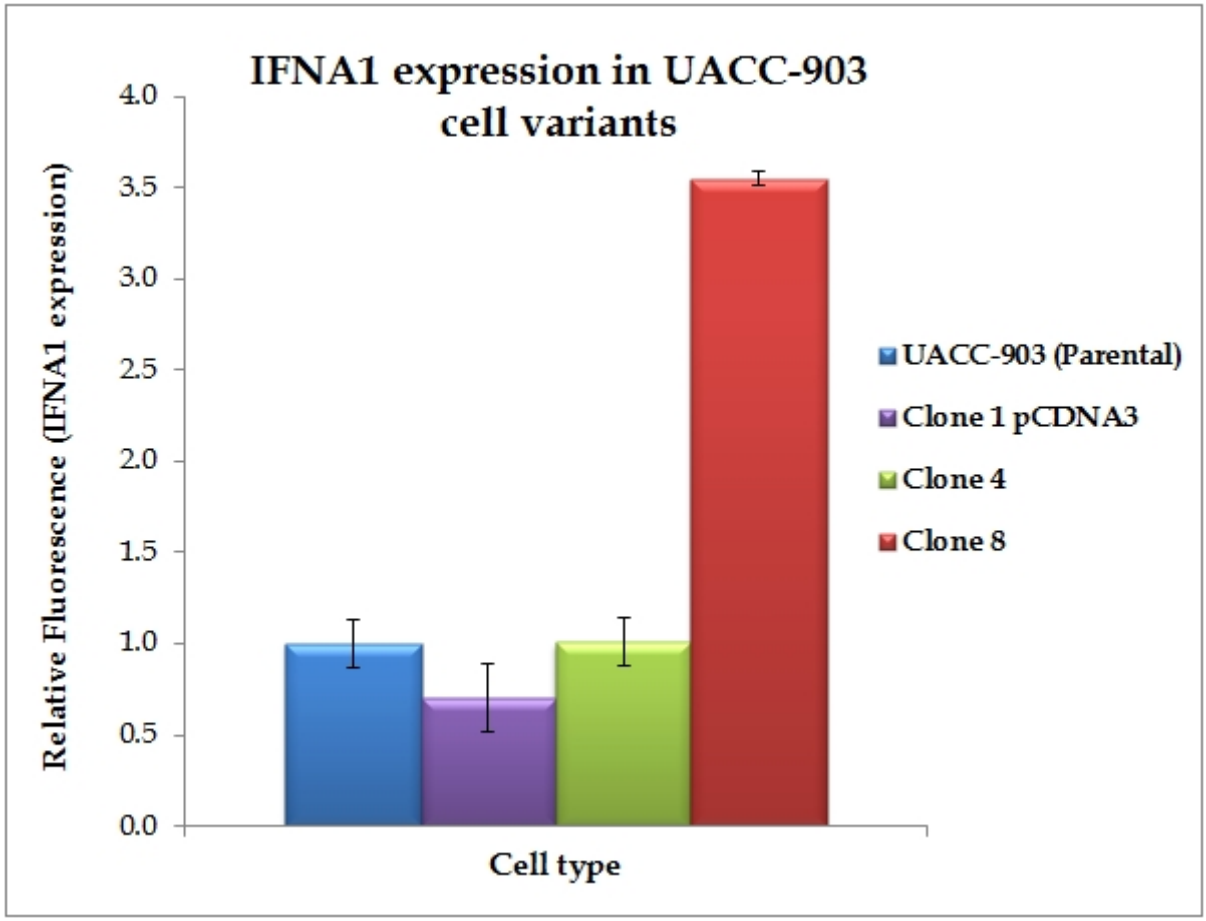

Figure 6.10: Relative fluorescence levels of IFNA1 expression in UACC-903 cell variants. Relative fluorescence of IFNA1 expression, ranging from 0.7-3.55, was calculated by dividing the fluorescence levels of each clone by the fluorescence exhibited in the parental cell line (control). Error bars represent standard deviations from the mean values. Data shown is the representative of two independent experiments in which approximately 10,000 cells were collected and analysed.

6.4. DISCUSSION

As previously demonstrated, IFNA1 cDNA was stably transfected in UACC-903 cells; therefore, it seemed critical to assay the levels of IFNA1 protein. Using a double-antibody sandwich ELISA, wherein the antibodies are directed against two or more distinct epitopes, cell culture supernatants were tested for IFNA1 production in a quantitative manner, in which the optical density of the tested samples was interpolated into a standard curve, prepared from a serial dilution of human IFN-α standard solution, provided at 10,000pg/mL.

Given that IFNA1 is secreted extracellularly, it appeared promising to detect high levels of this cytokine in media. The lower end of the extended range of the IFN-α ELISA was 156pg/mL; however, IFNA1 could only be detected at lower levels, between 132.5pg/mL and 148pg/mL; hence, below the detection limit of the used kit. It is well-established that gene mutations can result in a malfunctioning or missing protein. OD values demonstrated no significant variation between the tested samples and the tumourigenic controls. Altogether, this indubitably implies that the target protein could not be detected, which either would suggest that IFNA1 mRNA was produced but not translated, or that the translated mRNA yielded an inactive product as the result of a mutation.

It may seem paradoxical that mRNA expression levels did not correlate with protein abundance, however, high interferon gene expression without detectable secretion of the protein has been previously reported by Shuttleworth and colleagues, in which the treatment of human lymphoblastoid (Namalwa) cells

with Sendai virus induced the IFN-β gene expression without protein secretion (Shuttleworth et al., 1983).

Although mRNA is eventually translated into protein, this does not signify that there should be a direct correlation between the levels of mRNA and protein abundance. Initially, post-transcriptional modifications are vital for the final synthesis of the native protein, however, there are several complicated and varied post-transcriptional mechanisms involved between transcription and translation which can affect the post-translational modifications. On the other hand, proteins can differ substantially in their half-lives as a result of varied protein synthesis and degradation (Greenbaum et al., 2003). Therefore, the general lack of correlation between mRNA levels and protein abundance could be attributed to experimental challenges, and/or the complex fundamental biological factors that take place between transcription and translation processes.

Since we could not detect the target protein extracellularly, imaging flow cytometry was the alternative method to assess IFNA1 protein levels intracellularly. Based on the morphometric cellular analysis that depicts the fluorescence features of the two-dimensional images, and the statistical analysis of their fluorescence features, ImageStream enabled us to detect and localise the target protein.

Using the parental UACC-903, clone 1pcDNA3 empty vector, and clone 4— which exhibited the highest growth ability (98%) for anchorage independence in soft agar and displayed very low mRNA expression levels in qRT-PCR, as controls, we tested clone 8 for intracellular IFNA1 protein expression. The latter

has previously showed significant suppression (0%) in soft agar and considerably the highest mRNA expression levels.

After running the test samples through the ImageStream^{x}, the system generated an automated quantitation of events (figure 6.10). All the analysed images depicted clearly stained nuclei with Draq 5, and while IFNA1-AF488 immunoreactivity seemed very weak in the controls (figure 6.8), the green fluorescence in clone 8 (figure 6.9) appeared briskly within the cellular membrane, which suggests the localisation of the target protein. The intracellular IFNA1 protein expression was 3.55-fold higher in clone 8 than the tumourigenic controls.

The endoplasmic reticulum (ER) is essential for the folding and processing of proteins. In order for secretory proteins to fold properly, this protein-folding machinery should maintain a dynamic balance between the ER protein load and the ER folding capacity. However, perturbations to ER homeostasis cause accumulation of unfolded or misfolded proteins in the ER (Oslowski and Urano, 2011).

Attempts to detect IFNA1 protein by imaging flow cytometry were successful, since the antibody recognised the target protein and generated a vivid green fluorescence. Since the extracellular signalling cytokine appeared to be accumulated within the cells, this could suggest that the cells suffer from endoplasmic reticulum stress. The accumulation of misfolded or unfolded proteins in the ER trigger ER stress, eliciting the unfolded protein response (UPR), which subsequently lead to a major reduction of protein synthesis (Cohen-Cymberknoh et al., 2013).

CHAPTER 7

THE RELATIONSHIP BETWEEN *IFNA1* EXPRESSION AND INDUCTION OF APOPTOSIS IN UACC-903

8.1. INTRODUCTION

Although IFN-α antitumour effects have been widely documented, the precise mechanisms that trigger and potentiate this behaviour are not fully elucidated. Given that some of the transfected clones failed to grow colonies in soft agar, I investigated the possible pro-apoptotic effects of *IFNA1* in mediating the growth inhibition in these clones. In this study, I have examined the relationship between *IFNA1* expression and apoptosis induction in the transfected UACC-903 clones by monitoring the process through imaging flow cytometry using annexin V-FITC assay.

Cellular homeostasis is maintained through an orchestrated balance between cell proliferation and cell death. This latter typically follows one of two types, namely apoptosis and necrosis, both involving a series of biochemical and morphological

events ultimately leading to cell death. In 1972, Kerr *et al*. introduced the concept of apoptosis to describe distinct form of cell death by necrosis with fundamentally different morphological features [reviewed in (Teraki and Shiohara, 1999)]. The morphological characteristics of apoptosis are manifested by the formation of apoptotic bodies, which involve chromatin condensation of nucleus and cytoplasm, nuclear fragmentation, and separation of protuberances on the cell surface. These apoptotic bodies are rapidly phagocytosed and degraded by other cells without any inflammatory phenomena (Kerr et al., 1972)

The apoptotic process can be triggered through two main pathways, either the extrinsic pathway or the intrinsic pathway (figure 7.1). The extrinsic pathway is initiated by a signal of death receptors on the cell surface, which are activated upon binding to their respective ligands— such as TNF-α (tumour necrosis factor-α) or FasL (Fas ligand). A signalling cascade is mediated, which in turn recruits adaptor proteins leading to the death-inducing signalling complex (DISC) formation and the subsequent activation of the initiator caspase-8 or caspase-10. On the other hand, the intrinsic pathway is tightly triggered by the interacting pro- and anti-apoptotic members of Bcl-2 (B cell lymphoma-2) protein family, which regulates the integrity of the outer mitochondrial membrane. The activation or up-regulation of the latter leads to mitochondrial outer membrane permeabilisation, and results in the activation of initiator caspase-9 (Rodrigues et al., 2012).

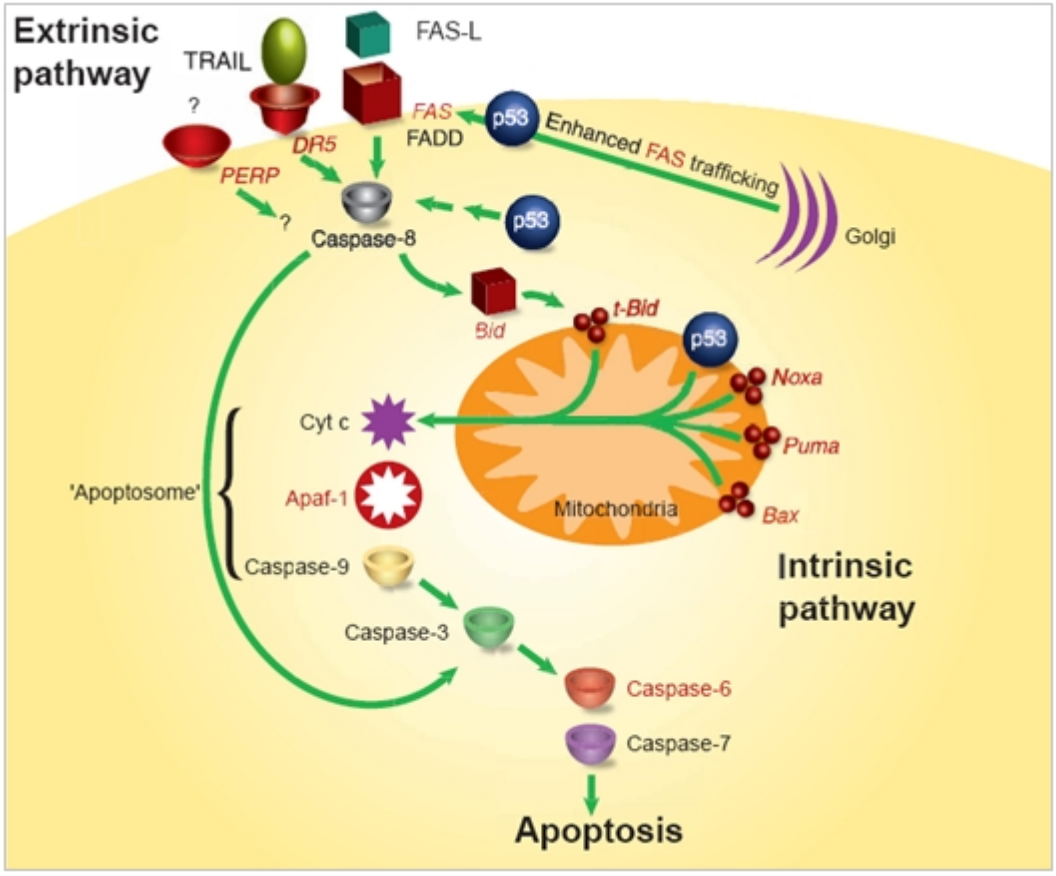

Figure 7.1: A model for p53-mediated apoptosis in the intrinsic and extrinsic pathways. p53 target genes are shown in red. In response to diverse cellular insults, such as DNA damage, p53 activates the intrinsic mitochondrial apoptotic pathway by inducing the expression of at least three Bcl-2 pro-apoptotic members (Bax, Bak, Bid, NOXA, and PUMA), shifting the balance toward pro-apoptotic effects. p53 can activate the extrinsic pathway through the induction of genes encoding Fas, DR5, and PERP transmembrane proteins, which in turn promotes cell death through caspase-8 (Haupt et al., 2003).

The malignant transformation of normal cells is attributed to the malfunctioning of apoptosis. Inactivation of pro-apoptotic signalling, or activation of anti-apoptotic pathways confer a survival advantage to tumour cells (Ghavami et al., 2009). Several reports have implicated mutations within caspase family proteases in cancer development. For instance, Soung and colleagues screened 162 cases of

gastric carcinomas, 185 non–small cell lung cancers, 93 breast carcinomas, and 88 acute leukemias to explore the possible contribution of caspase-8 mutation in the development of malignancy. Their results suggested that caspase-8 mutation strongly contribute to the pathogenesis of gastric cancers, especially at the late stage of gastric carcinogenesis (Soung et al., 2005). In addition, Bernstorff *et al*. suggested that pancreatic cancer cells become resistant to apoptosis by evading immune surveillance *in vivo*. In pancreatic adenocarcinomas, partial or complete loss of Fas expression has been associated with the malignant phenotype (Bernstorff et al., 2002). Moreover, there is evidence indicating that polymorphisms in the promoter region of the caspase-9 gene are significantly associated with the risk of developing lung cancer in smokers (Park et al., 2006).

Life and death of cells is determined based on a delicate balance between pro-apoptotic and anti-apoptotic mechanisms. Malignant melanoma is notoriously resistant to treatment, although the mechanisms by which melanoma cells bypass the apoptotic machinery are still unclear. To identify survival-apoptosis molecular signalling pathways in melanoma, Zhang and colleagues used UACC-903 and chromosome 6-mediated suppressed cell line UACC-903(+6). These genetically linked cell lines exhibit distinctive phenotypic characteristics along with different levels of resistance to apoptosis, in which UACC-903 is highly resistant and UACC-903(+6) is sensitive. This study identified 154 differentially expressed genes, including pro-apoptotic and anti-apoptotic, underlying resistance and sensitivity to apoptosis. Interestingly, expression of 10 pro-apoptotic genes—*FDX1*, *BCAP31*, *BNIP1*, *VDAC1*, *FDXR*, *BAK1* [encoded by 6p21.3], *TNFSF10*,

FAS, *CASP6* and *CASP3*— were up-regulated in UACC-903(+6) and down-regulated in UACC-903 before UV treatment. Conversely, in response to the UV treatment, UACC-903 displayed up-regulation of all 10 genes. In addition, the expression patterns of the anti-apoptotic genes — *CLN3*, *MCL1* and *BCL2L1* — were up-regulated in UACC-903(+6) and down-regulated in UACC-903 before UV treatment. However, once induced with UV treatment, the UACC-903(+6) displayed down-regulation of *MCL1* and *BCL2L1*, wherein UACC-903 displayed up-regulation of all 3 genes. Taken together, the apoptotic differences between these two cell lines strongly suggest the presence of differential molecules that regulate survival and apoptosis (Zhang et al., 2008).

Interferon-alpha is a pleiotropic cytokine that has been extensively used in the treatment of a variety of cancers, though its antitumoural activity and mechanism of action are incompletely characterised (Thyrell et al., 2002). It has been suggested that IFNα exerts its apoptotic pathways as a possible anti-tumour mechanism (Luchetti et al., 1998). In addition, it has been previously established that IFNα can directly induce apoptosis on human squamous cancer (Rodriguez-Villanueva and McDonnell, 1995). Furthermore, a study by Sangfelt *et al*. reported that IFNα is a direct inducer of apoptosis, stating that this biological phenomenon occurs independently of cell growth inhibition (Sangfelt et al., 1997).

Stimulating the apoptotic sensitivity with IFN treatment has been previously documented. For instance, investigation on myeloma and glioma cell lines

suggested that long term treatment with IFN sensitised cells to Fas-induced apoptosis. Furthermore, effects of IFNα2 in basal cell carcinoma may mediate apoptosis. In fact, injection of IFNα2 into basal cell carcinomas induces FasR and leads to tumour regression [reviewed in (Caraglia et al., 2005)].

The biological responses of cells to the clinical anti-tumour effects of IFN treatment are pleiotropic. IFNα therapy is beneficial for some neoplasms whereas other types could be partially or completely resistant. *In vitro* studies suggested that the alteration of JAK-STAT (Janus kinases-signal transducers and activators of transcription) components of the IFNα-induced signalling could most possibly be the mechanism behind drug resistance. In fact, the resistance to the antitumoural effects of IFNα has been correlated to altered signal transduction pathways of STAT protein in several types of cancer. Wong *et al*. established that the non-responsiveness of melanoma cell lines to the antiproliferative effects of IFNs arises from STATs deficiency, and this may represent a general mechanism underlying IFN resistance that many cancers develop [Reviewed in (Caraglia et al., 2005)].

7.2. MATERIALS AND METHODS

The ImageStream^{x} technology was employed to accurately analyse the prevalence of apoptotic cells using a commercial kit of Annexin V-FITC assay (BD Biosciences, San Diego, CA).

7.2.1. Cell Staining

Cells were routinely cultured in growth medium supplemented with 10% foetal bovine serum and 2mM L-glutamine, and grown as monolayers at 37°C in a humidified atmosphere of 10% CO_2 air. For staining, cells were washed twice with cold Dulbecco's PBS (with Ca^{2+} and Mg^{2+}) and then gently detached by adding 1ml of Accutase^{TM} (PAA) to each culture dish. Rather than using Trypsin-EDTA, Accutase seemed to be a better alternative since it is less damaging to the cell membranes and surface epitopes, leaving the structure and function of the surface proteins intact. Thus, reducing the chances of developing false positive staining.

The 10X binding buffer (0.1 M Hepes/NaOH (pH 7.4), 1.4 M NaCl, 25 mM CaCl2) (BD Pharmingen) contains optimal calcium concentration that is required for annexin V binding to phosphatidylserine (PS) on the cell surface. The 10X binding buffer was diluted 1:10 in ddH2O and kept at room temperature. The cells were re-suspended in 1X binding buffer at a concentration of 1×10^{6} cells/ml. Then 100µl of re-suspended solution was transferred to an Eppendorf tube. Annexin V-FITC/PI staining solution was prepared by adding 5µl of fluorescein

isothiocyanate (FITC) and 5µl of propidium iodide (PI) to the cell suspension. Two other samples were prepared for fluorescence compensation, in which either FITC or PI was omitted from the process. All 3 tubes were gently vortexed and incubated in the dark for 15 minutes at room temperature. After the incubation period, 100µl of 1X binding buffer was added to each tube and analysed using the ImageStream^{x} within 1 hour.

7.2.2. Imaging Flow Cytometry

Using the Inspire^{TM} data acquisition software, images of 5000 cells were captured on channel 1 for brightfield (BF), which shows cell size and morphology; on channel 2 for FITC green staining; and on channel 4 for PI orange staining of the nuclear region. Subsequently, images of 500 positively stained cells with FITC only and PI only were captured without the BF illumination and used for generating the compensation matrix.

7.2.3. Image Compensation

Compensation files were digitally calculated and were applied to all subsequent analysis as appropriate.

7.2.4. ImageStream Analysis

Initially, single cells from the BF images were visually identified from a heterogeneous population of single and doublet cells as well as cellular debris, and were gated using the polygon region tool. Subsequently, single cells were distributed in histogram bins and the ones in focus were defined based on visual inspection of the images within each individual bin and were selected using the line region tool. Finally, the 'Fluorescence Positive Two Colours' tool generated a scatter of stained single cells in focus whereby a polygon tool was used to gate and enumerate the cells stained with both FITC and PI. Staining patterns in these apoptotic cells were visually confirmed by assessing their appearance in the image gallery (figures 7.2, 7.3, 7.4).

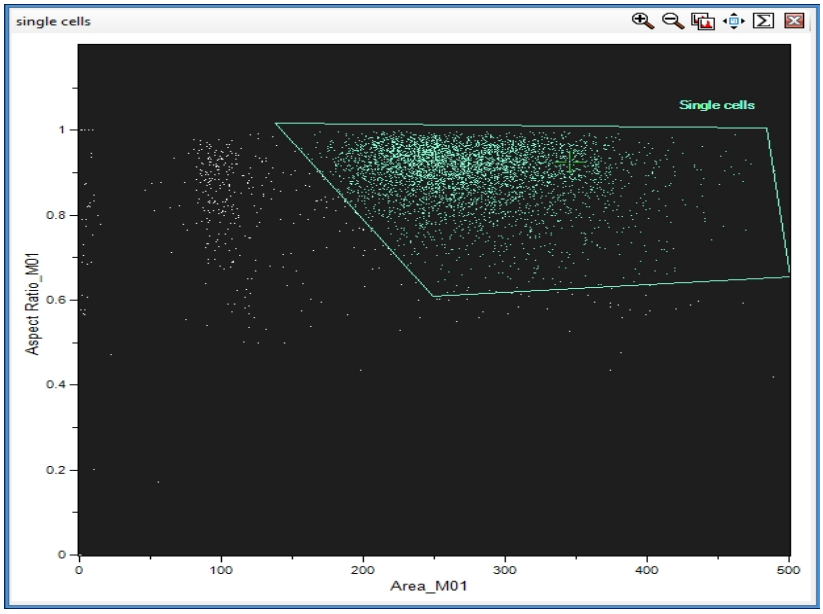

Figure 7.2: Gating for single cell population. The scatterplot single cell region was gated using the polygon tool after visually validating the BF images. The cells outside the polygon represent debris and doublet cells.

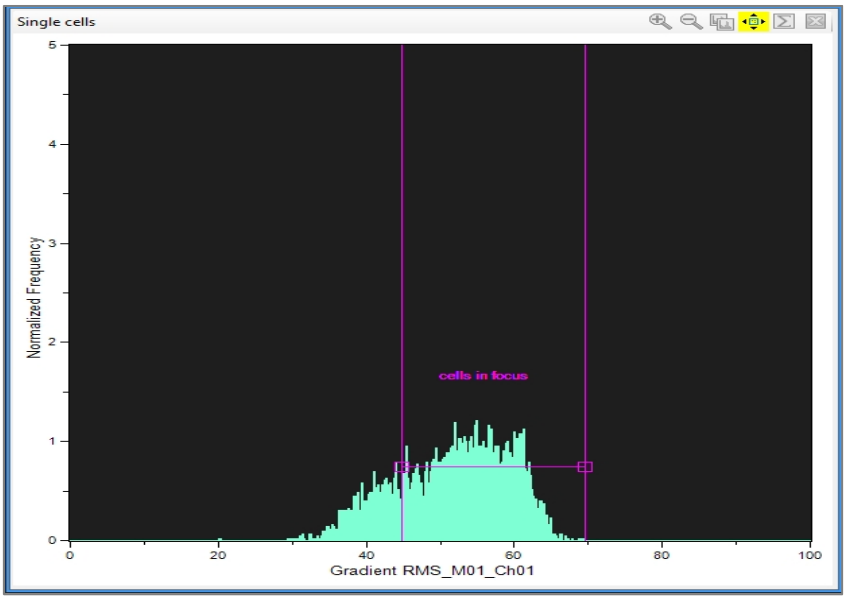

Figure 7.3: Gating for single cells in focus. The figure represents a population of single cells that were distributed in histogram bins based on the calculated focus of the BF images. Single cells in focus were visually validated and then gated using the line region tool highlighted in purple.

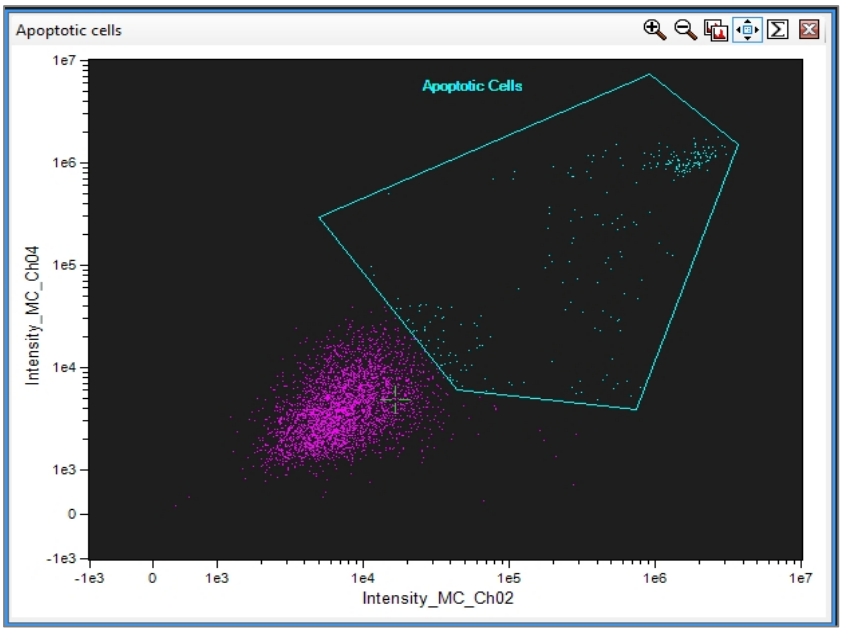

Figure 7.4: Gating for single cells in focus stained for both FITC and PI. Apoptotic cells (FITC and PI +ve) were gated using the polygon tool highlighted in blue. The fluorescence intensity of green FITC (480-560nm) is plotted on the x-axis, while the fluorescence intensity of orange PI (595-642nm) is plotted on the y-axis.

7.3. RESULTS

Inspire™ analysis software identified and quantitated apoptotic cells based on the intensity of the double-positive staining as a result of annexin V-FITC detection of the exposed phosphatidylserine and the increased uptake of PI caused by cell membrane permeability. Figure 7.5 shows different stages of apoptosis.

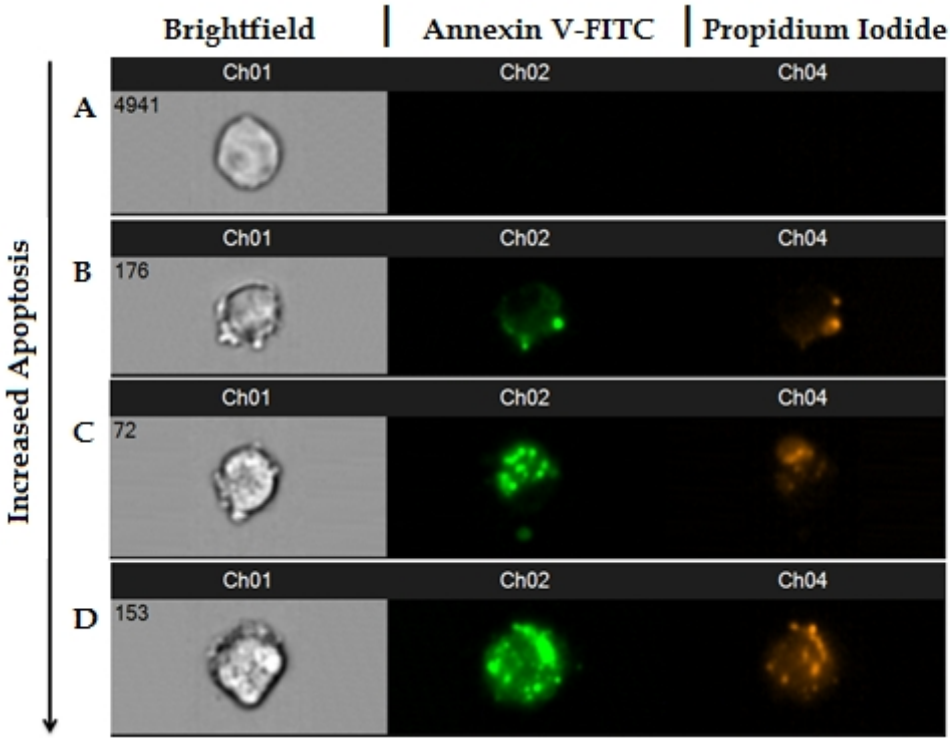

Figure 7.5: Illustrative Images derived from imagestream analysis showing BF images along with annexin V-FITC and PI staining. (A) Represents a normal non-apoptotic cell and (B to D) showing cells at different stages of apoptosis with increased intracellular staining with annexin V-FITC and PI, ranging from early apoptotic cells with light fluorescence to late apoptotic cells with membrane blebbing and intense fluorescence.

Apoptotic populations expressing the given markers were relatively assessed to two controls; unirradiated NB1-Tert cells, and treated cells with 2Gy gamma radiation from a ^{60}Coblat source. The IC_{50} for this cell line has been previously defined as the therapeutically relevant radiation dose of 2Gy (Ulus-Senguloglu et al., 2012).

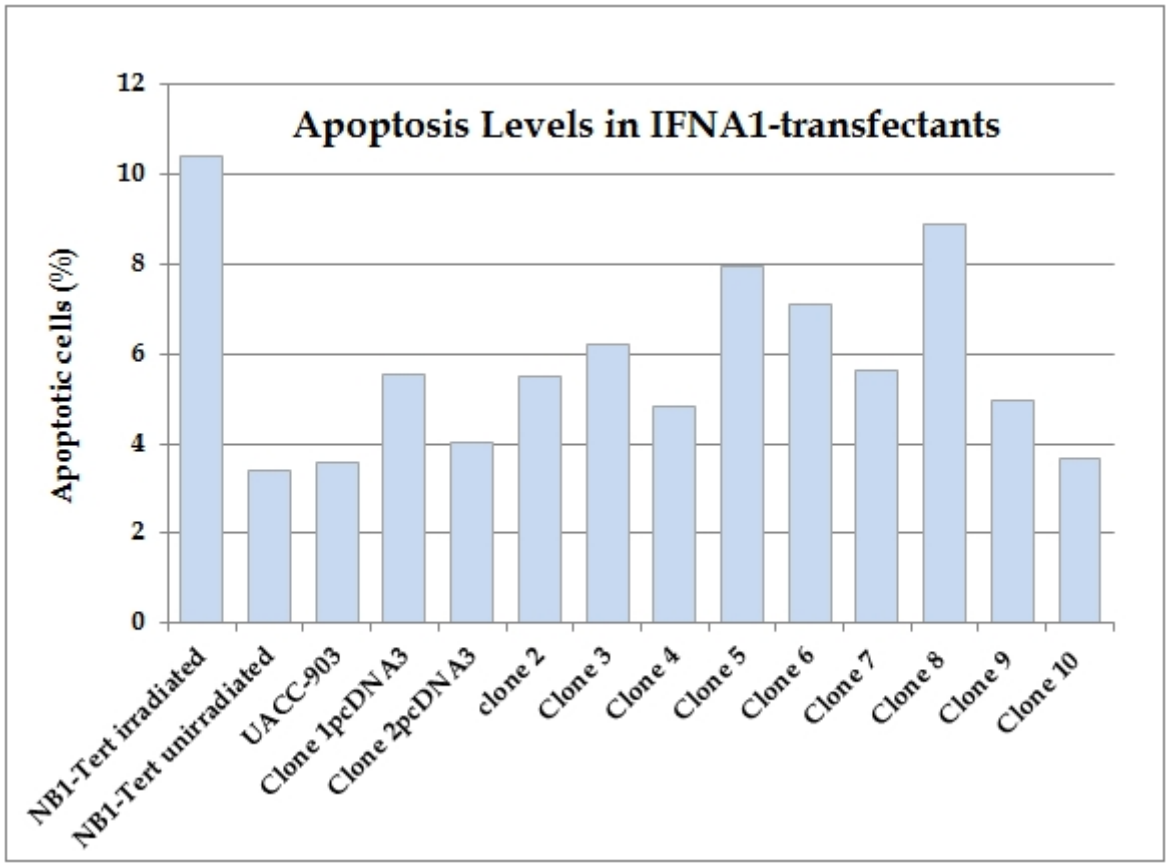

Figure 7.6: Apoptosis levels in the transfected clones. These levels were determined by annexin V-FITC and PI staining, and data were derived from analysing ≤ 5000 cells. The difference in apoptosis levels between the non-apoptotic controls (NB1-Tert unirradiated, UACC-903 and both transfected with empty pcDNA3) and the transfected clones was evaluated with *Student's* two sample test (two-tailed, with unequal variances). The results revealed a statistically significant difference in apoptosis levels (p = 0.024).

7.4. DISCUSSION

Loss of membrane integrity is one of the earliest changes in apoptotic cells, wherein the membrane phospholipid phosphatidylserine (PS) is externalised on the outer leaflet of the plasma membrane. Annexin V is a 35-36 kDa calcium dependent phospholipids-binding protein that has a high affinity for PS. An annexin V conjugate labelled with a fluorochrome such as FITC can be used to identify apoptotic cells by binding to the exposed PS. In cytometric analysis, staining with Annexin V-FITC is conjugated with a vital dye such as PI to discriminate viable from apoptotic cells (Sutton and Tchounwou, 2007).

According to the protocol provided by the manufacturer, viable cells with intact membranes are both Annexin V-FITC and PI -ve; early apoptotic cells are Annexin V-FITC +ve/ PI -ve; and cells both Annexin V-FITC and PI +ve are either in end stage apoptosis or already dead. The latter highlights the fact that this assay does not discriminate cells that have undergone apoptotic death from those that died of a necrotic pathway, as in both cases the dead cells will stain PI +ve. However, in the present study the movement of cells through these three stages indicated an apoptotic phenomenon and not necrotic.

The imagestream^{x} provides multi-spectral imaging of heterogeneous cell populations by combining the capacities of fluorescent microscopy and flow cytometry in a single platform. In this study, I have analysed a total of 5000 cells per clone in one empirical set. In comparison with the immunocytochemistry procedure, which analyses a total of 100 cells spread on a microscopic slide and

generally requires repeats, the robustness of the system we used coupled with the high analysed number did not require repeating the process multiple times.

Our data display variable levels of apoptosis in the transfected clones which were comparatively measured to the irradiated NB1-Tert cells. Since this assay was designated to investigate the possible pro-apoptotic effects of *IFNA1* in inhibiting growth in soft agar, I have conducted a correlation to establish the relationship between the two phenomena.

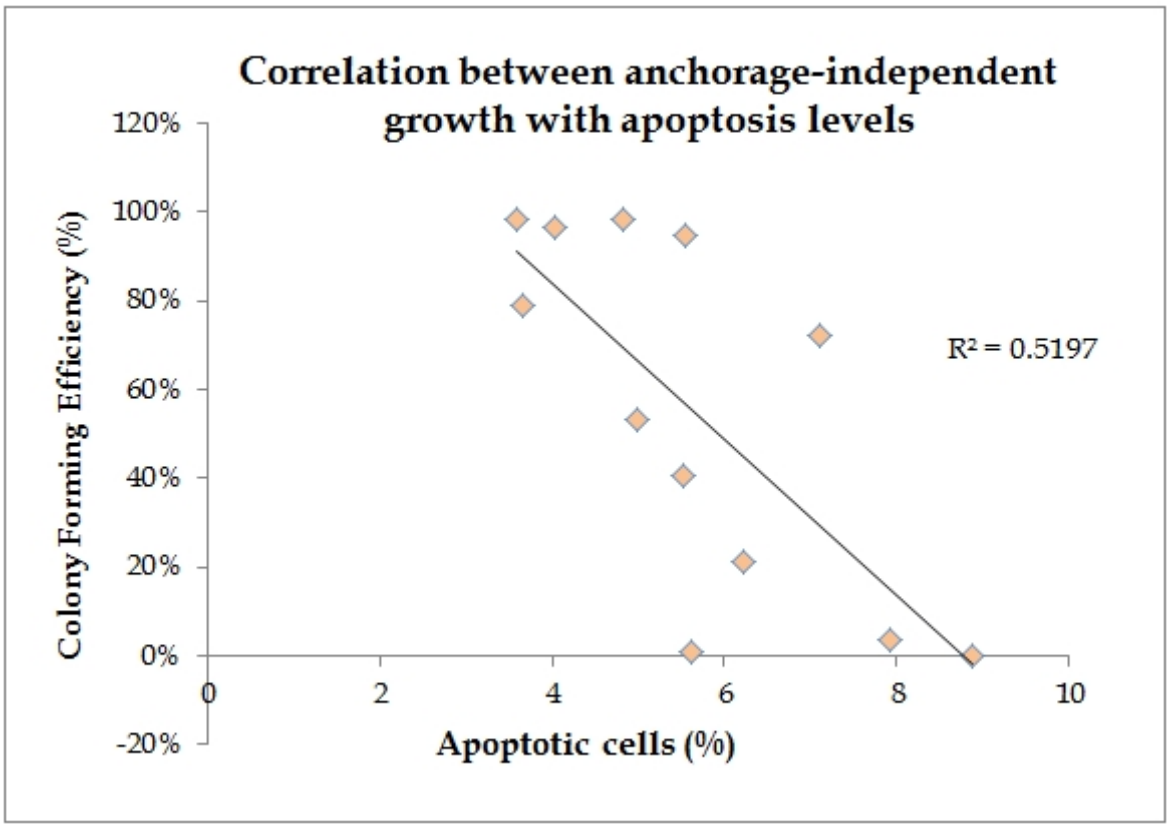

Figure 7.7: A scatter diagram showing a weak negative correlation between anchorage-independence growth in soft agar and apoptosis levels. Growth in soft agar was expressed as percentage of colony formation, and apoptosis was measured by gating the apoptotic populations.

The diagram above shows a moderate relationship between reduced efficiency of anchorage-independent growth in soft agar and high apoptotic levels. However, this correlation is rather unpersuasive in comparison with the previously documented magnitude effects of IFNα, and it probably reflects the fact that growth inhibition could well be associated with another pathway. Although our findings are not conclusive, it seems that apoptosis might not be the pathway controlling the growth in soft agar.

Although the molecular mechanisms underlying IFNα anti-tumour activity are not fully understood, Fiddler and collaborators demonstrated that IFNα-mediated antiangiogenic mechanisms may well influence the anti-tumour effects (Eggermont, 2001). In fact, IFNs exert selective effects on tumour vasculature and decrease formation of capillary-like structures *in vitro* by inhibiting collagen synthesis and ECM formation. Moreover, IFNα was reported to block tumour necrosis factor alpha (TNFα) or Interleukin-1 (IL-1)-stimulated IL-8 (angiogenic chemokine) production in human malignant melanoma cell lines (Lindner, 2002). Altogether, this postulate that *IFNA1* expression could have been influenced by the presence of angiogenic factor expression, causing growth inhibition in soft agar rather than exerting its actions through an apoptotic pathway.

CHAPTER 8

CONCLUSION AND FURTHER RESEARCH

8.1. GENERAL DISCUSSION AND CONCLUSION

Cutaneous malignant melanoma is the least common yet the most lethal form of skin cancer. It has been known to mankind since antiquity and is increasing at an alarming rate globally despite the high level of awareness. Because of its capricious behaviour, the mechanisms underlying melanoma development and progression have not been fully elucidated. Nevertheless, the aetiology of melanoma is heterogeneous and complex, whereby both environmental insults and genetic predisposition are the major well established causative factors. Allelic deletions at chromosomes 1p, 6q, 9p or 10q, 11q and 17q have been frequently observed during the development and progression of CMM; therefore, suggesting that several putative tumour suppressor genes and oncogenic factors reside in these regions.

Loss or structural rearrangement of chromosome 9 during early stages of melanoma fuelled considerable debate at the possibility that this region harbours

tumour suppressor loci. Reports demonstrated that one of the most frequently targeted regions in melanoma was within the vicinity of the IFNA gene cluster on 9p22-pter (Fountain et al., 1992). Moreover, studies of melanoma-prone families reported that susceptibly to melanoma is partially controlled by a locus known as *MLM*, located on chromosome 9p. Genetic predisposition for melanoma in these families is inherited as a dominant Mendelian trait closely linked to the IFNA gene family. Therefore, it has been proposed that a putative tumour suppressor gene lies within a region of less than 40 kb centromere-proximal to the IFNA gene cluster (Weaver-Feldhaus et al., 1994).

Parris and colleagues provided the first functional evidence of a novel melanoma tumour suppressor gene(s) that resides in the vicinity of the *INK4* locus. By means of transferring two chromosome 9 derivatives into tumourigenic UACC-903 cell line, they have demonstrated that the region spanning between IFNA (telomeric) to D9S171 (centromeric) harbours tumour suppressor(s) that functions independently of the *INK4* locus and would confer tumourigenicity if deleted.

Our previous research group study has pursued several approaches in attempt to identify genes that are responsible for tumour suppression in melanoma. Microcell mediated chromosome transfer (MMCT) was used to develop several monochromosome hybrids. This panel of hybrids was created by transferring a variant 9a chromosome derived from a normal human fibroblast primary cell line (1BR3) and maintained in a murine A9 cell background that was then transferred into UACC-903 cell line. The derivative of chromosome 9 carried a deletion at the

INK4 locus only. After selection with hygromycin B, a total of 22 resistant hybrid constructs have been assessed for anchorage-independent growth in soft agar to evaluate any suppression activity in the presence of single chromosome 9 deleted for the *INK4* locus. Interestingly, ten of these hybrids showed segregation (non-suppressors), whereas twelve of them demonstrated growth suppression (suppressors).

RT-PCR was used to evaluate the gene expression of all the functional genes mapped between markers IFNA and MTAP (figure 8.1), as previously described in Parris et al., 1999. According to the NCBI search, some of the genes in this region were pseudogenes, which are defined as non-functional copies of genes that lost their protein-coding ability. To detect any differences in gene expression patterns between the segregant and suppressor hybrids, a total of 23 functional genes were assessed. Interestingly, *IFNA1* was the only gene that was expressed in all the suppressor hybrids and in only one of the non-suppressors. This expression was further evaluated using real-time PCR, which revealed that expression of *IFNA1* gene is higher in the suppressor than its expression in the non-suppressor hybrids. Altogether, this study suggested *IFNA1* as a candidate tumour suppressor gene in CMM development.

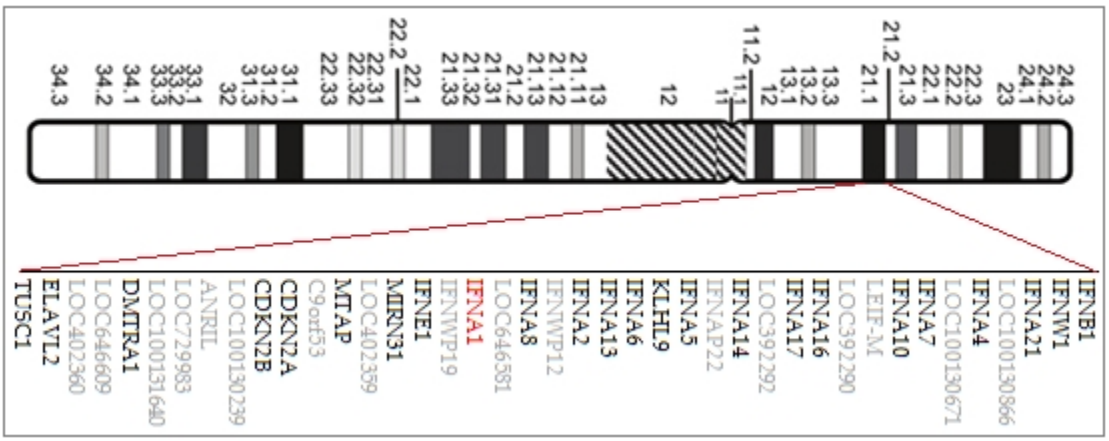

Figure 8.1: Chromosomal region 9p21 showing all the genes mapped between the markers D9S1846 and D9S171. Functional genes are in black and pseudogenes are in grey

To further validate its tumour-suppressive function, IFNA1 cDNA was cloned into pcDNA3 vector and transfected into UACC-903 cell line. Stably *IFNA1*-expressing clones were selected to further study their anchorage-independent growth in soft agar. The ability to thrive in a semi-solid medium was variable; however, two populations were observed; (a) clones that preserved their tumourigenic phenotype and demonstrated a high number of large colonies, and (b) clones that displayed a reduced ability for anchorage-independence and demonstrated few and small-sized colonies or clones that failed to grow, a rather reversed tumourigenic phenotype.

QRT-PCR was used to determine whether *IFNA1* gene expression would correlate with the tumourigenicity in soft agar. Interestingly, the analysis revealed that the gene expression patterns reflect the level of tumourigenicity in these clones, where the expression was low in the highly tumourigenic clones and substantially

higher in the less tumourigenic clones, reaching its peak in those clones that failed to grow. However, there were particular exceptions to this observation when clones 7 and 10 were assessed. Their growth in soft agar and gene expression demonstrated an inverse correlation pattern compared to the other clones. In other terms, clone 7 displayed no growth and low gene expression and clone 10 displayed growth in soft agar and high *IFNA1* expression.

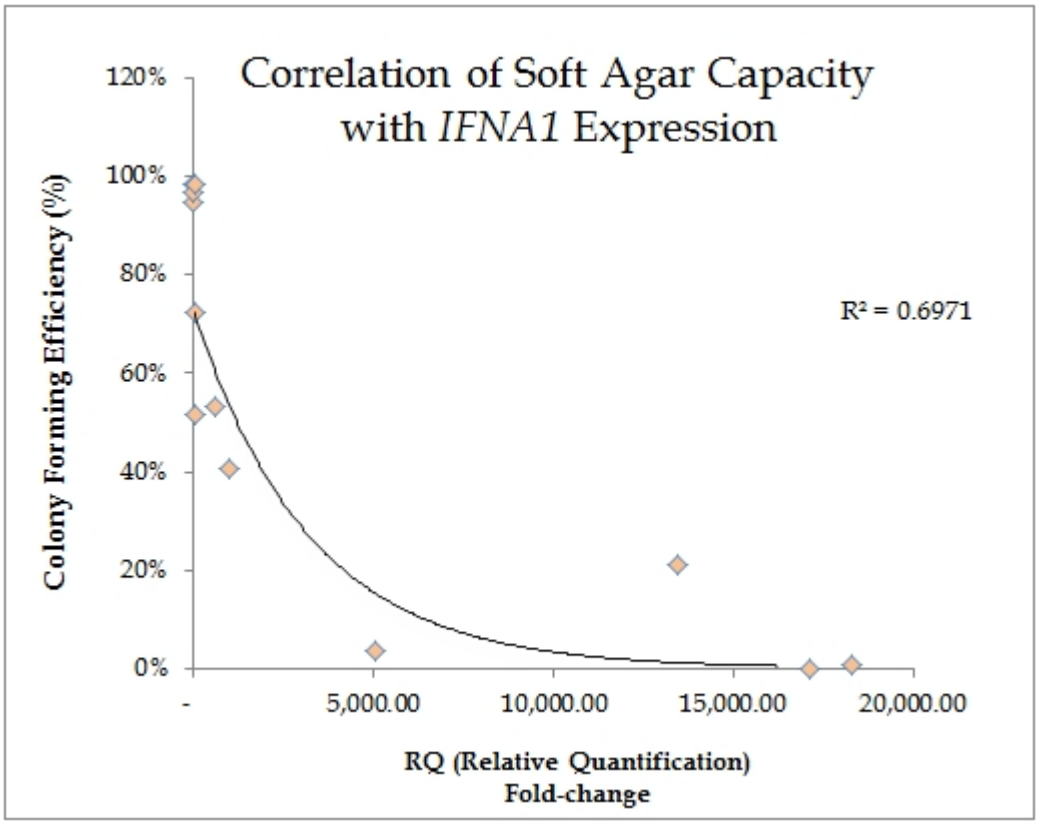

Figure 8.2: A scatter graph showing a strong correlation between anchorage-independent growth in soft agar and *IFNA1* expression in qRT-PCR. Growth in soft agar was expressed as percentage of colony formation, and real-time PCR analysis assessed the fold-change of *IFNA1* expression relative to parental UACC-903. The present trendline has a negative gradient showing that the more *IFNA1* is expressed, the less growth is observed. This correlation excluded clones 7 and 10.

IFNA1 protein expression was also tested using ELISA and imaging flow cytometry. Absent extracellular IFNA1 protein expression was observed in all clones using ELISA; nevertheless, the imaging flow cytometry analyses detected and localised the target protein intracellularly. These analyses showed that intracellular IFNA1 protein expression in clone 8 was 3.55-fold higher than in the tumourigenic controls. While this cytokine is expected to localise in extracellular spaces, the findings derived from these approaches demonstrated that the target protein is retained intracellularly, which could suggest that the transfected cells suffer from endoplasmic reticulum stress, due to the accumulation of misfolded or unfolded proteins in the ER, and subsequent reduction of protein synthesis.

IFN-α has been employed extensively in the treatment of a variety of cancers, although its antitumoural mechanisms are incompletely characterised. It has been previously reported that IFN-α can directly induce apoptosis on human squamous cancer (Rodriguez-Villanueva and McDonnell, 1995). Hence, it has been proposed that IFN-α exerts pleiotropic actions through apoptosis (Luchetti et al., 1998).

Given that UACC-903 cells are highly resistant to apoptosis, I have examined whether *IFNA1* could sensitize this resistance in the transfected clones. The process was monitored through imaging flow cytometry by using annexin V-FITC assay. This quantitative assay measures apoptosis by annexin V-FITC and PI staining by analysing approximately 5000 cells per clone.

The analysis displayed variable levels of apoptosis in the transfected clones relative to treated NB1-Tert cells with 2Gy gamma radiation. Growth in soft agar and apoptosis levels in the transfected clones showed a moderate negative correlation demonstrating that apoptosis levels get higher with reduced ability of anchorage-independence. Due to the weak correlation, the findings derived from this approach suggested that apoptosis might not be the pathway controlling anchorage-dependent growth in the suppressed clones.

Alternatively, reduced proliferation and invasion could be manipulated by the presence angiogenic factor expression. These findings, although inconclusive due to the use of only one highly tumourigenic melanoma cell line, suggest that *IFNA1* might not entirely exert its actions through apoptosis but it could also modulate angiogenesis.

8.2. RESEARCH LIMITATIONS AND FUTURE WORK

Like any research project, this study was limited by several constraints that may serve as a starting point for further research. Initially, although anchorage-independent growth in soft agar is a well-established method for assessing tumourigenicity *in vitro*, animal studies would have provided a robust and efficient way for evaluating the antitumourigenic potency of *IFNA1* in the transfected clones.

This study was carried out using only one melanoma cell line, UACC-903, which was another constraint. Considering a panel of different melanoma cell lines and

melanoma tumour samples at different stages would be useful for further investigation.

Detecting ER stress in the transfected clones, by examining the enlargement of the ER lumen using electron microscopy (Oslowski and Urano, 2011), could lead us to understand if the target protein is retained intracellularly instead of being expressed extracellularly.

The functional complementation of MMCT documented in our previous research group along with gene expression analysis and functional characterisation in the present study lend weight to strongly suggest *IFNA1* as a candidate tumour suppressor gene in melanoma pathogenesis. However, it is appealing to consider testing the gene expression status of miR-31, a neighbouring gene of *IFNA1* (figure 8.1), wherein the parent gene is located on 9p21.3 within the intron of a long non-coding RNA.

MicroRNAs (miRNAs) are central in regulating gene expression at the posttranscriptional level in the cytoplasm as well as in the nucleus (Kim et al., 2008). Some miRNAs are aberrantly expressed in human cancers, suggesting that they may play significant roles in carcinogenesis. A functional study has reported that miR-31 is overexpressed in murine lung cancers. LATS2 and PPP2R2A were identified as tumour-suppressive mRNA targets in human and mouse lung cancer cell lines. Both of these target mRNAs were downregulated by miR-31, and the expression of each was augmented by engineered knockdown, which in turn conferred marked repression of lung cancer growth *in vitro* and *in vivo*. Notably,

miR-31 and these target mRNAs were inversely expressed. Altogether, these findings revealed that miR-31 acts as an oncogenic miRNA in lung cancer by causing repression of specific tumour suppressors (Liu et al., 2010).

Down-regulation by both genomic deletion and epigenetic silencing of miR-31 gene expression is a common event in melanomas. In fact, transient overexpression of miR-31-mediated attenuation on migration and invasion was reported in various melanoma cell lines; however, its inhibitory effects have been accounted for only a subset of melanoma cell lines. Moreover, miR-31 targets multiple oncogenic kinases, which include SRC, MET, NIK (MAP3K14), and RAB27A. These findings suggested a role for miR-31 as a tumour suppressive miR in melanoma, emphasising a novel therapeutic target and a promising anti-neoplastic agent (Asangani et al., 2012).

Taken together, it would be intriguing to assess the expression of miR-31 for inhibitory effects or potential oncogenic role in the transfected clones. This analysis would sequentially elicit any antitumour responses and in turn generates a conclusive answer.

REFERENCES

ABBASI, N. R., SHAW, H. M., RIGEL, D. S., FRIEDMAN, R. J., MCCARTHY, W. H., OSMAN, I., KOPF, A. W. & POLSKY, D. 2004. Early diagnosis of cutaneous melanoma: revisiting the ABCD criteria. *JAMA,* 292**,** 2771-6.

ABDULLA, F. R., FELDMAN, S. R., WILLIFORD, P. M., KROWCHUK, D. & KAUR, M. 2005. Tanning and skin cancer. *Pediatr Dermatol,* 22**,** 501-12.

ALAPETITE, C., WACHTER, T., SAGE, E. & MOUSTACCHI, E. 1996. Use of the alkaline comet assay to detect DNA repair deficiencies in human fibroblasts exposed to UVC, UVB, UVA and gamma-rays. *Int J Radiat Biol,* 69**,** 359-69.

ALBERT, M. R. & OSTHEIMER, K. G. 2003. The evolution of current medical and popular attitudes toward ultraviolet light exposure: part 3. *J Am Acad Dermatol,* 49**,** 1096-106.

ANWAR, J., WRONE, D. A., KIMYAI-ASADI, A. & ALAM, M. 2004. The development of actinic keratosis into invasive squamous cell carcinoma: evidence and evolving classification schemes. *Clin Dermatol,* 22**,** 189-96.

ARENBERGER, P., ARENBERGEROVA, M., VOHRADNIKOVA, O. & KREMEN, J. 2008. Early detection of melanoma progression by quantitative real-time RT-PCR analysis for multiple melanoma markers. *Keio J Med,* 57**,** 57-64.

ARICO, E., CASTIELLO, L., URBANI, F., RIZZA, P., PANELLI, M. C., WANG, E., MARINCOLA, F. M. & BELARDELLI, F. 2011. Concomitant detection of IFNalpha signature and activated monocyte/dendritic cell precursors in the peripheral blood of IFNalpha-treated subjects at early times after repeated local cytokine treatments. *J Transl Med,* 9**,** 67.

ARMSTRONG, B. K. & KRICKER, A. 1994. Cutaneous melanoma. *Cancer Surv,* 19-20**,** 219-40.

ATILLASOY, E. S., SEYKORA, J. T., SOBALLE, P. W., ELENITSAS, R., NESBIT, M., ELDER, D. E., MONTONE, K. T., SAUTER, E. & HERLYN, M. 1998. UVB induces atypical melanocytic lesions and melanoma in human skin. *Am J Pathol,* 152**,** 1179-86.

AUGUSTINE, C. K., YOO, J. S., POTTI, A., YOSHIMOTO, Y., ZIPFEL, P. A., FRIEDMAN, H. S., NEVINS, J. R., ALI-OSMAN, F. & TYLER, D. S. 2009. Genomic and molecular profiling predicts response to temozolomide in melanoma. *Clin Cancer Res,* 15**,** 502-10.

BALAGURUMOORTHY, P., ADELSTEIN, S. J. & KASSIS, A. I. 2008. Method to eliminate linear DNA from mixture containing nicked circular, supercoiled, and linear plasmid DNA. *Anal Biochem,* 381**,** 172-4.

BALCH, C. M., BUZAID, A. C., SOONG, S. J., ATKINS, M. B., CASCINELLI, N., COIT, D. G., FLEMING, I. D., GERSHENWALD, J. E., HOUGHTON, A., JR., KIRKWOOD, J. M., MCMASTERS, K. M., MIHM, M. F., MORTON, D. L., REINTGEN, D. S., ROSS, M. I., SOBER, A., THOMPSON, J. A. & THOMPSON, J. F. 2001. Final version of the American Joint Committee on Cancer staging system for cutaneous melanoma. *J Clin Oncol,* 19**,** 3635-48.

BANDARCHI, B., MA, L., NAVAB, R., SETH, A. & RASTY, G. 2010. From melanocyte to metastatic malignant melanoma. *Dermatol Res Pract,* 2010.

BAR-SAGI, D. 2001. A Ras by any other name. *Mol Cell Biol,* 21**,** 1441-3.

BART, R. S., PORZIO, N. R., KOPF, A. W., VILCEK, J. T., CHENG, E. H. & FARCET, Y. 1980. Inhibition of growth of B16 murine malignant melanoma by exogenous interferon. *Cancer Res,* 40**,** 614-9.

BERG, J. M., TYMOCZKO, J. L. & STRYER, L. 2002. *Biochemistry,* New York, W. H. Freeman and Co. ; [Basingstoke : Palgrave] [distributor], 2001.

BIECHE, I., LAURENDEAU, I., TOZLU, S., OLIVI, M., VIDAUD, D., LIDEREAU, R. & VIDAUD, M. 1999. Quantitation of MYC gene expression in sporadic breast tumors with a real-time reverse transcription-PCR assay. *Cancer Res,* 59**,** 2759-65.

BISHOP, D. T., DEMENAIS, F., GOLDSTEIN, A. M., BERGMAN, W., BISHOP, J. N., BRESSAC-DE PAILLERETS, B., CHOMPRET, A., GHIORZO, P., GRUIS, N., HANSSON, J., HARLAND, M., HAYWARD, N., HOLLAND, E. A., MANN, G. J., MANTELLI, M., NANCARROW, D., PLATZ, A. & TUCKER, M. A. 2002. Geographical variation in the penetrance of CDKN2A mutations for melanoma. *J Natl Cancer Inst,* 94**,** 894-903.

BOURTON, E. C., PLOWMAN, P. N., ZAHIR, S. A., SENGULOGLU, G. U., SERRAI, H., BOTTLEY, G. & PARRIS, C. N. 2012. Multispectral imaging flow cytometry reveals distinct frequencies of gamma-H2AX foci induction in DNA double strand break repair defective human cell lines. *Cytometry A,* 81**,** 130-7.

BOYLE, P., DORE, J. F., AUTIER, P. & RINGBORG, U. 2004. Cancer of the skin: a forgotten problem in Europe. *Ann Oncol,* 15**,** 5-6.

BRENNER, S. & TAMIR, E. 2002. Early detection of melanoma: the best strategy for a favorable prognosis. *Clin Dermatol,* 20**,** 203-11.

BRESSAC-DE-PAILLERETS, B., AVRIL, M. F., CHOMPRET, A. & DEMENAIS, F. 2002. Genetic and environmental factors in cutaneous malignant melanoma. *Biochimie,* 84**,** 67-74.

BRIELE, H. A. & DAS GUPTA, T. K. 1979. Natural history of cutaneous malignant melanoma. *World J Surg,* 3**,** 255-70.

BRISTOW, I. R. & ACLAND, K. 2008. Acral lentiginous melanoma of the foot and ankle: A case series and review of the literature. *J Foot Ankle Res,* 1**,** 11.

BUSTIN, S. A. 2000. Absolute quantification of mRNA using real-time reverse transcription polymerase chain reaction assays. *J Mol Endocrinol,* 25**,** 169-93.

CANCER-RESEARCH-UK. 2012. *Skin cancer statistics* [Online]. Available: http://www.cancerresearchuk.org/cancer-info/cancerstats/types/skin/ [Accessed 30/10/12].

CANNON-ALBRIGHT, L. A., GOLDGAR, D. E., MEYER, L. J., LEWIS, C. M., ANDERSON, D. E., FOUNTAIN, J. W., HEGI, M. E., WISEMAN, R. W., PETTY, E. M., BALE, A. E. & ET AL. 1992. Assignment of a locus for familial melanoma, MLM, to chromosome 9p13-p22. *Science,* 258**,** 1148-52.

CAPON, D. J., SHEPARD, H. M. & GOEDDEL, D. V. 1985. Two distinct families of human and bovine interferon-alpha genes are coordinately expressed and encode functional polypeptides. *Mol Cell Biol,* 5**,** 768-79.

CHAO, W. S. 2008. Real-Time PCR as a Tool to Study Weed Biology. *Weed Science,* 56**,** 290-296.

CHAPMAN, P. B., HAUSCHILD, A., ROBERT, C., HAANEN, J. B., ASCIERTO, P., LARKIN, J., DUMMER, R., GARBE, C., TESTORI, A., MAIO, M., HOGG, D., LORIGAN, P., LEBBE, C., JOUARY, T., SCHADENDORF, D., RIBAS, A., O'DAY, S. J., SOSMAN, J. A., KIRKWOOD, J. M., EGGERMONT, A. M., DRENO, B., NOLOP, K., LI, J., NELSON, B., HOU, J., LEE, R. J., FLAHERTY, K. T. & MCARTHUR, G. A. 2011. Improved survival with vemurafenib in melanoma with BRAF V600E mutation. *N Engl J Med,* 364**,** 2507-16.

CHIA, A., MORENO, G., LIM, A. & SHUMACK, S. 2007. Actinic keratoses. *Aust Fam Physician,* 36**,** 539-43.

CHIN, L., GARRAWAY, L. A. & FISHER, D. E. 2006. Malignant melanoma: genetics and therapeutics in the genomic era. *Genes Dev,* 20**,** 2149-82.

CHIN, L., MERLINO, G. & DEPINHO, R. A. 1998. Malignant melanoma: modern black plague and genetic black box. *Genes Dev,* 12**,** 3467-81.

CHIN, L., POMERANTZ, J., POLSKY, D., JACOBSON, M., COHEN, C., CORDON-CARDO, C., HORNER, J. W., 2ND & DEPINHO, R. A. 1997. Cooperative effects of INK4a and ras in melanoma susceptibility in vivo. *Genes Dev,* 11**,** 2822-34.

CHO, E., ROSNER, B. A. & COLDITZ, G. A. 2005. Risk factors for melanoma by body site. *Cancer Epidemiol Biomarkers Prev,* 14**,** 1241-4.

CHUDNOVSKY, Y., KHAVARI, P. A. & ADAMS, A. E. 2005. Melanoma genetics and the development of rational therapeutics. *Journal of Clinical Investigation,* 115**,** 813-824.

CHURCH, S. L., GRANT, J. W., RIDNOUR, L. A., OBERLEY, L. W., SWANSON, P. E., MELTZER, P. S. & TRENT, J. M. 1993. Increased manganese superoxide dismutase expression suppresses the malignant phenotype of human melanoma cells. *Proc Natl Acad Sci U S A,* 90**,** 3113-7.

CIFONE, M. A. & FIDLER, I. J. 1980. Correlation of patterns of anchorage-independent growth with in vivo behavior of cells from a murine fibrosarcoma. *Proc Natl Acad Sci U S A,* 77**,** 1039-43.

CLARK, W. H., JR., FROM, L., BERNARDINO, E. A. & MIHM, M. C. 1969. The histogenesis and biologic behavior of primary human malignant melanomas of the skin. *Cancer Res,* 29**,** 705-27.

CLINGEN, P. H., ARLETT, C. F., ROZA, L., MORI, T., NIKAIDO, O. & GREEN, M. H. 1995. Induction of cyclobutane pyrimidine dimers, pyrimidine(6-4)pyrimidone photoproducts, and Dewar valence isomers by natural sunlight in normal human mononuclear cells. *Cancer Res,* 55**,** 2245-8.

COBBEN, D. C., KOOPAL, S., TIEBOSCH, A. T., JAGER, P. L., ELSINGA, P. H., WOBBES, T. & HOEKSTRA, H. J. 2002. New diagnostic techniques in staging in the surgical treatment of cutaneous malignant melanoma. *Eur J Surg Oncol,* 28**,** 692-700.

COHEN-CYMBERKNOH, M., KEREM, E., FERKOL, T. & ELIZUR, A. 2013. Airway inflammation in cystic fibrosis: molecular mechanisms and clinical implications. *Thorax,* 68**,** 1157-62.

COLLADO, M. & SERRANO, M. 2006. The power and the promise of oncogene-induced senescence markers. *Nat Rev Cancer,* 6**,** 472-6.

COSTIN, G. E. & HEARING, V. J. 2007. Human skin pigmentation: melanocytes modulate skin color in response to stress. *FASEB J,* 21**,** 976-94.

COWAN, J. M., HALABAN, R. & FRANCKE, U. 1988. Cytogenetic analysis of melanocytes from premalignant nevi and melanomas. *J Natl Cancer Inst,* 80**,** 1159-64.

CROWSON, A. N., MAGRO, C. M., KADIN, M. E. & STRANC, M. 1996. Differential expression of the bcl-2 oncogene in human basal cell carcinoma. *Hum Pathol,* 27**,** 355-9.

CURTIN, J. A., FRIDLYAND, J., KAGESHITA, T., PATEL, H. N., BUSAM, K. J., KUTZNER, H., CHO, K. H., AIBA, S., BROCKER, E. B., LEBOIT, P. E., PINKEL, D. & BASTIAN, B. C. 2005. Distinct sets of genetic alterations in melanoma. *N Engl J Med,* 353**,** 2135-47.

DAVIES, H., BIGNELL, G. R., COX, C., STEPHENS, P., EDKINS, S., CLEGG, S., TEAGUE, J., WOFFENDIN, H., GARNETT, M. J., BOTTOMLEY, W., DAVIS, N., DICKS, E., EWING, R., FLOYD, Y., GRAY, K., HALL, S., HAWES, R., HUGHES, J., KOSMIDOU, V., MENZIES, A., MOULD, C., PARKER, A., STEVENS, C., WATT, S., HOOPER, S., WILSON, R., JAYATILAKE, H., GUSTERSON, B. A., COOPER, C., SHIPLEY, J., HARGRAVE, D., PRITCHARD-JONES, K., MAITLAND, N., CHENEVIX-TRENCH, G., RIGGINS, G. J., BIGNER, D. D., PALMIERI, G., COSSU, A., FLANAGAN, A., NICHOLSON, A., HO, J. W., LEUNG, S. Y., YUEN, S. T., WEBER, B. L., SEIGLER, H. F., DARROW, T. L., PATERSON, H., MARAIS, R., MARSHALL, C. J., WOOSTER, R., STRATTON, M. R. & FUTREAL, P. A. 2002. Mutations of the BRAF gene in human cancer. *Nature,* 417**,** 949-54.

DE SNOO, F. A. & HAYWARD, N. K. 2005. Cutaneous melanoma susceptibility and progression genes. *Cancer Lett,* 230**,** 153-86.

DHANOYA, A., CHAIN, B. M. & KESHAVARZ-MOORE, E. 2011. The impact of DNA topology on polyplex uptake and transfection efficiency in mammalian cells. *J Biotechnol,* 155**,** 377-86.

DIEFFENBACH, C. W., LOWE, T. M. & DVEKSLER, G. S. 1993. General concepts for PCR primer design. *PCR Methods Appl,* 3**,** S30-7.

DIEPGEN, T. L. & MAHLER, V. 2002. The epidemiology of skin cancer. *Br J Dermatol,* 146 Suppl 61**,** 1-6.

EGGERMONT, A. M. 2001. The role interferon-alpha in malignant melanoma remains to be defined. *Eur J Cancer,* 37**,** 2147-53.

ENGESAETER, B., ENGEBRAATEN, O., FLORENES, V. A. & MAELANDSMO, G. M. 2012. Dacarbazine and the Agonistic TRAIL Receptor-2 Antibody Lexatumumab Induce Synergistic Anticancer Effects in Melanoma. *PLoS One,* 7**,** e45492.

ESTEVE-PUIG, R., CANALS, F., COLOME, N., MERLINO, G. & RECIO, J. A. 2009. Uncoupling of the LKB1-AMPKalpha energy sensor pathway by growth factors and oncogenic BRAF. *PLoS One,* 4**,** e4771.

FEGHALI, C. A. & WRIGHT, T. M. 1997. Cytokines in acute and chronic inflammation. *Front Biosci,* 2**,** d12-26.

FELGNER, P. L., GADEK, T. R., HOLM, M., ROMAN, R., CHAN, H. W., WENZ, M., NORTHROP, J. P., RINGOLD, G. M. & DANIELSEN, M. 1987.

Lipofection: a highly efficient, lipid-mediated DNA-transfection procedure. *Proc Natl Acad Sci U S A,* 84**,** 7413-7.

FERRANTINI, M. & BELARDELLI, F. 2000. Gene therapy of cancer with interferon: lessons from tumor models and perspectives for clinical applications. *Semin Cancer Biol,* 10**,** 145-57.

FERRANTINI, M., CAPONE, I. & BELARDELLI, F. 2007. Interferon-alpha and cancer: mechanisms of action and new perspectives of clinical use. *Biochimie,* 89**,** 884-93.

FERRE, F. 1992. Quantitative or semi-quantitative PCR: reality versus myth. *PCR Methods Appl,* 2**,** 1-9.

FLAHERTY, K. T., INFANTE, J. R., DAUD, A., GONZALEZ, R., KEFFORD, R. F., SOSMAN, J., HAMID, O., SCHUCHTER, L., CEBON, J., IBRAHIM, N., KUDCHADKAR, R., BURRIS, H. A., 3RD, FALCHOOK, G., ALGAZI, A., LEWIS, K., LONG, G. V., PUZANOV, I., LEBOWITZ, P., SINGH, A., LITTLE, S., SUN, P., ALLRED, A., OUELLET, D., KIM, K. B., PATEL, K. & WEBER, J. 2012. Combined BRAF and MEK inhibition in melanoma with BRAF V600 mutations. *N Engl J Med,* 367**,** 1694-703.

FLORES, J. F., POLLOCK, P. M., WALKER, G. J., GLENDENING, J. M., LIN, A. H., PALMER, J. M., WALTERS, M. K., HAYWARD, N. K. & FOUNTAIN, J. W. 1997. Analysis of the CDKN2A, CDKN2B and CDK4 genes in 48 Australian melanoma kindreds. *Oncogene,* 15**,** 2999-3005.

FOUNTAIN, J. W., KARAYIORGOU, M., ERNSTOFF, M. S., KIRKWOOD, J. M., VLOCK, D. R., TITUS-ERNSTOFF, L., BOUCHARD, B., VIJAYASARADHI, S., HOUGHTON, A. N., LAHTI, J. & ET AL. 1992. Homozygous deletions within human chromosome band 9p21 in melanoma. *Proc Natl Acad Sci U S A,* 89**,** 10557-61.

FREEDMAN, V. H. & SHIN, S. I. 1974. Cellular tumorigenicity in nude mice: correlation with cell growth in semi-solid medium. *Cell,* 3**,** 355-9.

FRISCH, S. M. & RUOSLAHTI, E. 1997. Integrins and anoikis. *Curr Opin Cell Biol,* 9**,** 701-6.

GARBE, C., MCLEOD, G. R. & BUETTNER, P. G. 2000. Time trends of cutaneous melanoma in Queensland, Australia and Central Europe. *Cancer,* 89**,** 1269-78.

GARBE, C., TERHEYDEN, P., KEILHOLZ, U., KOLBL, O. & HAUSCHILD, A. 2008. Treatment of melanoma. *Dtsch Arztebl Int,* 105**,** 845-51.

GILES, G. G., MARKS, R. & FOLEY, P. 1988. Incidence of non-melanocytic skin cancer treated in Australia. *Br Med J (Clin Res Ed),* 296**,** 13-7.

GIMONA, M., KAZZAZ, J. A. & HELFMAN, D. M. 1996. Forced expression of tropomyosin 2 or 3 in v-Ki-ras-transformed fibroblasts results in distinct phenotypic effects. *Proc Natl Acad Sci U S A,* 93**,** 9618-23.

GINZINGER, D. G. 2002. Gene quantification using real-time quantitative PCR: an emerging technology hits the mainstream. *Exp Hematol,* 30**,** 503-12.

GOLDMAN, G. D. 1998. Squamous cell cancer: a practical approach. *Semin Cutan Med Surg,* 17**,** 80-95.

GRAY-SCHOPFER, V., WELLBROCK, C. & MARAIS, R. 2007. Melanoma biology and new targeted therapy. *Nature,* 445**,** 851-7.

GREEN, M. R. & SAMBROOK, J. 2012. *Molecular cloning : a laboratory manual,* Cold Spring Harbor, N.Y., Cold Spring Harbor Laboratory Press.

GREENBAUM, D., COLANGELO, C., WILLIAMS, K. & GERSTEIN, M. 2003. Comparing protein abundance and mRNA expression levels on a genomic scale. *Genome Biol,* 4**,** 117.

GRIMM, S. 2004. The art and design of genetic screens: mammalian culture cells. *Nat Rev Genet,* 5**,** 179-89.

GROB, J. J., JOUARY, T., DRENO, B., ASSELINEAU, J., GUTZMER, R., HAUSCHILD, A., LECCIA, M. T., LANDTHALER, M., GARBE, C., SASSOLAS, B., HERBST, R. A., GUILLOT, B., CHENE, G. & PEHAMBERGER, H. 2012. Adjuvant therapy with pegylated interferon alfa-2b (36months) versus low-dose interferon alfa-2b (18months) in melanoma patients without macrometastatic nodes: An open-label, randomised, phase 3 European Association for Dermato-Oncology (EADO) study. *Eur J Cancer*.

GUTTERMAN, J. U. 1994. Cytokine therapeutics: lessons from interferon alpha. *Proc Natl Acad Sci U S A,* 91**,** 1198-205.

HAASS, N. K., SMALLEY, K. S. & HERLYN, M. 2004. The role of altered cell-cell communication in melanoma progression. *J Mol Histol,* 35**,** 309-18.

HAMBURGER, A. & SALMON, S. E. 1977. Primary bioassay of human myeloma stem cells. *J Clin Invest,* 60**,** 846-54.

HARDY, M. P., OWCZAREK, C. M., JERMIIN, L. S., EJDEBACK, M. & HERTZOG, P. J. 2004. Characterization of the type I interferon locus and identification of novel genes. *Genomics,* 84**,** 331-45.

HAUPT, S., BERGER, M., GOLDBERG, Z. & HAUPT, Y. 2003. Apoptosis - the p53 network. *J Cell Sci,* 116**,** 4077-85.

HIGUCHI, R., DOLLINGER, G., WALSH, P. S. & GRIFFITH, R. 1992. Simultaneous amplification and detection of specific DNA sequences. *Biotechnology (N Y),* 10**,** 413-7.

HIGUCHI, R., FOCKLER, C., DOLLINGER, G. & WATSON, R. 1993. Kinetic PCR analysis: real-time monitoring of DNA amplification reactions. *Biotechnology (N Y),* 11**,** 1026-30.

HOCKER, T. L., SINGH, M. K. & TSAO, H. 2008. Melanoma genetics and therapeutic approaches in the 21st century: moving from the benchside to the bedside. *J Invest Dermatol,* 128**,** 2575-95.

HODI, F. S., O'DAY, S. J., MCDERMOTT, D. F., WEBER, R. W., SOSMAN, J. A., HAANEN, J. B., GONZALEZ, R., ROBERT, C., SCHADENDORF, D., HASSEL, J. C., AKERLEY, W., VAN DEN EERTWEGH, A. J., LUTZKY, J., LORIGAN, P., VAUBEL, J. M., LINETTE, G. P., HOGG, D., OTTENSMEIER, C. H., LEBBE, C., PESCHEL, C., QUIRT, I., CLARK, J. I., WOLCHOK, J. D., WEBER, J. S., TIAN, J., YELLIN, M. J., NICHOL, G. M., HOOS, A. & URBA, W. J. 2010. Improved survival with ipilimumab in patients with metastatic melanoma. *N Engl J Med,* 363**,** 711-23.

HOLLENBEAK, C. S., TODD, M. M., BILLINGSLEY, E. M., HARPER, G., DYER, A. M. & LENGERICH, E. J. 2005. Increased incidence of melanoma in renal transplantation recipients. *Cancer,* 104**,** 1962-7.

HOWELL, A. N. & SAGER, R. 1978. Tumorigenicity and its suppression in cybrids of mouse and Chinese hamster cell lines. *Proc Natl Acad Sci U S A,* 75**,** 2358-62.

HUSSEIN, M. R. 2004. Genetic pathways to melanoma tumorigenesis. *J Clin Pathol,* 57**,** 797-801.

HUSSEIN, M. R. 2005. Ultraviolet radiation and skin cancer: molecular mechanisms. *J Cutan Pathol,* 32**,** 191-205.

HUSSEIN, M. R., SUN, M., ROGGERO, E., SUDILOVSKY, E. C., TUTHILL, R. J., WOOD, G. S. & SUDILOVSKY, O. 2002. Loss of heterozygosity, microsatellite instability, and mismatch repair protein alterations in the radial growth phase of cutaneous malignant melanomas. *Mol Carcinog,* 34**,** 35-44.

JACOB, A. 1827. Observations respecting an ulcer of peculiar character, which attacks the eyelids and other parts of the face. *Dublin Hospital Rep Commun Med Surg,* 4**,** 232–239.

JAIN, K. K. 2010. *The handbook of biomarkers,* New York, Springer.

JAMUR, M. C. & OLIVER, C. 2010. Permeabilization of cell membranes. *Methods Mol Biol,* 588**,** 63-6.

JONES, P. A., LAUG, W. E., GARDNER, A., NYE, C. A., FINK, L. M. & BENEDICT, W. F. 1976. In vitro correlates of transformation in C3H/10T1/2 clone 8 mouse cells. *Cancer Res,* 36**,** 2863-7.

JONES, W. O., HARMAN, C. R., NG, A. K. & SHAW, J. H. 1999. Incidence of malignant melanoma in Auckland, New Zealand: highest rates in the world. *World J Surg,* 23**,** 732-5.

KAHN, R. A., COSSETTE, I. & FRIEDMAN, L. I. 1976. Optimum centrifugation conditions for the preparation of platelet and plasma products. *Transfusion,* 16**,** 162-5.

KAIDO, T., BANDU, M. T., MAURY, C., FERRANTINI, M., BELARDELLI, F. & GRESSER, I. 1995. IFN-alpha 1 gene transfection completely abolishes the tumorigenicity of murine B16 melanoma cells in allogeneic DBA/2 mice and decreases their tumorigenicity in syngeneic C57BL/6 mice. *Int J Cancer,* 60**,** 221-9.

KAIGHN, M. E., NARAYAN, K. S., OHNUKI, Y., LECHNER, J. F. & JONES, L. W. 1979. Establishment and characterization of a human prostatic carcinoma cell line (PC-3). *Invest Urol,* 17**,** 16-23.

KAMB, A., SHATTUCK-EIDENS, D., EELES, R., LIU, Q., GRUIS, N. A., DING, W., HUSSEY, C., TRAN, T., MIKI, Y., WEAVER-FELDHAUS, J. & ET AL. 1994. Analysis of the p16 gene (CDKN2) as a candidate for the chromosome 9p melanoma susceptibility locus. *Nat Genet,* 8**,** 23-6.

KANETSKY, P. A., REBBECK, T. R., HUMMER, A. J., PANOSSIAN, S., ARMSTRONG, B. K., KRICKER, A., MARRETT, L. D., MILLIKAN, R. C., GRUBER, S. B., CULVER, H. A., ZANETTI, R., GALLAGHER, R. P., DWYER, T., BUSAM, K., FROM, L., MUJUMDAR, U., WILCOX, H., BEGG, C. B. & BERWICK, M. 2006. Population-based study of natural variation in the melanocortin-1 receptor gene and melanoma. *Cancer Res,* 66**,** 9330-7.

KANTAK, S. S. & KRAMER, R. H. 1998. E-cadherin regulates anchorage-independent growth and survival in oral squamous cell carcinoma cells. *J Biol Chem,* 273**,** 16953-61.

KASPER, M., JAKS, V., HOHL, D. & TOFTGARD, R. 2012. Basal cell carcinoma - molecular biology and potential new therapies. *J Clin Invest,* 122**,** 455-63.

KEFFORD, R. F., NEWTON BISHOP, J. A., BERGMAN, W. & TUCKER, M. A. 1999. Counseling and DNA testing for individuals perceived to be genetically predisposed to melanoma: A consensus statement of the Melanoma Genetics Consortium. *J Clin Oncol,* 17**,** 3245-51.

KERR, J. F., WYLLIE, A. H. & CURRIE, A. R. 1972. Apoptosis: a basic biological phenomenon with wide-ranging implications in tissue kinetics. *Br J Cancer,* 26**,** 239-57.

KHALIL, I. A., KOGURE, K., AKITA, H. & HARASHIMA, H. 2006. Uptake pathways and subsequent intracellular trafficking in nonviral gene delivery. *Pharmacol Rev,* 58**,** 32-45.

KIM, S. H., TURNBULL, J. & GUIMOND, S. 2011. Extracellular matrix and cell signalling: the dynamic cooperation of integrin, proteoglycan and growth factor receptor. *J Endocrinol,* 209**,** 139-51.

KOYANAGI, K., KUO, C., NAKAGAWA, T., MORI, T., UENO, H., LORICO, A. R., JR., WANG, H. J., HSEUH, E., O'DAY, S. J. & HOON, D. S. 2005. Multimarker quantitative real-time PCR detection of circulating melanoma cells in peripheral blood: relation to disease stage in melanoma patients. *Clin Chem,* 51**,** 981-8.

KUBISTA, M., ANDRADE, J. M., BENGTSSON, M., FOROOTAN, A., JONAK, J., LIND, K., SINDELKA, R., SJOBACK, R., SJOGREEN, B., STROMBOM, L., STAHLBERG, A. & ZORIC, N. 2006. The real-time polymerase chain reaction. *Mol Aspects Med,* 27**,** 95-125.

KVAM, E. & TYRRELL, R. M. 1999. The role of melanin in the induction of oxidative DNA base damage by ultraviolet A irradiation of DNA or melanoma cells. *J Invest Dermatol,* 113**,** 209-13.

LEE, K. M., CHOI, K. H. & OUELLETTE, M. M. 2004. Use of exogenous hTERT to immortalize primary human cells. *Cytotechnology,* 45**,** 33-8.

LENGYEL, P. 1982. Biochemistry of interferons and their actions. *Annu Rev Biochem,* 51**,** 251-82.

LENS, M. B. & DAWES, M. 2004. Global perspectives of contemporary epidemiological trends of cutaneous malignant melanoma. *Br J Dermatol,* 150**,** 179-85.

LINDNER, D. J. 2002. Interferons as antiangiogenic agents. *Curr Oncol Rep,* 4**,** 510-4.

LODISH H, B. A., ZIPURSKY SL, ET AL. 2000. *Molecular Cell Biology,* New York, W. H. Freeman.

LOO, J. C., PATERSON, A. D., HAO, A., SHENNAN, M., PERETZ, H., SIDI, Y., HOGG, D. & YAKOBSON, E. 2005. Search for genetic variants associated with cutaneous malignant melanoma in the Ashkenazi Jewish population. *J Med Genet,* 42**,** e30.

MAELLARO, E., PACENTI, L., DEL BELLO, B., VALENTINI, M. A., MANGIAVACCHI, P., DE FELICE, C., RUBEGNI, P., LUZI, P. & MIRACCO, C. 2003. Different effects of interferon-alpha on melanoma cell lines: a study on telomerase reverse transcriptase, telomerase activity and apoptosis. *Br J Dermatol,* 148**,** 1115-24.

MARKOVIC, S. N., ERICKSON, L. A., RAO, R. D., WEENIG, R. H., POCKAJ, B. A., BARDIA, A., VACHON, C. M., SCHILD, S. E., MCWILLIAMS, R. R., HAND, J. L., LAMAN, S. D., KOTTSCHADE, L. A., MAPLES, W. J., PITTELKOW, M. R., PULIDO, J. S., CAMERON, J. D. & CREAGAN, E. T. 2007. Malignant melanoma in the 21st century, part 1: epidemiology, risk factors, screening, prevention, and diagnosis. *Mayo Clin Proc,* 82**,** 364-80.

MARKS, R., RENNIE, G. & SELWOOD, T. 1988. The relationship of basal cell carcinomas and squamous cell carcinomas to solar keratoses. *Arch Dermatol,* 124**,** 1039-42.

MARROT, L., BELAIDI, J. P., MEUNIER, J. R., PEREZ, P. & AGAPAKIS-CAUSSE, C. 1999. The human melanocyte as a particular target for UVA radiation and an endpoint for photoprotection assessment. *Photochem Photobiol,* 69**,** 686-93.

MATSUTA, M., IMAMURA, Y., SASAKI, K. & KON, S. 1997. Detection of numerical chromosomal aberrations in malignant melanomas using fluorescence in situ hybridization. *J Cutan Pathol,* 24**,** 201-5.

MEYER, L. J. & ZONE, J. H. 1994. Genetics of cutaneous melanoma. *J Invest Dermatol,* 103**,** 112S-116S.

MOCELLIN, S., PASQUALI, S., ROSSI, C. R. & NITTI, D. 2010. Interferon alpha adjuvant therapy in patients with high-risk melanoma: a systematic review and meta-analysis. *J Natl Cancer Inst,* 102**,** 493-501.

MOLIFE, R. & HANCOCK, B. W. 2002. Adjuvant therapy of malignant melanoma. *Crit Rev Oncol Hematol,* 44**,** 81-102.

MORITA, R., FUJIMOTO, A., HATTA, N., TAKEHARA, K. & TAKATA, M. 1998. Comparison of genetic profiles between primary melanomas and their metastases reveals genetic alterations and clonal evolution during progression. *J Invest Dermatol,* 111**,** 919-24.

MORRISON, T. B., WEIS, J. J. & WITTWER, C. T. 1998. Quantification of low-copy transcripts by continuous SYBR Green I monitoring during amplification. *Biotechniques,* 24**,** 954-8, 960, 962.

MORTIER, L., MARCHETTI, P., DELAPORTE, E., MARTIN DE LASSALLE, E., THOMAS, P., PIETTE, F., FORMSTECHER, P., POLAKOWSKA, R. & DANZE, P. M. 2002. Progression of actinic keratosis to squamous cell carcinoma of the skin correlates with deletion of the 9p21 region encoding the p16(INK4a) tumor suppressor. *Cancer Lett,* 176**,** 205-14.

NEWTON, J. A. 1994. Genetics of melanoma. *Br Med Bull,* 50**,** 677-87.

NOURI, K. 2008. *Skin cancer,* New York, McGraw-Hill Medical.

OLSZEWSKA-SLONINA, D. M., STYCZYNISK, J., DREWA, T. A., OLSZEWSKI, K. J. & CZAJKOWSKI, R. 2005. B16 and cloudman S91 mouse melanoma cells susceptibility to apoptosis after dacarbazine treatment. *Acta Pol Pharm,* 62**,** 473-83.

OSLOWSKI, C. M. & URANO, F. 2011. Measuring ER stress and the unfolded protein response using mammalian tissue culture system. *Methods Enzymol,* 490**,** 71-92.

PALMER, J. S., DUFFY, D. L., BOX, N. F., AITKEN, J. F., O'GORMAN, L. E., GREEN, A. C., HAYWARD, N. K., MARTIN, N. G. & STURM, R. A. 2000. Melanocortin-1 receptor polymorphisms and risk of melanoma: is the association explained solely by pigmentation phenotype? *Am J Hum Genet,* 66**,** 176-86.

PAPP, T., PEMSEL, H., ZIMMERMANN, R., BASTROP, R., WEISS, D. G. & SCHIFFMANN, D. 1999. Mutational analysis of the N-ras, p53, p16INK4a, CDK4, and MC1R genes in human congenital melanocytic naevi. *J Med Genet,* 36**,** 610-4.

PARRIS, C. N., HARRIS, J. D., GRIFFIN, D. K., CUTHBERT, A. P., SILVER, A. J. & NEWBOLD, R. F. 1999. Functional evidence of novel tumor suppressor genes for cutaneous malignant melanoma. *Cancer Res,* 59**,** 516-20.

PEARCE, J., BARNETT, R. & KINGHAM, S. 2006. Slip! Slap! Slop! Cutaneous malignant melanoma incidence and social status in New Zealand, 1995-2000. *Health Place,* 12**,** 239-52.

PEEHL, D. M. & STANBRIDGE, E. J. 1981. Anchorage-independent growth of normal human fibroblasts. *Proc Natl Acad Sci U S A,* 78**,** 3053-7.

PESTKA, S. 2007. The interferons: 50 years after their discovery, there is much more to learn. *J Biol Chem,* 282**,** 20047-51.

PESTKA, S., LANGER, J. A., ZOON, K. C. & SAMUEL, C. E. 1987. Interferons and their actions. *Annu Rev Biochem,* 56**,** 727-77.

PETTI, C., MOLLA, A., VEGETTI, C., FERRONE, S., ANICHINI, A. & SENSI, M. 2006. Coexpression of NRASQ61R and BRAFV600E in human melanoma cells activates senescence and increases susceptibility to cell-mediated cytotoxicity. *Cancer Res,* 66**,** 6503-11.

PETTY, E. M., GIBSON, L. H., FOUNTAIN, J. W., BOLOGNIA, J. L., YANG-FENG, T. L., HOUSMAN, D. E. & BALE, A. E. 1993. Molecular definition of a chromosome 9p21 germ-line deletion in a woman with multiple melanomas and a plexiform neurofibroma: implications for 9p tumor-suppressor gene(s). *Am J Hum Genet,* 53**,** 96-104.

PFAFFL, M. W. 2001. A new mathematical model for relative quantification in real-time RT-PCR. *Nucleic Acids Res,* 29**,** e45.

PFAFFL, M. W. & HAGELEIT, M. 2001. Validities of mRNA quantification using recombinant RNA and recombinant DNA external calibration curves in real-time RT-PCR. *Biotechnology Letters,* 23**,** 275–282.

PIECHACZYK, M., BLANCHARD, J. M., MARTY, L., DANI, C., PANABIERES, F., EL SABOUTY, S., FORT, P. & JEANTEUR, P. 1984. Post-transcriptional regulation of glyceraldehyde-3-phosphate-dehydrogenase gene expression in rat tissues. *Nucleic Acids Res,* 12**,** 6951-63.

POLLOCK, P. M., HARPER, U. L., HANSEN, K. S., YUDT, L. M., STARK, M., ROBBINS, C. M., MOSES, T. Y., HOSTETTER, G., WAGNER, U., KAKAREKA, J., SALEM, G., POHIDA, T., HEENAN, P., DURAY, P., KALLIONIEMI, O., HAYWARD, N. K., TRENT, J. M. & MELTZER, P. S. 2003. High frequency of BRAF mutations in nevi. *Nat Genet,* 33**,** 19-20.

PORRAS, B. H. & COCKERELL, C. J. 1997. Cutaneous malignant melanoma: classification and clinical diagnosis. *Semin Cutan Med Surg,* 16**,** 88-96.

POSALAKY, Z., MCGINLEY, D., CUTLER, B. & KATZ, H. I. 1979. Intercellular junctional specializations in human basal cell carcinoma. A freeze-fracture study. *Virchows Arch A Pathol Anat Histol,* 384**,** 53-63.

RAASCH, B., MACLENNAN, R., WRONSKI, I. & ROBERTSON, I. 1998. Body site specific incidence of basal and squamous cell carcinoma in an exposed population, Townsville, Australia. *Mutat Res,* 422**,** 101-6.

REBOUÇAS, E. L., COSTA, J. J. N., PASSOS, M. J., PASSOS, J. R. S., HURK, R. & SILVA, J. R. V. 2013. Real-Time PCR and Importance of Housekeepings Genes for Normalization and Quantification of mRNA Expression in Different Tissues. *Brazillian archives of biology and technology,* 56**,** 143-154.

REDEI, G. P. 2008. *Encyclopedia of genetics, genomics, proteomics and informatics,* [London], Springer.

RICOTTI, C., BOUZARI, N., AGADI, A. & COCKERELL, C. J. 2009. Malignant skin neoplasms. *Med Clin North Am,* 93**,** 1241-64.

RIDKY, T. W. 2007. Nonmelanoma skin cancer. *J Am Acad Dermatol,* 57**,** 484-501.

RIZOS, H., PUIG, S., BADENAS, C., MALVEHY, J., DARMANIAN, A. P., JIMENEZ, L., MILA, M. & KEFFORD, R. F. 2001. A melanoma-associated germline mutation in exon 1beta inactivates p14ARF. *Oncogene,* 20**,** 5543-7.

ROBERTSON, G., COLEMAN, A. & LUGO, T. G. 1996. A malignant melanoma tumor suppressor on human chromosome 11. *Cancer Res,* 56**,** 4487-92.

RODRIGUES, V., CORDEIRO-DA-SILVA, A., LAFORGE, M., OUAISSI, A., SILVESTRE, R. & ESTAQUIER, J. 2012. Modulation of mammalian apoptotic pathways by intracellular protozoan parasites. *Cell Microbiol,* 14**,** 325-33.

ROWERT-HUBER, J., PATEL, M. J., FORSCHNER, T., ULRICH, C., EBERLE, J., KERL, H., STERRY, W. & STOCKFLETH, E. 2007. Actinic keratosis is an early in situ squamous cell carcinoma: a proposal for reclassification. *Br J Dermatol,* 156 Suppl 3**,** 8-12.

RUBIN, K. M., VONA, K., MADDEN, K., MCGETTIGAN, S. & BRAUN, I. M. 2012. Side effects in melanoma patients receiving adjuvant interferon alfa-2b therapy: a nurse's perspective. *Support Care Cancer,* 20**,** 1601-11.

SAGEBIEL, R. W. 1993. Melanocytic nevi in histologic association with primary cutaneous melanoma of superficial spreading and nodular types: effect of tumor thickness. *J Invest Dermatol,* 100**,** 322S-325S.

SAUTER, E. R. & HERLYN, M. 1998. Molecular biology of human melanoma development and progression. *Mol Carcinog,* 23**,** 132-43.

SAUTER, E. R., YEO, U. C., VON STEMM, A., ZHU, W., LITWIN, S., TICHANSKY, D. S., PISTRITTO, G., NESBIT, M., PINKEL, D., HERLYN, M. & BASTIAN, B. C. 2002. Cyclin D1 is a candidate oncogene in cutaneous melanoma. *Cancer Res,* 62**,** 3200-6.

SCHLAAK, M., SCHMIDT, P., BANGARD, C., KURSCHAT, P., MAUCH, C. & ABKEN, H. 2012. Regression of metastatic melanoma in a patient by antibody targeting of cancer stem cells. *Oncotarget,* 3**,** 22-30.

SCHOOLEY, A. M., ANDREWS, N. M., ZHAO, H. & ADDISON, C. L. 2012. beta1 integrin is required for anchorage-independent growth and invasion of tumor cells in a context dependent manner. *Cancer Lett,* 316**,** 157-67.

SERRANO, M., HANNON, G. J. & BEACH, D. 1993. A new regulatory motif in cell-cycle control causing specific inhibition of cyclin D/CDK4. *Nature,* 366**,** 704-7.

SETLOW, R. B., WOODHEAD, A. D. & GRIST, E. 1989. Animal model for ultraviolet radiation-induced melanoma: platyfish-swordtail hybrid. *Proc Natl Acad Sci U S A,* 86**,** 8922-6.

SHAH, V., BHARADWAJ, S., KAIBUCHI, K. & PRASAD, G. L. 2001. Cytoskeletal organization in tropomyosin-mediated reversion of ras-transformation: Evidence for Rho kinase pathway. *Oncogene,* 20**,** 2112-21.

SHARPLESS, E. & CHIN, L. 2003. The INK4a/ARF locus and melanoma. *Oncogene,* 22**,** 3092-8.

SHIN, S. I., FREEDMAN, V. H., RISSER, R. & POLLACK, R. 1975. Tumorigenicity of virus-transformed cells in nude mice is correlated specifically with anchorage independent growth in vitro. *Proc Natl Acad Sci U S A,* 72**,** 4435-9.

SHUTTLEWORTH, J., MORSER, J. & BURKE, D. C. 1983. Expression of interferon-alpha and interferon-beta genes in human lymphoblastoid (Namalwa) cells. *Eur J Biochem,* 133**,** 399-404.

SIEGEL, R., WARD, E., BRAWLEY, O. & JEMAL, A. 2011. Cancer statistics, 2011: the impact of eliminating socioeconomic and racial disparities on premature cancer deaths. *CA Cancer J Clin,* 61**,** 212-36.

SMITH, K. J., SKELTON, H. G., HEIMER, W., BAXTER, D., ANGRITT, P., FRISMAN, D. & WAGNER, K. F. 1993. Melanocytic activation in HIV-1 disease: HMB-45 staining in common acquired nevi. Military Medical Consortium for the Advancement of Retroviral Research. *J Am Acad Dermatol,* 29**,** 539-44.

SOUFIR, N., AVRIL, M. F., CHOMPRET, A., DEMENAIS, F., BOMBLED, J., SPATZ, A., STOPPA-LYONNET, D., BENARD, J. & BRESSAC-DE PAILLERETS, B. 1998. Prevalence of p16 and CDK4 germline mutations in 48 melanoma-prone families in France. The French Familial Melanoma Study Group. *Hum Mol Genet,* 7**,** 209-16.

STAHL, J. M., SHARMA, A., CHEUNG, M., ZIMMERMAN, M., CHENG, J. Q., BOSENBERG, M. W., KESTER, M., SANDIRASEGARANE, L. & ROBERTSON, G. P. 2004. Deregulated Akt3 activity promotes development of malignant melanoma. *Cancer Res,* 64**,** 7002-10.

STEWART, W. E., 2ND 1974. Distinct molecular species of interferons. *Virology,* 61**,** 80-6.

STRATIGOS, A. J., DIMISIANOS, G., NIKOLAOU, V., POULOU, M., SYPSA, V., STEFANAKI, I., PAPADOPOULOS, O., POLYDOROU, D., PLAKA, M., CHRISTOFIDOU, E., GOGAS, H., TSOUTSOS, D., KASTANA, O., ANTONIOU, C., HATZAKIS, A., KANAVAKIS, E. & KATSAMBAS, A. D. 2006. Melanocortin receptor-1 gene polymorphisms and the risk of cutaneous melanoma in a low-risk southern European population. *J Invest Dermatol,* 126**,** 1842-9.

STUCHBURY, G. & MUNCH, G. 2010. Optimizing the generation of stable neuronal cell lines via pre-transfection restriction enzyme digestion of plasmid DNA. *Cytotechnology,* 62**,** 189-94.

TARTOUR, E., GEY, A., SASTRE-GARAU, X., PANNETIER, C., MOSSERI, V., KOURILSKY, P. & FRIDMAN, W. H. 1994. Analysis of interleukin 6 gene expression in cervical neoplasia using a quantitative polymerase chain reaction

assay: evidence for enhanced interleukin 6 gene expression in invasive carcinoma. *Cancer Res,* 54**,** 6243-8.

TELFER, N. R., COLVER, G. B. & MORTON, C. A. 2008. Guidelines for the management of basal cell carcinoma. *Br J Dermatol,* 159**,** 35-48.

TENCOMNAO, T., RAKKHITAWATTHANA, V. & SUKHONTASING, K. 2008. Evaluation of a novel luciferase reporter construct: a positive control plasmid for reporter gene assay. *African Journal of Biotechnology,* 7**,** 2124-2127.

TERAKI, Y. & SHIOHARA, T. 1999. Apoptosis and the skin. *Eur J Dermatol,* 9**,** 413-25; quiz 426.

TESTORI, A., RUTKOWSKI, P., MARSDEN, J., BASTHOLT, L., CHIARION-SILENI, V., HAUSCHILD, A. & EGGERMONT, A. M. 2009. Surgery and radiotherapy in the treatment of cutaneous melanoma. *Ann Oncol,* 20 Suppl 6**,** vi22-9.

THE-UNIVERSITY-OF-CHICAGO-MEDICINE. 2012. *Skin Cancer Screening (PDQ®)* [Online]. Available: http://www.uchospitals.edu/online-library/content=CDR258037 [Accessed 01/11/12].

THOMPSON, F. H., EMERSON, J., OLSON, S., WEINSTEIN, R., LEAVITT, S. A., LEONG, S. P., EMERSON, S., TRENT, J. M., NELSON, M. A., SALMON, S. E. & ET AL. 1995. Cytogenetics of 158 patients with regional or disseminated melanoma. Subset analysis of near-diploid and simple karyotypes. *Cancer Genet Cytogenet,* 83**,** 93-104.

THOMPSON, J. F., SCOLYER, R. A. & KEFFORD, R. F. 2005. Cutaneous melanoma. *Lancet,* 365**,** 687-701.

TITUS-ERNSTOFF, L., PERRY, A. E., SPENCER, S. K., GIBSON, J. J., COLE, B. F. & ERNSTOFF, M. S. 2005. Pigmentary characteristics and moles in relation to melanoma risk. *Int J Cancer,* 116**,** 144-9.

TRENT, J. M., STANBRIDGE, E. J., MCBRIDE, H. L., MEESE, E. U., CASEY, G., ARAUJO, D. E., WITKOWSKI, C. M. & NAGLE, R. B. 1990. Tumorigenicity in human melanoma cell lines controlled by introduction of human chromosome 6. *Science,* 247**,** 568-71.

TSAO, H., ZHANG, X., BENOIT, E. & HALUSKA, F. G. 1998. Identification of PTEN/MMAC1 alterations in uncultured melanomas and melanoma cell lines. *Oncogene,* 16**,** 3397-402.

TSAO, H., ZHANG, X., FOWLKES, K. & HALUSKA, F. G. 2000. Relative reciprocity of NRAS and PTEN/MMAC1 alterations in cutaneous melanoma cell lines. *Cancer Res,* 60**,** 1800-4.

TUTING, T., GAMBOTTO, A., BAAR, J., DAVIS, I. D., STORKUS, W. J., ZAVODNY, P. J., NARULA, S., TAHARA, H., ROBBINS, P. D. & LOTZE, M. T. 1997. Interferon-alpha gene therapy for cancer: retroviral transduction of fibroblasts and particle-mediated transfection of tumor cells are both effective strategies for gene delivery in murine tumor models. *Gene Ther,* 4**,** 1053-60.

ULUS-SENGULOGLU, G., ARLETT, C. F., PLOWMAN, P. N., PARNELL, J., PATEL, N., BOURTON, E. C. & PARRIS, C. N. 2012. Elevated expression of artemis in human fibroblast cells is associated with cellular radiosensitivity and increased apoptosis. *Br J Cancer,* 107**,** 1506-13.

URTEAGA, O. & PACK, G. T. 1966. On the antiquity of melanoma. *Cancer,* 19**,** 607-10.

VOLKOVOVA, K., BILANICOVA, D., BARTONOVA, A., LETASIOVA, S. & DUSINSKA, M. 2012. Associations between environmental factors and incidence of cutaneous melanoma. Review. *Environ Health,* 11 Suppl 1**,** S12.

WEINBERG, R. A. 1994. Oncogenes and tumor suppressor genes. *CA Cancer J Clin,* 44**,** 160-70.

WHEATLEY, K., IVES, N., HANCOCK, B. & GORE, M. 2002. Interferon as adjuvant treatment for melanoma. *Lancet,* 360**,** 878.

WHITEMAN, D. C., PARSONS, P. G. & GREEN, A. C. 1998. p53 expression and risk factors for cutaneous melanoma: a case-control study. *Int J Cancer,* 77**,** 843-8.

WITTWER, C. T., HERRMANN, M. G., MOSS, A. A. & RASMUSSEN, R. P. 1997. Continuous fluorescence monitoring of rapid cycle DNA amplification. *Biotechniques,* 22**,** 130-1, 134-8.

WORLD-HEALTH-ORGANIZATION. 2012 *Ultraviolet radiation and the INTERSUN Programme* [Online]. Available: http://www.who.int/uv/faq/skincancer/en/index1.html [Accessed 30/10/12].

YANOFSKY, V. R., MERCER, S. E. & PHELPS, R. G. 2011. Histopathological variants of cutaneous squamous cell carcinoma: a review. *J Skin Cancer,* 2011**,** 210813.

YOUNG, A. R., POTTEN, C. S., NIKAIDO, O., PARSONS, P. G., BOENDERS, J., RAMSDEN, J. M. & CHADWICK, C. A. 1998. Human melanocytes and keratinocytes exposed to UVB or UVA in vivo show comparable levels of thymine dimers. *J Invest Dermatol,* 111**,** 936-40.

ZHOU, X. P., GIMM, O., HAMPEL, H., NIEMANN, T., WALKER, M. J. & ENG, C. 2000. Epigenetic PTEN silencing in malignant melanomas without PTEN mutation. *Am J Pathol,* 157**,** 1123-8.

ZUO, L., WEGER, J., YANG, Q., GOLDSTEIN, A. M., TUCKER, M. A., WALKER, G. J., HAYWARD, N. & DRACOPOLI, N. C. 1996. Germline mutations in the p16INK4a binding domain of CDK4 in familial melanoma. *Nat Genet,* 12**,** 97-9.